BuMines OFR 132-78

PB 289716

# DEVELOPMENT OF A QUIET ROCK DRILL
# Volume 2: Sources of Drill Rod Noise

Prepared for

UNITED STATES DEPARTMENT OF THE INTERIOR
BUREAU OF MINES

By

IVOR HAWKES ASSOCIATES
14 Parkhurst Street
Lebanon, New Hampshire 03766

IHA

Final Report, Volume 2

CONTRACT NO. J0155099
Development of Other Pneumatic Drills

June 1977

Bureau of Mines Open File Report 132-78

REPRODUCED BY
NATIONAL TECHNICAL
INFORMATION SERVICE
U. S. DEPARTMENT OF COMMERCE
SPRINGFIELD, VA. 22161

Reference to specific brands, equipment, or trade names in this report is made to facilitate understanding and does not imply endorsement by the Bureau of Mines.

The views and conclusions contained in this document are those of the authors and should not be interpreted as necessarily representing the official policies or recommendations of the Interior Department's Bureau of Mines or of the U.S. Government.

NOTICE

THIS DOCUMENT HAS BEEN REPRODUCED FROM THE BEST COPY FURNISHED US BY THE SPONSORING AGENCY. ALTHOUGH IT IS RECOGNIZED THAT CERTAIN PORTIONS ARE ILLEGIBLE, IT IS BEING RELEASED IN THE INTEREST OF MAKING AVAILABLE AS MUCH INFORMATION AS POSSIBLE.

50272-101

| REPORT DOCUMENTATION PAGE | 1. REPORT NO. BuMines OFR 132-78 | 2. | 3. Recipient's Accession No. PB289716 |
|---|---|---|---|

**4. Title and Subtitle**
DEVELOPMENT OF A QUIET ROCK DRILL
Volume 2: Sources of Drill Rod Noise

**5. Report Date** June 1977

**6.**

**7. Author(s)**
Ivor Hawkes, David D. Wright and P. K. Dutta

**8. Performing Organization Rept. No.**

**9. Performing Organization Name and Address**
Ivor Hawkes Associates
14 Parkhurst Street
Lebanon, New Hampshire 03766

**10. Project/Task/Work Unit No.**

**11. Contract(C) or Grant(G) No.**
(C) J0155099
(G)

**12. Sponsoring Organization Name and Address**
Office of the Assistant Director--Mining
Bureau of Mines
U.S. Department of the Interior
Washington, D.C. 20241

**13. Type of Report & Period Covered**
Contract research
June 1975 - June 1977

**14.**

**15. Supplementary Notes**
Approved by the Director of the Bureau of Mines for placement on open file, November 17, 1978

**16. Abstract (Limit: 200 words)**
This report describes how longitudinal and bending stress waves in percussive drill rods generate noise. It is shown that in practical drills the largest noise source is the bending waves, which are mainly generated because of imperfections in the piston, chuck, and drill rod alignment. Equations are presented which enable the noise spectra generated by the bending and longitudinal waves to be precisely predicted. Means for reducing the amplitude of the bending waves are discussed.

**17. Document Analysis a. Descriptors**
Drilling
Drilling machines
Drills
Machinery noise
Mining engineering
Noise
Noise reduction
Rock drilling
(DDC Retrieval and Indexing Terminology, 1975)

**b. Identifiers/Open-Ended Terms**

**c. COSATI Field/Group** 08I, 05E

**18. Availability Statement**
Unlimited release by NTIS.

**19. Security Class (This Report)**

**20. Security Class (This Page)**

**22. Price** A05-A01

(See ANSI-Z39.18) See Instructions on Reverse

OPTIONAL FORM 272 (4-77)
(Formerly NTIS-35)
Department of Commerce

# DO NOT PRINT THESE INSTRUCTIONS AS A PAGE IN A REPORT

## INSTRUCTIONS

Optional Form 272, Report Documentation Page is based on Guidelines for Format and Production of Scientific and Technical Reports, ANSI Z39.18–1974 available from American National Standards Institute, 1430 Broadway, New York, New York 10018. Each separately bound report—for example, each volume in a multivolume set—shall have its unique Report Documentation Page.

1. Report Number. Each individually bound report shall carry a unique alphanumeric designation assigned by the performing organization or provided by the sponsoring organization in accordance with American National Standard ANSI Z39.23–1974, Technical Report Number (STRN). For registration of report code, contact NTIS Report Number Clearinghouse, Springfield, VA 22161. Use uppercase letters, Arabic numerals, slashes, and hyphens only, as in the following examples: FASEB/NS–75/87 and FAA/RD–75/09.
2. Leave blank.
3. Recipient's Accession Number. Reserved for use by each report recipient.
4. Title and Subtitle. Title should indicate clearly and briefly the subject coverage of the report, subordinate subtitle to the main title. When a report is prepared in more than one volume, repeat the primary title, add volume number and include subtitle for the specific volume.
5. Report Date. Each report shall carry a date indicating at least month and year. Indicate the basis on which it was selected (e.g., date of issue, date of approval, date of preparation, date published).
6. Sponsoring Agency Code. Leave blank.
7. Author(s). Give name(s) in conventional order (e.g., John R. Doe, or J. Robert Doe). List author's affiliation if it differs from the performing organization.
8. Performing Organization Report Number. Insert if performing organization wishes to assign this number.
9. Performing Organization Name and Mailing Address. Give name, street, city, state, and ZIP code. List no more than two levels of an organizational hierarchy. Display the name of the organization exactly as it should appear in Government indexes such as Government Reports Announcements & Index (GRA & I).
10. Project/Task/Work Unit Number. Use the project, task and work unit numbers under which the report was prepared.
11. Contract/Grant Number. Insert contract or grant number under which report was prepared.
12. Sponsoring Agency Name and Mailing Address. Include ZIP code. Cite main sponsors.
13. Type of Report and Period Covered. State interim, final, etc., and, if applicable, inclusive dates.
14. Performing Organization Code. Leave blank.
15. Supplementary Notes. Enter information not included elsewhere but useful, such as: Prepared in cooperation with . . . Translation of . . . Presented at conference of . . . To be published in . . . When a report is revised, include a statement whether the new report supersedes or supplements the older report.
16. Abstract. Include a brief (200 words or less) factual summary of the most significant information contained in the report. If the report contains a significant bibliography or literature survey, mention it here.
17. Document Analysis. (a). Descriptors. Select from the Thesaurus of Engineering and Scientific Terms the proper authorized terms that identify the major concept of the research and are sufficiently specific and precise to be used as index entries for cataloging.

    (b). Identifiers and Open-Ended Terms. Use identifiers for project names, code names, equipment designators, etc. Use open-ended terms written in descriptor form for those subjects for which no descriptor exists.

    (c). COSATI Field/Group. Field and Group assignments are to be taken from the 1964 COSATI Subject Category List. Since the majority of documents are multidisciplinary in nature, the primary Field/Group assignment(s) will be the specific discipline, area of human endeavor, or type of physical object. The application(s) will be cross-referenced with secondary Field/Group assignments that will follow the primary posting(s).
18. Distribution Statement. Denote public releasability, for example "Release unlimited", or limitation for reasons other than security. Cite any availability to the public, with address, order number and price, if known.
19. & 20. Security Classification. Enter U.S. Security Classification in accordance with U.S. Security Regulations (i.e., UNCLASSIFIED).
21. Number of pages. Insert the total number of pages, including introductory pages, but excluding distribution list, if any.
22. Price. Enter price in paper copy (PC) and/or microfiche (MF) if known.

☆ U.S. GPO: 1977-0-241-530 3461

CONTENTS



ILLUSTRATIONS





Preceding page blank

TABLES

## EXECUTIVE SUMMARY

Excluding exhaust air, drill rod vibrations are the most serious source of noise in percussive drills, with levels on the order of 105-110 dBA at the operator's position. The objective of the study reported here and funded by the U.S. Bureau of Mines under the Coal Mines Health and Safety Act of 1969 was to study the sources of noise in drill rods and relate the causes to the relevant drill design features.

This report is Volume 2 of the final report of a study to conceive and evaluate rock drill design changes that will significantly reduce their noise levels. Volume 1 dealt with the general problem and described the development of a percussive drill incorporating noise-reducing features which reduced the noise levels at 1 meter from around 114 DBA to around 95 dBA without significantly changing the drilling rate.

The current report, which deals solely with drill-rod-associated noise, is in three main sections. The first describes in detail the nature and generation of longitudinal and bending waves in drill rods. The second section describes how the longitudinal and bending waves generate noise and shows that bending waves are the major source of noise emanating from drill rods. The final section concludes the report with a discussion of means of reducing the amplitude of bending waves in future designs.

Important conclusions from the study are as follows:

1. The individual contributions of the longitudinal and bending waves to the noise levels can be determined from spectrum analysis of the noise.

Spectrum analysis of drill rod noise produces discrete frequency peaks $f_n$ where

$$f_{Ln} = \frac{nC_s}{2L_r} : \text{ longitudinal waves}$$

and

$$f_{Bn} = \frac{n^2\pi DC_s}{8L_r^2}\left[1-1.2\left(\frac{nD}{L_r}\right)^2\right]\left(\frac{2n+1}{2n}\right)^2 : \text{ bending waves}$$

where $C_s$ = longitudinal wave speed, $D$ = rod diameter, $L_r$ = rod length, and $n$ = integer (1, 2, 3, 4,...).

2. In practical drills the bending waves contribute the bulk of the noise and they arise primarily because of misalignments of the drill cylinder, chuck and drill rod and nonparallel impact surfaces.

3. The amplitude of the bending waves can be reduced by: a) Using longer drill shanks, b) Reducing drill rod/shank tolerances, c) Mounting rubber collars on the drill rods, and d) Optimizing the drill machine thrust.

The above techniques for reducing drill rod noise are all being implemented into the design of six production prototype stoper drills currently being developed under USBM Contract J0177125. It is also expected that the technology reported here and in Volume 1 will be applicable in future designs of other quiet percussive drills.

## NOMENCLATURE

| | |
|---|---|
| $A_r$ | Rod area |
| $A_p$ | Piston area |
| $A_{ra}$ | Area ratio, piston/drill rod |
| $C_s$ | Longitudinal wave speed |
| $C_B$ | Bending wave speed |
| $D$ | Rod diameter |
| $E$ | Young's modulus |
| $E_b$ | Bending strain energy |
| $E_L$ | Longitudinal strain energy |
| $F$ | Force (subscript 0, initial deceleration force) |
| $f_B$ | Frequency (bending wave) |
| $f_L$ | Frequency (longitudinal wave) |
| $f_r$ | Frequency (ring) |
| $I$ | Moment of inertia |
| $k$ | Wave number |
| $L_r$ | Drill rod length |
| $L_p$ | Piston length |
| $M$ | Bending moment |
| $m$ | Mass of drill rod |
| $Q$ | Longitudinal stress wave exponential decay constant |
| $q$ | Wavelength (longitudinal wave in triangular approximation) |
| $R$ | Radius of curvature of drill rod |
| $R_0$ | Room constant |
| $r$ | Drill rod radius |
| $S_f$ | Longitudinal stress wave form modification factor |
| $T$ | Cycle time of the stress wave form |
| $t$ | Time |
| $u$ | Radial surface velocity |
| $u_b$ | (Peak) radial surface velocity due to bending wave - (Spatial peak) |
| $u_L$ | (Peak) radial surface velocity due to longitudinal wave |
| $u_0$ | (Peak) radial surface velocity due to bending wave - (Time and spatial peak) |
| $u_{rL}$ | RMS surface velocity due to longitudinal stress |
| $u_{rb}$ | RMS surface velocity due to bending stress |
| $V$ | Axial particle velocity (subscript r, rod; subscript p, piston) |
| $V_0$ | Piston impact velocity |
| $y$ | Lateral deflection of rod/beam |
| $y_0$ | Initial deflection of rod/beam |
| $\bar{\alpha}$ | Average absorption coefficient |
| $\omega$ | Angular velocity |
| $\rho$ | Mass density |
| $\varepsilon$ | Axial strain |
| $\varepsilon_0$ | Peak radial strain in both time and space |
| $\varepsilon_r$ | Radial strain |
| $\varepsilon_b$ | Peak bending strain in space |
| $\nu$ | Poisson's ratio |
| $\lambda_B$ | Wavelength (bending wave) |
| $\sigma$ | Stress |
| $\sigma_0$ | Initial peak stress (at instant of impact) |
| $\sigma_{mL}$ | Peak longitudinal stress |
| $\sigma_{mb}$ | Peak bending stress |
| $\tau$ | Rise time of a longitudinal stress wave |

# 1. INTRODUCTION

This report describes the results of a study on drill rod vibrations and the noise they generate. The work was undertaken as part of a comprehensive program to investigate techniques that will lead to the production of stoper drills with an overall noise level of 90 dBA or less. Volume 1 of the study, *Evaluation of Design Concepts*, issued in March 1977, includes a discussion of the overall problem and the techniques investigated to reduce drilling noise.

As part of the study described in Volume 1 a prototype stoper drill was built that drilled at rates comparable to those of a normal stoper but in which the noise levels were reduced from around 115 dBA to 96 dBA 1 meter away from the drill. Drill rod vibrations were the major source of noise in the prototype drill, with a noise level around 107 dBA. To reduce the radiated noise to 96 dBA, the drill rod was enclosed within a tubular member small enough to enter the drill hole with the bit. The technique was demonstrated to be a practical means of reducing the noise levels from the rod vibrations and it is expected that further developments will take place along these lines.

The scope of the study reported here was to investigate the nature of the two kinds of stress waves that are generated in drill rods, bending and longitudinal waves, and how they generate noise. Acoustic theory has been kept to a minimum and, because the majority of the measurements have been taken in "near" field conditions, where the sound field is extremely complex, no attempts have been made to correlate the noise levels with vibration amplitudes.

The report is laid out in three main sections. Section 2 provides background information. Section 3 deals in detail with the nature of longitudinal and bending waves in drill rods and the surface motions associated with them. Section 4 discusses the relative contribution of bending and longitudinal waves to noise generation and describes the effects of design features such as chuck clearance and the use of rubber collars. The report concludes with a section on the implications of the study in regard to future drill designs.

As part of the study, equipment was assembled to record longitudinal and bending waves, surface acceleration levels and sound pressure levels. Full details are given in Appendix A.

## 2. BACKGROUND

Many studies (e.g. Beiers 1966, Pretlove 1969, Summers and Murphy 1974, Visnapuu and Jensen 1975) have shown that the major source of mechanical noise in pneumatic drills and breakers is the ringing of the drill steel or moil. Noise levels on the order of 110 dBA at 1 meter have been reported by these workers and were confirmed by the studies reported in Volume 1.

The noise radiating from the drill rod contributes roughly 12% of the total noise power (Holdo 1958), and for a typical stoper drill represents 0.02% of the total power transmitted through the drill rod. Drill rod noise is generated by Poisson's ratio expansions and contractions of the rod as the longitudinal waves travel up and down it and by transverse rod motions induced by bending waves. The stress waves are generated by the impact of the piston on the end of the drill rod, by bit/rock impact, and by the impact of the drill rod collar on the shank. The longitudinal waves effectively transmit the impact force of the piston to the bit and are essential to the drilling process, while the bending waves, which result from non-centralized impact, worn chucks and rods, and bent drill rods, serve no useful purpose.

Drill rod noise and possible practical means for reducing it were discussed briefly in Volume 1:

1. Match the bit/rock stiffness to the stress wave form to ensure that as much energy as possible is used for rock breaking and a minimum amount is left in the rod to "ring."

2. Design a drill rod/bit assembly that will rapidly damp out the residual stress waves between impacts.

3. Design a chuck and drill rod shank which will minimize the generation of bending waves.

4. Isolate the drill rod collar from the drill rod to reduce the secondary stress waves generated in the rod by chuck/collar impacts.

5. Damp the transverse drill rod vibrations by coating the drill rod.

6. Shroud the drill rod to attenuate the noise which radiates from its surface.

The approach taken in developing the prototype L-47 quiet drill described in Volume 1 was to shroud the drill rod. However, to further develop this or any other concept it is first necessary to have a clear understanding of the basic nature of the problem. At the conceptual stage of the study it was thought that if the noise levels could be correlated with the wave form and stress amplitudes of the longitudinal stress waves, which contain the bulk of the impact energy, then it might be possible to

optimize these parameters to minimize the radiated noise. However, early in the investigation it was found that the noise levels from the bending waves far surpass those from the longitudinal waves, even with relatively low bending wave energies. Thus a large part of the study has been concerned with understanding the behavior of bending waves in drill rods and making tests to determine how they generate noise.

A considerable amount of time has been spent reviewing acoustical theory to determine how best to model the drill rod so that the sound field of the vibrating rod can be predicted. However, the region of interest, within 1 meter of the drill rod, is within the "near" field where waves from different parts of the body interact to a degree that makes the theory inexact and too complicated for ready application. Thus, while we have attempted to present our results in a form that might be useful to acoustic theoreticians we have not attempted to either model the drill rod or derive radiation efficiencies.

The test program undertaken as part of the study entailed impacting drill rods within a reverberant room and in free field conditions and making frequency and amplitude measurements of the bending waves, longitudinal waves, surface accelerations and radiated sound pressure levels. While the single impact test setup bears resemblance to a drilling situation there are three major differences which prevent direct application of the test data: first, in drilling, impacts are repeated at roughly 30 Hz; secondly, the ends of the rod are captured, either in the drill machine or the drill hole; and finally, the rod rotates at around 200 rpm.

## 3. STRESS WAVES IN DRILL RODS

The two most important stress waves generated in drill rods are longitudinal and bending waves. Torsional waves also exist but their amplitude is usually low and they contribute little to drilling rate or noise level.

Nearly all the published work on drill rod stress waves is concerned with the generation of longitudinal waves, which are primarily responsible for driving the bit tip into the rock to advance the drill hole. Bending waves arise only because of imperfections in the drill design or overthrusting, and as they make no contribution to the drilling rate they are usually of little interest in rock drilling studies. However, as the particle motion in bending waves is transverse to the rod axis they contribute greatly to noise generation and as such justify detailed study.

Stress waves in drill rods are usually measured using electrical resistance strain gauges bonded to the surface of the drill rod with their axes parallel to that of the rod. To measure the longitudinal waves, which produce a uniform strain across the rod cross section, gauges are mounted on opposite sides of the rod and coupled in series. Using this technique any bending stresses are canceled out and only the longitudinal strains are picked up. To measure the bending waves, two gauges, again mounted on opposite sides of the rod, are coupled into opposite arms of a bridge setup so that only the strain difference in the plane of the gauges is picked up. Full details of the techniques are given in Appendix A.

## 3.1 Longitudinal stress waves

The generation of longitudinal stress waves in drill rods has been studied by many workers and is well understood. The reader is referred to an excellent review of the subject by Hustrulid and Fairhurst (1971-72).

When the drill machine's piston strikes the drill rod shank the kinetic energy of the piston is transferred to the drill rod as a stress wave of speed $C_s$:

$$C_s = \sqrt{E/\rho} \tag{1}$$

where $E$ is the modulus of the rod material and $\rho$ is the mass density. In engineering units $C_s = 2\times10^5$ in./s.

The particle motion in the wave is along the rod axis and the energy is stored in equal parts, half as strain energy and half as kinetic energy. The energy transfer efficiency, impact energy to longitudinal stress wave energy, is typically around 95% (Arndt 1960, Hawkes and Chakravarty 1961). For machines of the stoper class, the stress wave duration is typically 400 microseconds, and a rod 3½ ft long or longer can contain all of the longitudinal stress wave energy before the head of the wave returns to the impact point. The energy not transferred is either lost as bending wave energy or retained in the piston as rebound energy. In worn or poorly designed machines a larger percentage of the energy appears in the bending wave energy but only limited data are available to quantify the relative energy levels with reference to the machine design or wear parameters.

The initial stress level amplitude $\sigma_0$ generated in the drill rod by piston impact is a function of the impact velocity $V_0$ and the cross-sectional areas of the drill rod ($A_r$) and piston ($A_p$).

It is well known that the relationship between particle velocity $V$ and stress $\sigma$ in a stress wave is given by

$$\sigma = \rho C_s V. \tag{2}$$

At the instant of impact, the interface velocity is equal to the particle velocity in the rod, and thus the particle velocity in the piston can be obtained by equating the forces across the interface:

$$V_r = \frac{V_0 A_p}{A_p + A_r}, \quad V_p = V_0 - V_r. \tag{3}$$

The initial impact stress $\sigma_0$ is given in terms of the area ratio $A_{ra}$ and impact velocity $V_0$ by:

$$\sigma_0 = C_s \rho V_0 \frac{A_{ra}}{1+A_{ra}}. \tag{4}$$

In engineering units,

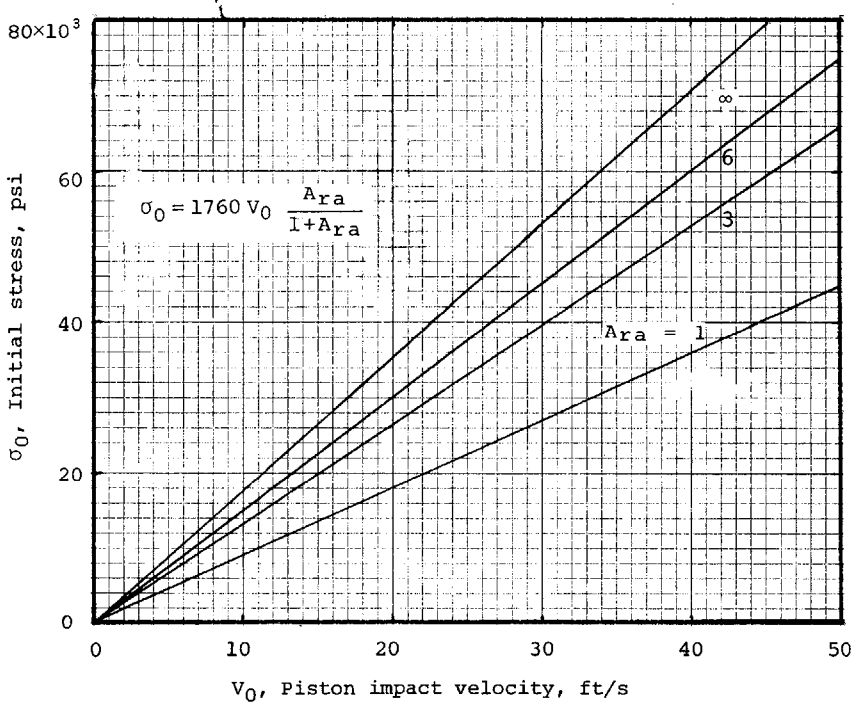


*Figure 1. Initial longitudinal stress levels in a drill rod.*

$$\sigma_0 = 1760\, V_0 \frac{A_{ra}}{1+A_{ra}} \qquad (5)$$

where $A_{ra} = A_p/A_r$ and $V_0$ is in ft/s and $\sigma_0$ in psi.

Figure 1 shows the initial impact stress of the drill rod as a function of piston velocity, calculated using eq 5. For an impact velocity of 30 ft/s, the stress rises from around 27,000 psi to 53,000 psi as the piston/drill rod area ratio varies from 1 to ∞. The area ratios for the L-47 piston* hitting $^7/_8$-in. and 1-in. hexagonal rods are 2.4 and 1.9 respectively. In practice, the peak stress levels will be higher than those shown in Figure 1 because of the non-uniform area of the piston. As discussed in Volume 1, the impact velocity of the drill piston is typically limited to around 35 ft/s to limit the stresses to around 35,000 psi and avoid excessive piston and drill rod breakage.

The length and shape of the stress wave are complicated functions of the piston shape and dimensions and drill rod diameter, and are best obtained by numerical techniques. A computer program to enable this to be done for any piston and drill rod configuration and bit/rock stiffness has been developed by Joy Manufacturing Co. based on a program originally written by Dutta (1968). Essentially, the program follows the numerous wave reflections in both the piston and drill rod and predicts the stresses existing at any point in these components at any time. Figure 2 shows theoretical longitudinal stress waves generated in $^7/_8$-in. and 1-in. drill rods by the piston of the L-47 drill impacting at 30 ft/s. Many workers have shown close correlation between predicted and measured longitudinal stress waves in rods. Figure 3a shows the predicted and measured wave

**The L-47 drill described in detail in Volume 1 is typical of rifle bar drills.*

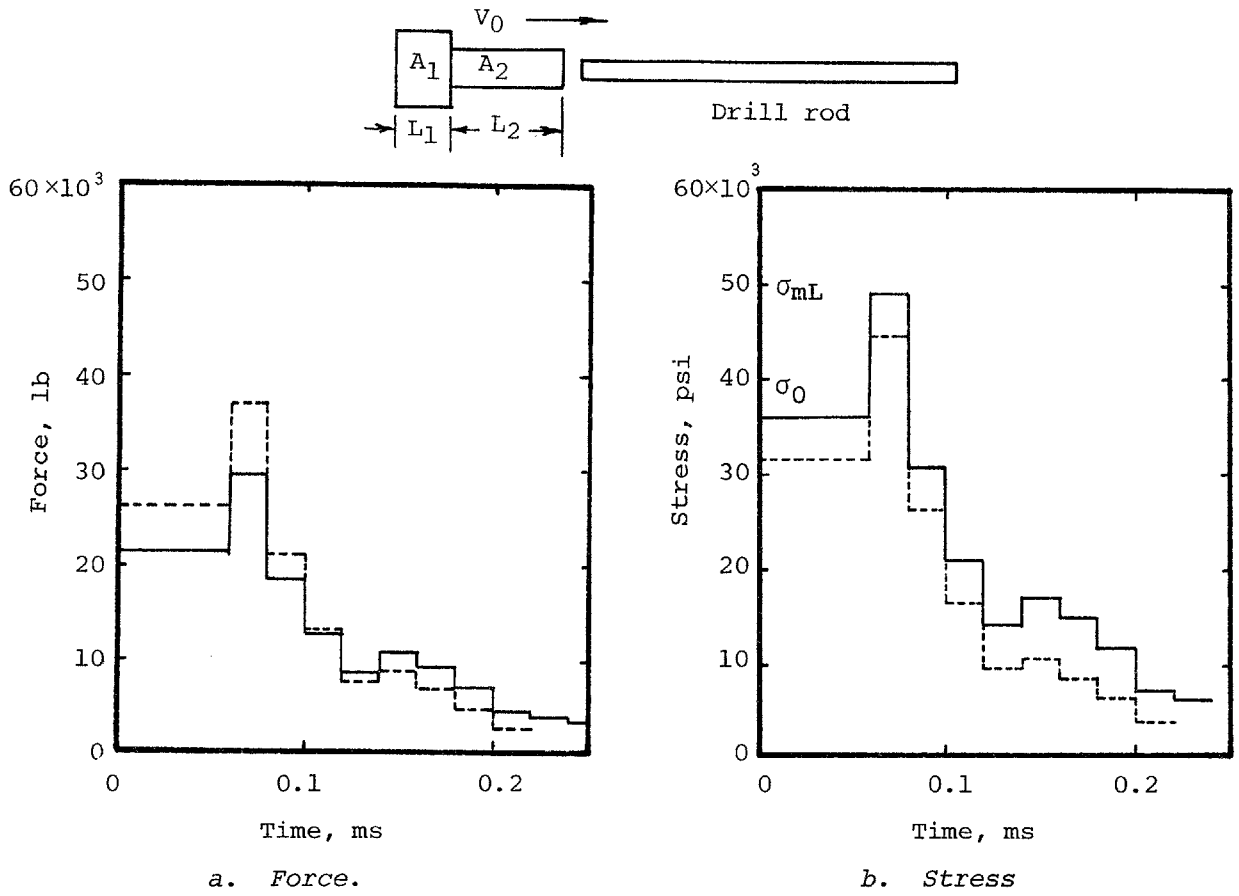


*a. Force.* *b. Stress*

*Figure 2. Initial longitudinal stress wave forms generated in 1-in. (dashed line) and $^7/_8$-in. (solid line) hexagonal drill rods by the Joy L-47 piston. L-47 piston, mass = 4 lb, $A_1$ = 3.63 in.$^2$, $A_2$ = 1.15 in.$^2$, $L_1$ = 2 in., $L_2$ = 6 in., $V_0$ = 30 ft/s.*

forms in a $^7/_8$-in. hexagonal rod impacted by a 2-in.-diameter piston 6 in. long, obtained during the current study. As might be expected there is some rounding off of the stress discontinuities but in general the shape and amplitude are well predicted. The waves appear as mirror images of each other as the wave oscillates backwards and forwards in the rod under free end conditions, as will be explained later.

Figure 4 shows the longitudinal stress waves generated in a 69.5-in.-long, $^7/_8$-in. hexagonal drill rod by manual impacts with two different hammers, 0.62 lb and 3.76 lb in weight. (For details of the procedures used to obtain these records see Appendix A.) As would be expected, the different hammers generate distinctly different wavelengths and shapes.

An alternative approach to predicting the initial stress levels and wave form in a rod impacted by a piston is to approximate the piston as a simple cylindrical mass. In this case the initial deceleration force $F_0$ on the piston is given by eq 4 as

$$F_0 = \sigma_0 A_r = C_s \rho V_0 \frac{A_{ra}}{1+A_{ra}} A_r. \qquad (6)$$

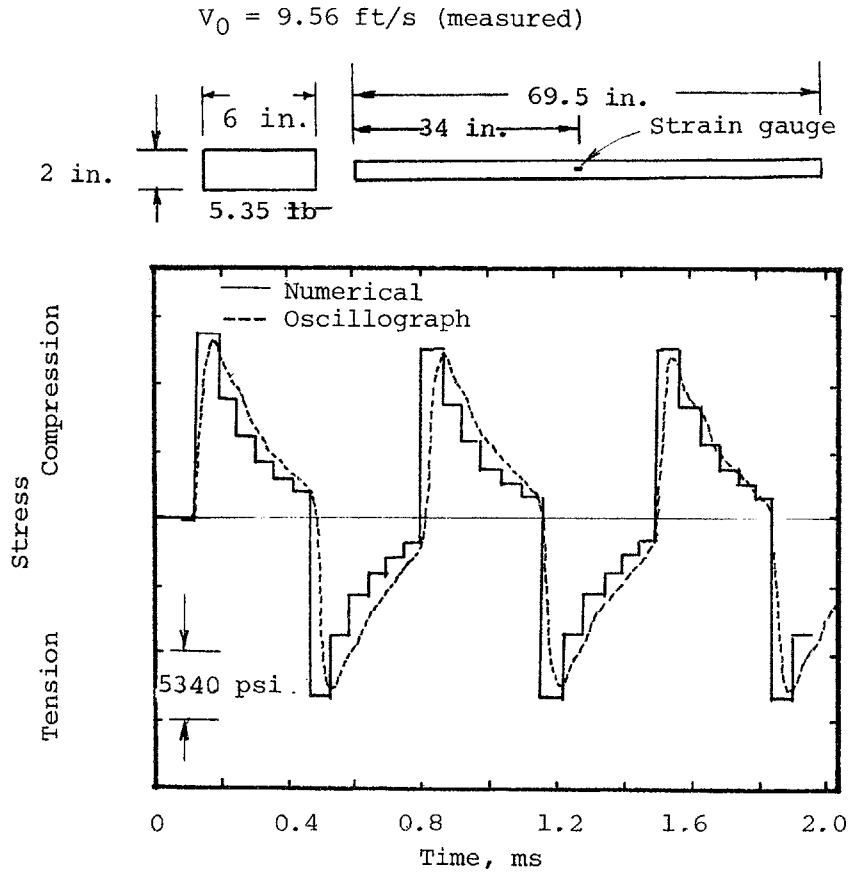


*a. Comparison of numerical prediction and measured stress wave (traced from original oscillograph record).*

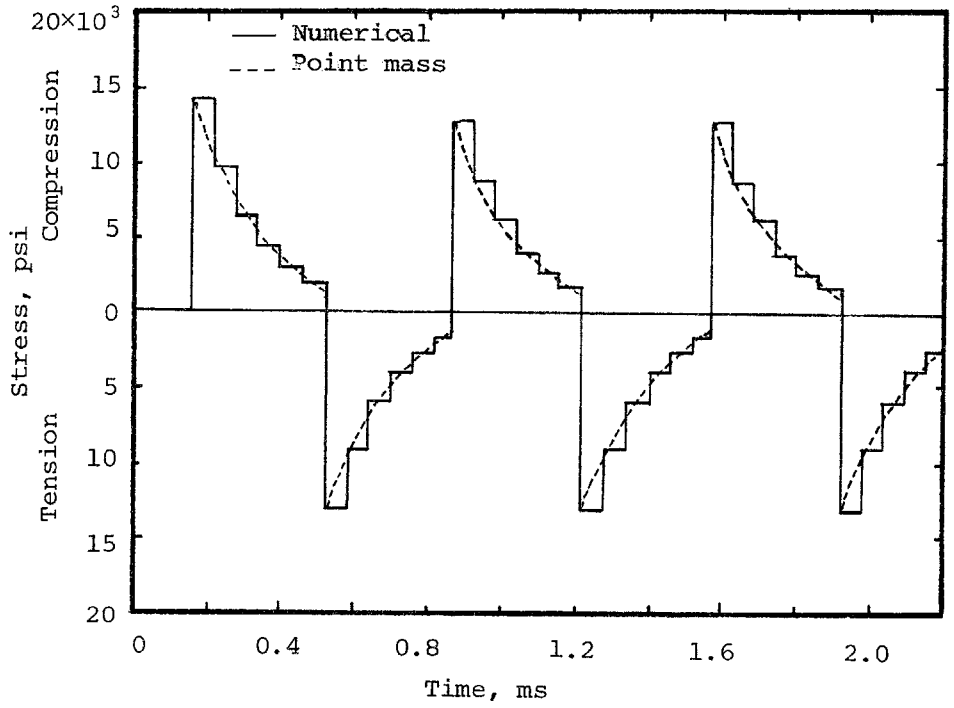


*b. Comparison of numerical and point mass techniques.*

*Figure 3. Predicted and measured longitudinal stress wave forms in $^{7}/_{8}$-in. hexagonal drill rods.*

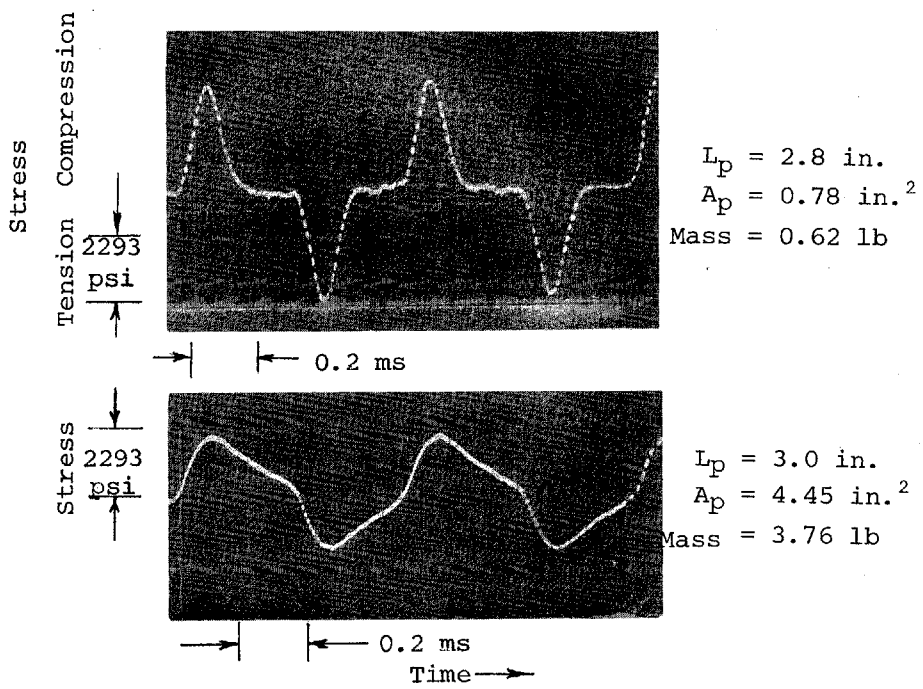


*Figure 4. Longitudinal stress wave forms generated in 69.5-in.-long, $\frac{7}{8}$-in. hexagonal drill rod by different piston masses. (Strain gauges mounted at the center of the rod.)*

This force decreases in proportion to the deceleration of the piston as governed by Newton's Second Law. Thus,

$$C_s \rho V_p A_r = -\rho A_p L_p \frac{dV_p}{dt} \tag{7}$$

where $L_p$ is the length of the piston. The solution to eq 7, using the initial condition prescribed by eq 6, is

$$\sigma = \frac{\rho C_s V_0 A_{ra} e^{-t/Q}}{1+A_{ra}} \tag{8}*$$

where

$$\frac{1}{Q} = \frac{C_s}{L_r(1+A_{ra})} .$$

This approximation is only valid when the piston has a larger diameter than the drill rod and is relatively short. The equation predicts an instantaneous rise to a peak stress followed by an exponential decay. Figure 3b shows the wave form for the impact case discussed earlier (6-in.-long, 2-in.-diameter piston impacting a 1-in.-diameter rod) compared with

** Equation 8 is similar to equations given by Timoshenko (1951).*

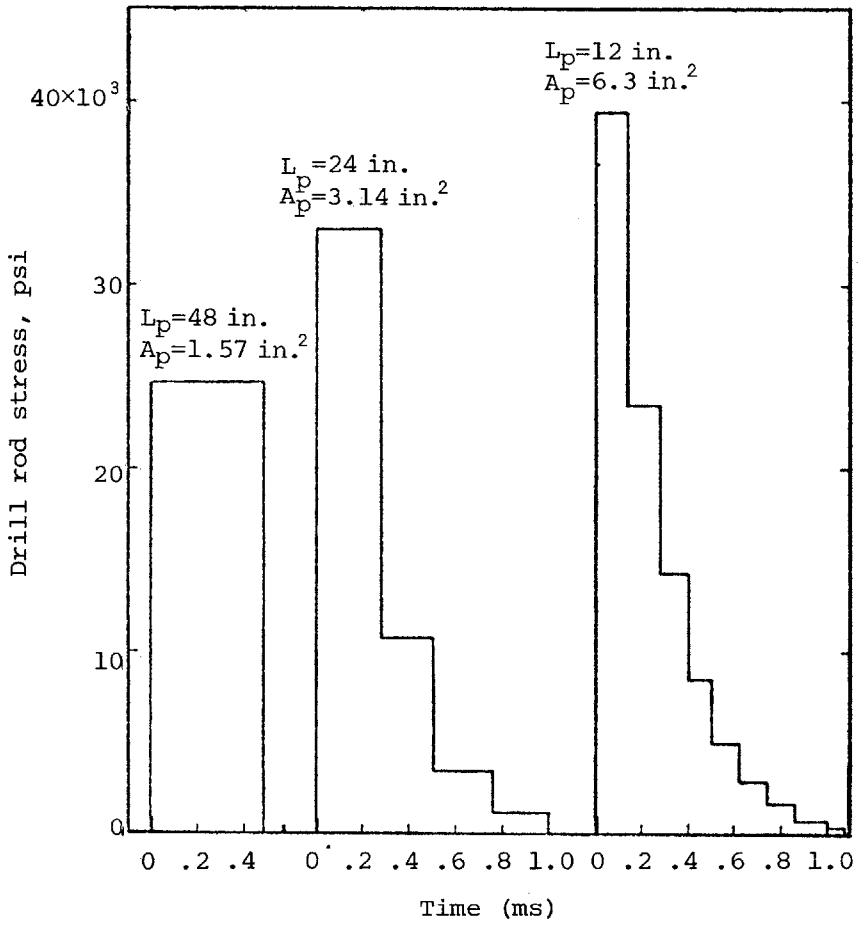


*Figure 5. Theoretical longitudinal stress wave forms generated by three different piston shapes with equal impact energies. Piston mass 21.3 lb, impact velocity 30 ft/s, rod area 1.57 in.$^2$*

the computer-derived wave form. For this particular case either method for calculating the wave form would be acceptable to give the peak stresses and general wave form. However, neither technique will predict the rise time, which is limited by the so called "ring" frequency of the rod $f_r$:

$$f_r = C_s/\pi D \tag{9}$$

where $D$ is the diameter of the rod. The ring frequency is the number of times that a stress wave can travel circumferentially around a drill rod and characterizes the high frequency vibration behavior of the rod.

For a 1-in.-diameter rod the ring frequency is 64 kHz. Fourier transform methods could possibly be used to predict the rise time but further analysis along these lines is beyond the scope of this report. Further discussion on rise time in relation to the radial surface velocity is given later in Section 3.2.

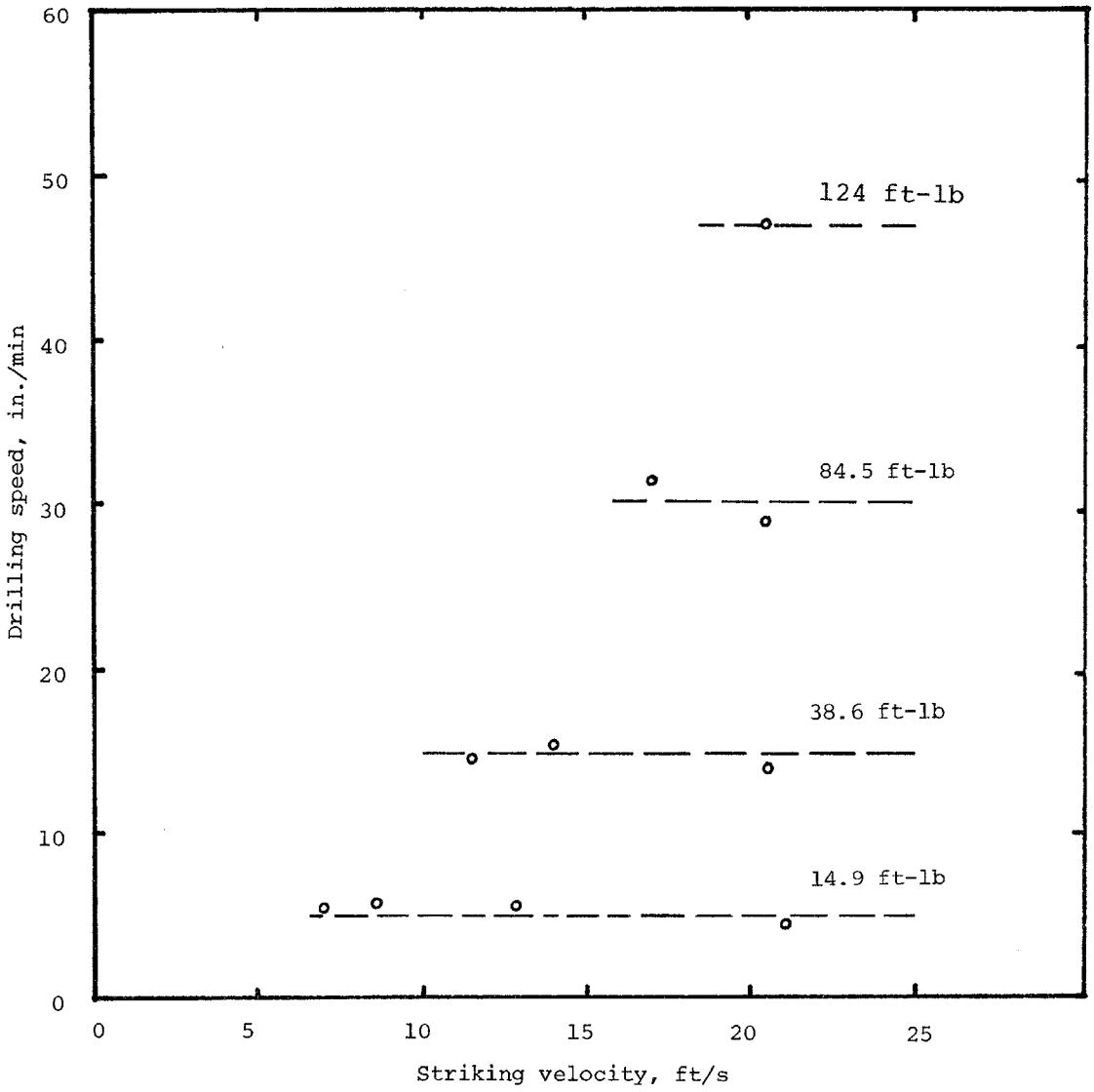


*Figure 6. Predicted drilling speeds versus striking velocity for constant blow energy drills (Barre granite, 1.5-in. 115xCS4 carset bit). (Shepherd 1954.)*

As discussed earlier, the piston's impact energy can be transmitted along the drill rod in a variety of wave forms, depending on the mass and shape of the piston and the piston/rod area ratios. As an example, Figure 5 shows the theoretical wave forms generated in drill rods by three differently shaped pistons, all having the same mass and impact velocity. Despite the large differences in peak stress levels and wavelength it is generally considered that the most important characteristic of the longitudinal stress wave relative to drilling rate is its total energy rather than the stress wave form. Figure 6 (after Shepherd 1954) shows the results of crater volume/blow energy tests which in general validate this conclusion.

Proper tuning of a drill system to a particular rock is well known to be effective, and theoretically wave shaping at constant energy can increase drilling rate. However, the effect of wave shaping is clearly secondary to total energy as a factor determining drilling rate. The design factors which determine the shape and amplitude of the stress wave, i.e. piston shape, mass and impact velocity, have been discussed in detail in Volume 1. Relative to noise generation, at the current stage of drill development there is no justification for radical changes in design philosophy solely for the purpose of shaping the longitudinal wave, particularly in view of the fact that the bending waves generate a large percentage of the noise radiating from the drill rod, as will be shown later.

Once the stress wave has been formed it travels along the drill rod until it reaches the bit/rock interface. Passage of the stress wave displaces the drill rod in the direction of the interface. As the drill bit moves into the rock a reaction force is generated and energy is taken from the wave to break out chips. Initially, the force required to drive the bit tip into the rock is lower than the force capability of the stress wave, so energy is reflected back from the rock as a tensile stress wave. As penetration continues, the required force eventually increases beyond that available from the stress wave, at which point the remaining portion of the incident compression wave is reflected as a compression wave. Thus the composite stress wave reflected from the bit/rock interface has a tensile leading edge and a compressive tail. When this composite reflected wave is reflected back from the drill rod shank towards the rock, the stresses are again reversed; the leading edge becomes compressive and the tail tensile.

When the wave which has been reflected back from the shank reaches the bit/rock interface, the compressive leading edge drives the bit still further into the rock. Penetration ceases when the force level required to drive the bit further is more than that available in the wave, or when the tensile tail of the wave reaches the interface. When this latter event occurs, the bit jumps away from the rock and the tensile tail of the incident wave is reflected completely as a compressive wave. For typical bit/rock stiffness ($10^5$-$10^6$ lb/in.) and typical stress wave forms, further penetration usually ceases after the second wave reflection and the drill rod bounces back. In practice this action is made more complicated by the fact that the bit does not penetrate smoothly, but in a series of jumps as chips are formed.

In analyzing the behavior of the drill rod during the passages of the longitudinal wave it must be remembered that reflected waves of opposite sign to the initial wave tend to cancel each other, while waves of the same sign add to the initial wave. Thus, nearly every point in the drill rod experiences different stresses after passage of the initial wavefront. The net stress levels become complicated to analyze after several reflections and the computations are best handled by computer. As an example of the type of behavior to be expected, Figure 7a shows the theoretical longitudinal stress waves at four different positions in 4-ft-long drill rods drilling into rock with a bit/rock stiffness of $1.5\times10^5$ lb/in.

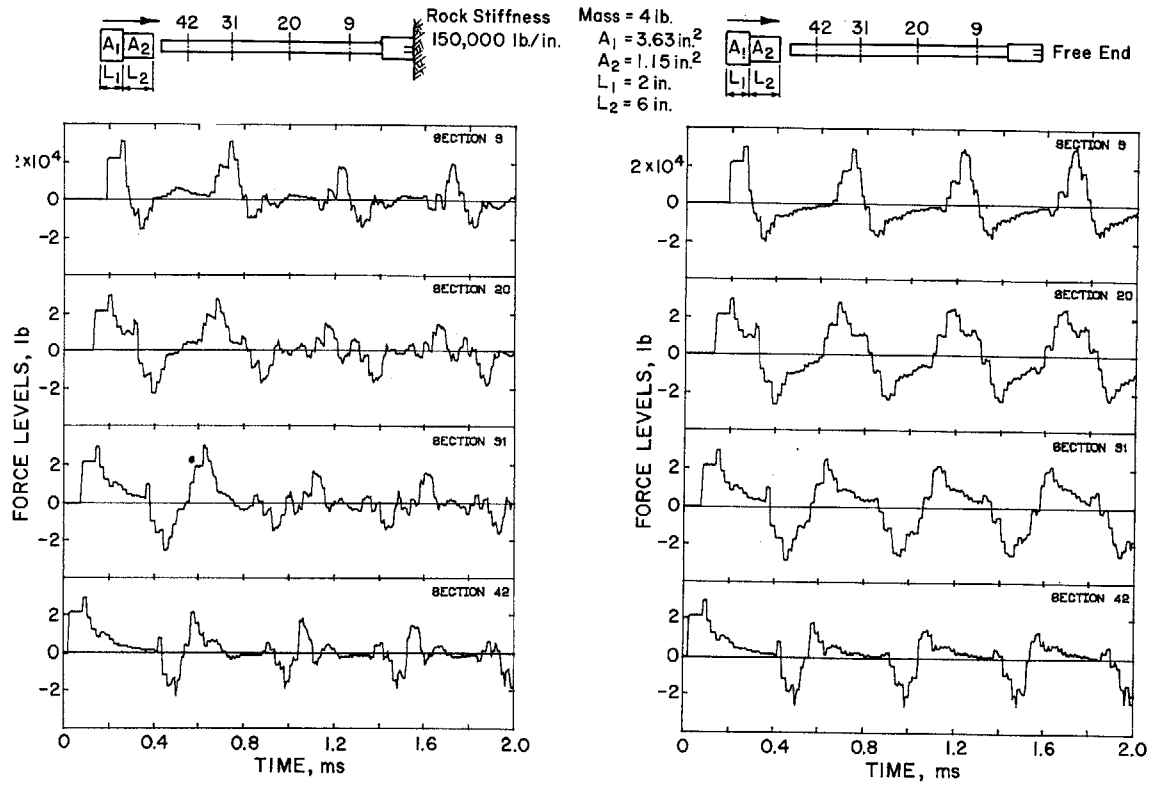


*a. Force wave forms in a rod drilling into rock.*

*b. Force wave forms in a drill rod with free end.*

*Figure 7. Theoretical net longitudinal forces on a $^{7}/_{8}$-in. hexagonal drill rod (piston mass 4 lb, impact velocity 30 ft/s, rod length 48 in.).*

After the rod has bounced from the rock it vibrates freely under the action of the residual stress wave energy left in the rod. This action is clearly shown in Figure 7a: after the first two waves, initial and first reflection, the wave form remains roughly constant and no further energy is removed from it. For comparison, Figure 7b shows the same initial stress wave in a rod with a free end condition (no rock present). In this latter case no energy has been removed from the wave and the wave form remains virtually unchanged during the numerous reflections.

From the above discussion and examples it will be apparent that even in these idealized examples it is difficult to predict the form of the longitudinal stress wave after the passage of the initial wave. In practice, the situation is rendered far more complicated by the additional impacts that take place between the chuck and collar and also between the bit and rock when the machine thrust again brings the bit back to the rock. To further complicate the situation, if the energy is not removed from the drill rod prior to the next blow, then the stress levels can rise to three times the level produced during a single blow (Hawkes and Chakravarty 1961).

The round trip time along the drill rod is $2L_r/C_s$ where $L_r$ is the length of the drill rod, so a spectrum analysis of the wave form produces

discrete peaks at frequency multiples of $C_s/2L_r$:

$$f_L = n \frac{C_s}{2L_r}, \quad n = 1, 2, 3... \tag{10}$$

## 3.2 Surface velocities in longitudinal stress waves

The important characteristic of the stress wave in relation to its noise-generating capability is the surface motion associated with the passage of the wave. Sound pressure in the plane wave approximation is proportional to particle velocity except in the so called "near" field where the low frequency pressure fluctuations tend to be proportional to acceleration. Most drill rod noise is at high frequencies (above 1000 Hz) and the most important surface motions characteristic of a drill rod relative to noise generation are the out-of-plane velocities. There are two sources of noise, radial motions of the drill rod surface and axial motions of the rod ends.

The particle motion in a longitudinal stress wave is predominantly axial, as discussed earlier, with Poisson's ratio expansion and contraction producing the radial surface motions. The axial particle velocity is given by eq 2:

$$V = \sigma/C_s\rho$$

or in engineering terms,

$$V = 6.82\times10^{-3}\sigma$$

where velocity $V$ is in in./s and stress $\sigma$ is in psi. The passage of the longitudinal wave produces a traveling bulge in the rod due to Poisson's ratio expansion, and the radial velocity associated with this bulging motion generates noise.

The radial strain $\varepsilon_r$ associated with the longitudinal strain $\varepsilon$ is given by

$$\varepsilon_r = \nu\varepsilon = \nu\sigma/E \tag{11}$$

and the surface displacement $y$ is given by

$$y = \int_0^{D/2} \varepsilon_r \, dr = \varepsilon_r \frac{D}{2} = \frac{\nu\sigma D}{2E}. \tag{12}$$

The radial surface velocity $u$ is the time rate of change of surface displacement:

$$u = \frac{dy}{dt} = \frac{\nu D}{2E} \frac{d\sigma}{dt}. \tag{13}$$

Figure 8 shows the radial surface velocity as a function of time calculated from the measured longitudinal stress wave produced by a 6-in.-long, 2-in.-diameter piston impacting a $^7/_8$-in. hexagonal rod.

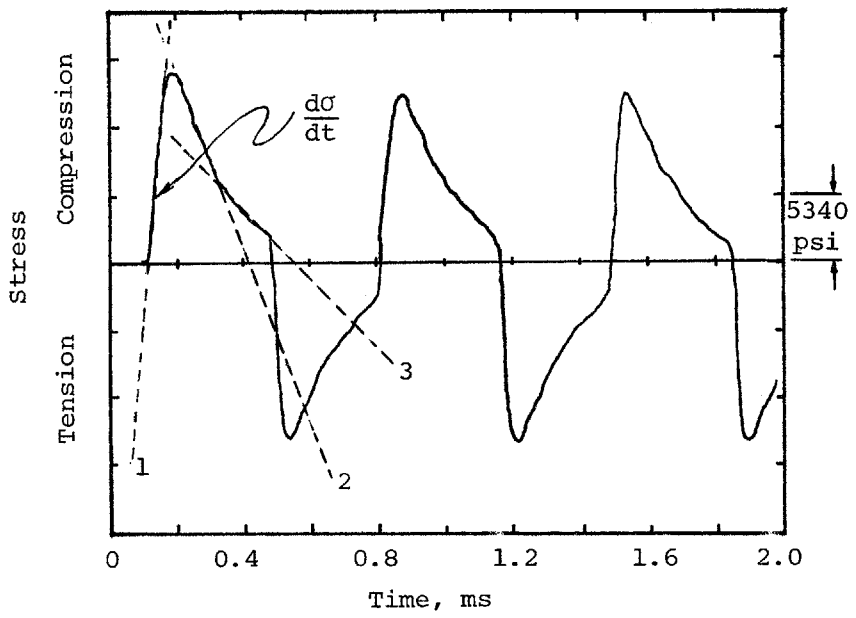


*a. Longitudinal stress wave form approximation.*

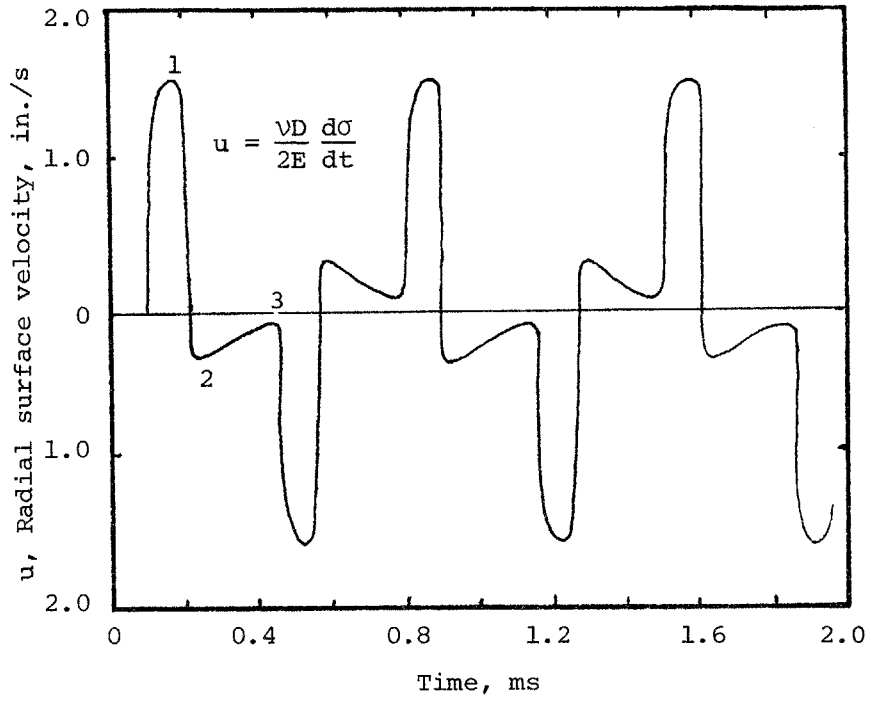


*b. Radial surface velocity calculated from slopes 1, 2 and 3 of the longitudinal stress wave.*

*Figure 8. Radial surface velocity due to longitudinal stress waves in 69.5-in.-long, 7/8-in. hexagonal drill rod. (Piston mass 5.35 lb, diam 2 in., length 6 in.; $V_0$ = 9.56 ft/s.)*

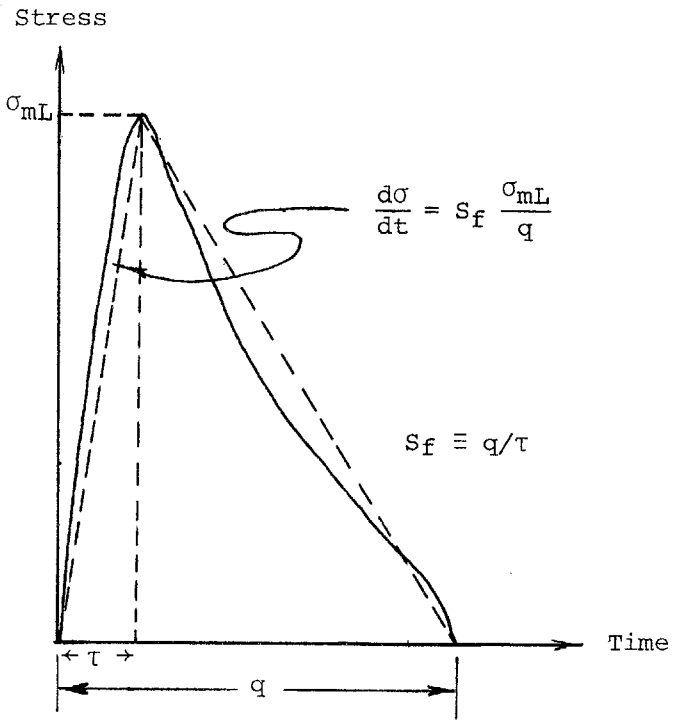


*Figure 9. Triangular approximation of stress wave form.*

From eq 13 it will be noted that the peak radial velocity is determined by the rise time of the stress wave. As discussed earlier, the simple theory which predicts the wave forms reasonably well fails to acknowledge the finite rise time and thus gives infinite radial velocities for the initial portion of the stress wave. An alternative approach is to approximate the wave form to a triangular shape defined by constant $S_f$. Referring to Figure 9, the initial rate of change of stress is given by

$$\frac{d\sigma}{dt} = S_f \frac{\sigma_{mL}}{q} . \tag{14}$$

Thus eq 13 can be used to calculate the peak radial velocity due to the passage of the longitudinal stress wave,

$$u_L = \frac{\nu D}{2E} S_f \frac{\sigma_{mL}}{q} \tag{15}$$

where $u_L$ is the peak radial velocity and $\sigma_{mL}$ is the peak longitudinal stress. The factor $S_f$ is obtained experimentally and varies from 4 to 8, depending upon blow energy.

In addition to the surface motion of the rod periphery, significant motions can take place at the rod ends when they are in a free condition. At a free interface the particle motion is double that which exists in the main body of the drill rod because here the strain energy in the rod is converted into kinetic energy. Thus in a drill rod freely vibrating

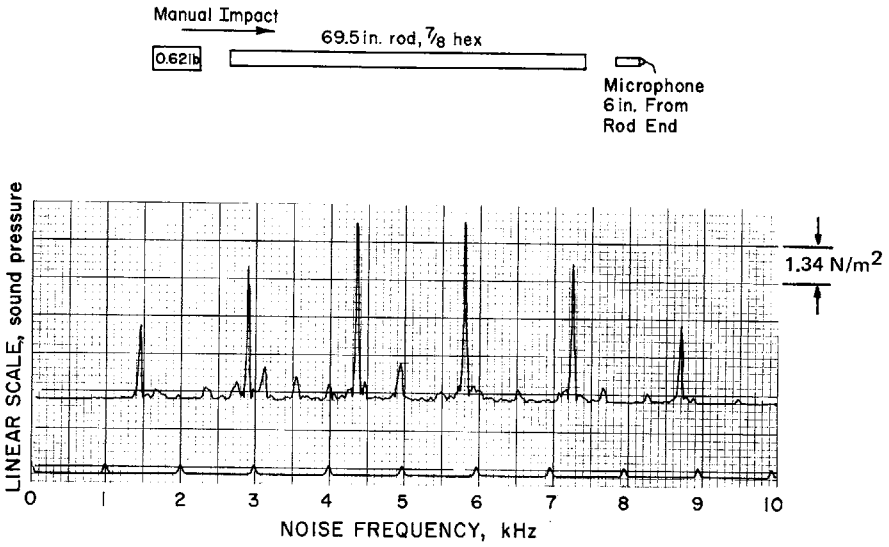


*a. End of drill rod.*

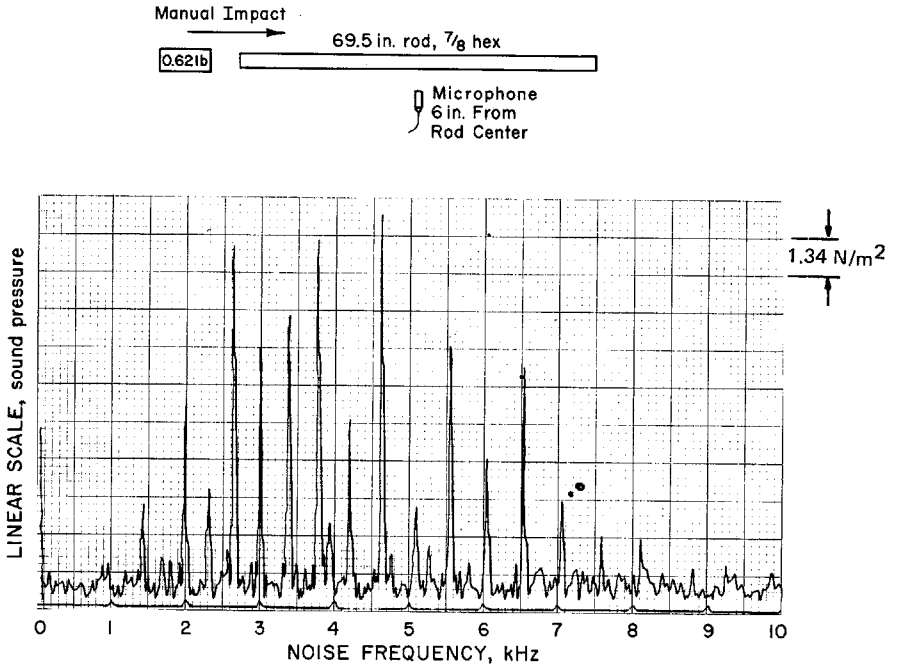


*b. Side of drill rod.*

*Figure 10. Noise frequency spectra records at the end and side of a drill rod.*

under the action of longitudinal waves, the two ends act as point noise-radiating sources with the peak surface velocity given by

$$u = 2\sigma_{mL}/(\rho C_S). \tag{16}$$

Figure 10 shows the noise spectrum for identical manual impacts on a drill rod end with the microphone mounted 6 in. from the rod end and 6 in. from the side of the rod. The noise spectrum at the end of the rod shows

the major frequency peaks coinciding with those of the longitudinal waves, while the noise spectrum at the side of the rods coincides with that of the bending wave, as will be discussed later. Note that the surface velocity of the ends is much greater than the radial surface velocity due to the bulging of the drill rod under the passage of the longitudinal wave.

Except when collaring, the noise radiating from the drill rod ends is not considered to be a major problem as the bit is enclosed by the rock and the impact end is enclosed by the drill chuck and body.

## 3.3 Bending waves

Bending waves in drill rods are extremely complicated and are not well understood. They cause the rod particles to vibrate transversely to the rod axis, and for comparable stress amplitudes are much more significant noise sources than longitudinal waves.

As discussed earlier, during the passage of a longitudinal stress wave, the complete cross-sectional area of the drill rod is subjected to a uniform stress and displacement. After the wave has passed, the rod is at rest and stress-free. The situation is quite different in the case of bending waves. Once the initial wave front has passed a point on the rod, that point then stays in motion until the wave is completely damped out, and the stresses are constantly changing, not only in time and with axial position but also across the rod section.

The theory for bending waves is developed in many sources, notably Cremer et al. (1973), Morse and Ingard (1968) and Harris and Crede (1976), upon which the following discussion is based.

The thin beam equation is well known:

$$M = EI \frac{d^2y}{dx^2} . \tag{17}$$

Differentiating twice, and setting $-d^2M/dx^2$, which is the rate of change of shear force with distance, equal to the acceleration of the rod per unit length, $\rho A_r(d^2y/dt^2)$, eq 17 becomes the bending wave equation:

$$\frac{d^4y}{dx^4} = - \left(\frac{\rho A_r}{EI}\right)\left(\frac{d^2y}{dt^2}\right). \tag{18}$$

To calculate the wave speed, assume that solutions to eq 18 may be written in the form of a wave, i.e.

$$y(x,t) = y_0 e^{-i(kx-\omega t)} . \tag{19}$$

Substituting the wave form, eq 19, into eq 18 reduces eq 18 to the form:

$$k^4 = \left(\frac{\rho A_r}{EI}\right)\omega^2. \tag{20}$$

The wave speed is defined as the relationship between $x$ and $t$ which keeps the factor $(kx-\omega t)$ constant. Thus

$$C_B = \frac{dx}{dt} = \frac{\omega}{k}.$$

The role of $k$, the wave number, is analogous in space to the role of $\omega$, the wave circular frequency in time. For instance, $k$ is related to wavelength just as $\omega$ is related to wave period, and it is convenient to conceptualize $k$ as spatial frequency. Substituting for $k$ using eq 20 and solving for $C_B$, the bending wave speed becomes

$$C_B = \sqrt{\omega}\left(\frac{EI}{\rho A_r}\right)^{1/4}$$

$$= \sqrt{(\pi/2)(Df_B C_S)} \qquad \text{(for round rods)}. \tag{21}$$

It will be noted from eq 21 that the bending waves exhibit dispersion. The wave speed is not constant; the higher frequency components travel faster than the lower frequency ones according to the square root of frequency. This effect can be clearly observed in the bending wave records shown in Figure 11 (after Roberts et al. 1962). In Figure 11 the low frequency components that predominate at the head of the wave for the first 1 or 2 feet of drill rod are rapidly overtaken by the higher frequency components further along the rod. (Compare the wave forms at 6 and 12 in. with those at 60 and 115 in.)

Initially the bending wave contains a broad band of frequencies. After the waves have oscillated up and down the rod, the only frequency components persisting are those which are an integer number of half wavelengths of the drill rod. The change from broad band to discrete standing wave frequencies occurs gradually as the waves are reflected back and forth along the drill rod. However, as shown in Figure 10b, most if not all of the radiated noise is associated with these standing wave vibrations which occur at the drill rod natural frequencies.

The natural frequencies of the rod are calculated from the well known relationship between frequency $f_B$, wavelength $\lambda_B$ and wave speed $C_B$:

$$C_B = f_B \lambda_B.$$

Substituting for $C_B$ from eq 21 leads to the expression:

$$f_B = \frac{\pi D C_S}{2\lambda_B^2}. \tag{22}$$

This expression can be simplified by writing the wavelength in terms of the rod length. Assuming that the ends of the rod are free (more general end conditions will be imposed later), the rod length is an integer number of half wavelengths of the bending wave, or:

$$L_r = n\frac{\lambda_B}{2}.$$

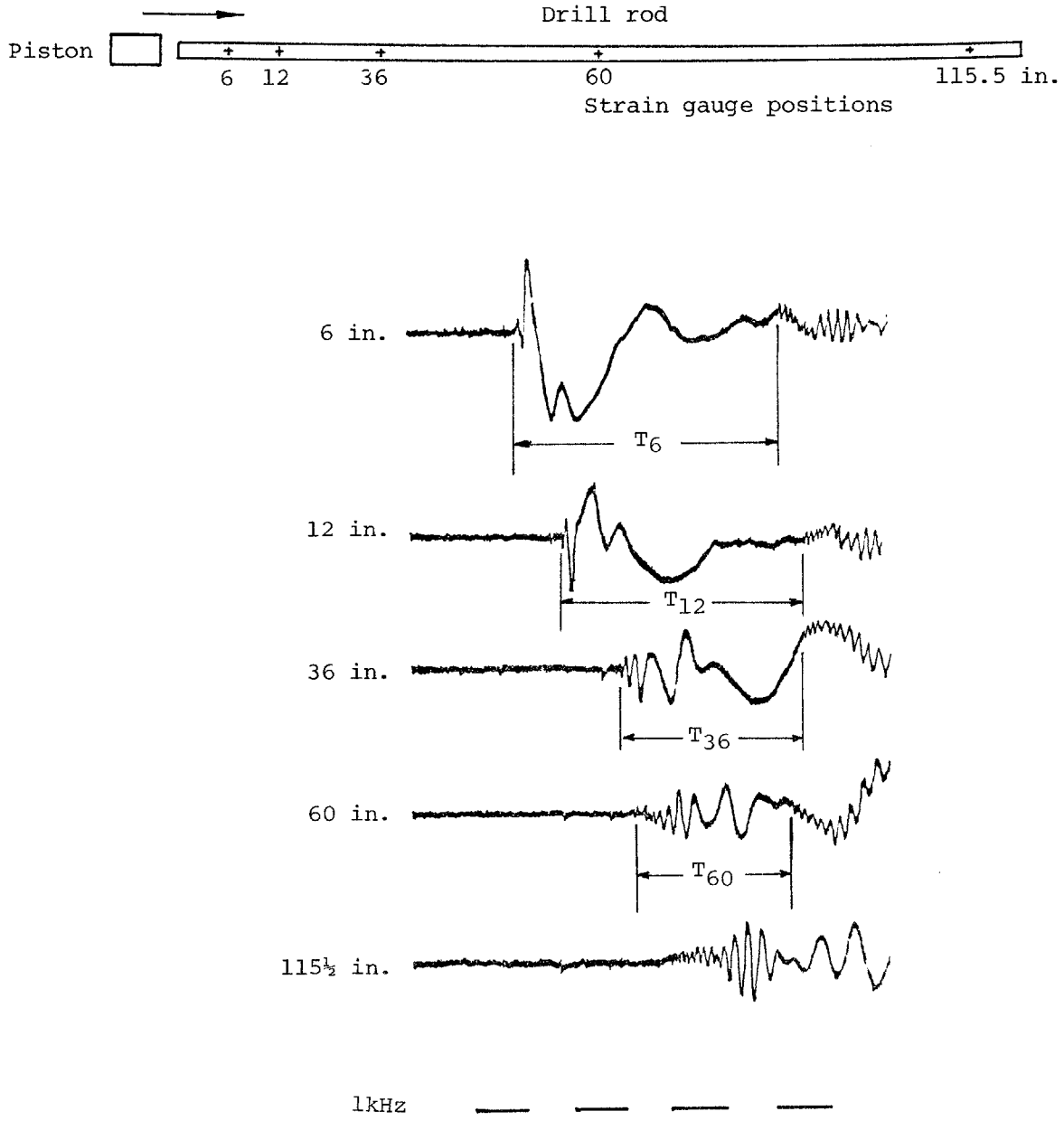


*Figure 11. Bending waves recorded at different positions along a 120-in.-long, 0.742-in.-diam drill rod (1/4 in. offset eccentric impact). Piston mass 2.67 lb, diam 2 in. T = time from wave head to time at which high frequency components occur. (After Roberts et al. 1962.)*

Substituting into eq 22 to eliminate $\lambda_B$ gives:

$$f_{Bn} = \frac{n^2 \pi D C_s}{8 L_r^2}, \qquad n = 1, 2, 3... \tag{23}$$

This equation gives the natural frequencies of a thin beam with free ends in bending. To accurately model drill rods, two correction factors are required: a correction for rod thickness at high frequency and a correction for the end conditions at low frequency.

Equation 23 can be corrected for thickness to include the effects of rotary inertia and shear force using the "Timoshenko beam theory." An approximate expression, valid for circular steel bars, is given in Harris and Crede (1976) as

$$f_{Bn} = \frac{n^2 \pi D C_s}{8 L_r^2} \left[1 - 1.2 \left(\frac{nD}{L_r}\right)^2\right] \quad \text{for } \frac{nD}{L_r} < 0.4. \tag{24}$$

The Timoshenko theory predicts that the rod frequencies will be more closely spaced at high frequency than the simple theory predicts.

The second correction factor, which depends on the end conditions, is summarized in Table 1, derived from Harris and Crede (1976).

Table 1. Correction factors for low frequency bending wave frequencies.

| *End condition** | *H - H* | *C - C* | *C - H* | *F - F* |
|---|---|---|---|---|
| *n* *Correction factor* | *1* | $\left(\frac{2n+1}{2n}\right)^2$ | $\left(\frac{4n+1}{4n}\right)^2$ | $\left(\frac{2n+1}{2n}\right)^2$ |
| 1 (half wave) | 1.0 | 2.25 | 1.56 | 2.25 |
| 2 (full wave) | 1.0 | 1.56 | 1.27 | 1.56 |
| 3 (3/2 wave) | 1.0 | 1.36 | 1.17 | 1.36 |
| 4 | 1.0 | 1.27 | 1.13 | 1.27 |
| 5 | 1.0 | ≃1 | ≃1 | ≃1 |

*Notation: C - clamped; H - hinged; F - free.

The correction factor affects only the lower frequencies of bending vibrations and accounts for the fact that the effective termination of the beam for the bending wave reflection is not precisely at the half wavelength position. For a vibrating drill rod, free-free end conditions apply and eq 24 becomes

$$f_{Bn} = \frac{n^2 \pi D C_s}{8 L_r^2} \left[1 - 1.2 \left(\frac{nD}{L_r}\right)^2\right] \left(\frac{2n+1}{2n}\right)^2. \tag{25}$$

The two multiplication factors are nearly unity over most of the range of interest. In Tables 2 and 3 the predictions of eq 25 are compared with spectrum analysis data for the bending waves in $^7/_8$-in. hexagonal drill rods, 69.5 and 21.9 in. long. It will be noted that all of the frequencies measured can be accurately predicted (to within 3%) from eq 25.

Table 2. Predicted and measured bending wave frequencies for 69.5-in.-long, 7/8-in. hexagonal drill rod. $L_r$ = 69.5 in., $D$ = 0.922 in., $C_s$ = $2 \times 10^5$ in./s

| Number | Frequency $f_B$ (Hz) | | Number | Frequency $f_B$ (Hz) | |
|---|---|---|---|---|---|
| | Predicted (eq 25) | Measured | | Predicted (eq 25) | Measured |
| 1 | 33 | 30 | 15 | 3431 | 3500 |
| 2 | 94 | 90 | 16 | 3861 | 3950 |
| 3 | 183 | 185 | 17 | 4311 | 4450 |
| 4 | 302 | 310 | 18 | 4780 | 4900 |
| 5 | 451 | 450 | 19 | 5266 | 5420 |
| 6 | 628 | 650 | 20 | 5768 | 5950 |
| 7 | 834 | 850 | 21 | 6284 | 6500 |
| 8 | 1068 | 1050 | 22 | 6814 | 7050 |
| 9 | 1329 | 1350 | 23 | 7354 | 7600 |
| 10 | 1618 | 1640 | 24 | 7904 | 8210 |
| 11 | 1932 | 1950 | 25 | 8462 | 8680 |
| 12 | 2271 | 2320 | 26 | 9025 | 8850 |
| 13 | 2635 | 2700 | 27 | 9592 | 9500 |
| 14 | 3022 | 3100 | | | |

Table 3. Predicted and measured bending wave frequencies for 21.9-in.-long, 7/8-in. hexagonal drill rod. $L_r$ = 21.9 in., $D$ = 0.922 in., $C_s$ = $2 \times 10^5$ in./s

| Number | Frequency $f_B$ (Hz) | |
|---|---|---|
| | Predicted (eq 25) | Measured |
| 1 | 339 | 300 |
| 2 | 936 | 1000 |
| 3 | 1814 | 1900 |
| 4 | 2953 | 3150 |
| 5 | 4324 | 4550 |
| 6 | 5891 | 6180 |
| 7 | 7608 | 7950 |
| 8 | 9424 | 9350 |
| 9 | 11279 | -- |

The shear and rotary inertia terms included in eq 25 become appreciable at frequencies near 10 kHz, and at these high frequencies the simple bending wave speed equation, eq 21, no longer applies. The upper limit of bending wave speed is predicted by the shear wave speed, which for steel is 10,400 ft/s. This would correspond to a frequency around 50,000 Hz for a 1-in.-diameter rod, if eq 21 were still valid.

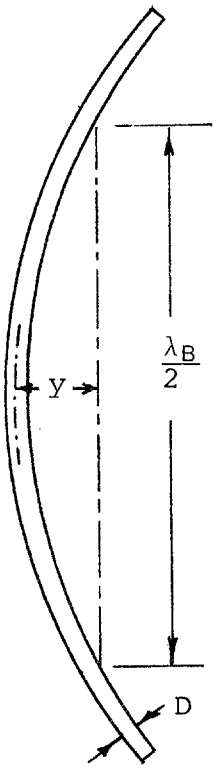


*Figure 12. Rod bending into a circular arc.*

## 3.4 Surface velocities in bending waves

As briefly discussed earlier in Section 3.2 the particle motions which generate noise are those in the radial direction, normal to the drill rod axis, and in bending waves the particle motions are predominantly in this direction.

Strain gauge measurements of bending waves essentially measure the difference in the surface strains between two diametrically opposite surfaces of the drill rod. (See Appendix A for details.) To the best of the writers' knowledge there is no published derivation of the relationship between the bending surface stress and the surface radial velocities.

A simple derivation is presented here which shows that the surface velocities are directly proportional to the bending strains. A more rigorous proof is given in Appendix B.

With reference to Figure 12, consider a wave of length $\lambda_B$ in a rod of diameter $D$, which produces a lateral deflection of the rod $y$ and peak surface strains $\pm \varepsilon_b$.

The radius of curvature of a circular arc of length $\lambda_B/2$ and deflection $y$ is given by the approximate formula, valid for $y$ small compared to $\lambda_B$,

$$R \simeq \left(\frac{\lambda_B}{2}\right)^2 \frac{1}{8y}. \tag{26}$$

It is easy to show that strain on the surface of the rod and in the plane of bending is to a first approximation $+D/2R$ on the outer surface and $-D/2R$ on the inner surface. Thus the surface strain is given by

$$\varepsilon_b = \pm \frac{16Dy}{\lambda_B^2}. \tag{27}$$

Solving eq 27 for $y$ and substituting for $\lambda_B$ from eq 22 gives

$$y = \frac{\varepsilon_b \pi C_s}{32 f_B}. \tag{28}$$

The surface velocity is calculated from the time rate of displacement of the surface assuming that the surface strain varies sinusoidally, i.e. $\varepsilon_b = \varepsilon_0 \cos 2\pi f_B t$, then the derivative of eq 28 gives the surface velocity:

$$u_b = \frac{dy}{dt} = \frac{\varepsilon_0 \pi^2 C_s}{16} \tag{29}$$

or in engineering units

$$u_b = 0.123\varepsilon_0 \text{ in./s} \tag{30}$$

where $\varepsilon_0$, the peak bending strain, is in microstrain units ($10^{-6}$). This very important equation means that *the surface radial velocity is directly proportional to the bending wave strains* as measured by electrical resistance strain gauges.

A more rigorous derivation of eq 29, which does not require the shape to be approximated by a circular arc, is presented in Appendix B. It is shown that the proportionality factor with the more rigorous treatment is 0.10 (in engineering units).

A strain gauge mounted at random on a drill rod measures an unknown quantity relative to peak strain amplitudes, and the readings are best represented as the *spatial RMS* average strain. Assuming the spatial RMS is measured by the strain gauge, the proportionality factor becomes 0.14. These different factors are summarized in Table 4.

Table 4. Relationships between radial velocity and bending strains.

| *Assumed condition* | *Equation* | *Engineering units** |
|---|---|---|
| 1. Circular arc bending | $u_b = (\pi^2/16)C_s\varepsilon_b$ | $0.12\,\varepsilon_b$ |
| 2. Sinusoidal mode bending | $u_b = (1/2)C_s\varepsilon_b$ | $0.10\,\varepsilon_b$ |
| 3. RMS average strain | $u_b = (\sqrt{2}/2)C_s\varepsilon_{rms}$ | $0.14\,\varepsilon_{rms}$ |

* $\varepsilon_b$ is in microstrain units and $u_b$ is in in./s.

## 3.5 Generation of bending waves

Bending wave theory is not sufficiently developed to enable the vibration amplitudes to be calculated from the impact parameters, either for the initial impact or the steady state vibrations. The factors causing bending waves in drill rods have been studied by Roberts et al. (1962) and the results presented by these workers, together with those obtained during the study reported here, represent the bulk of the available data on the subject. The important factors which determine the nature and amplitude of the bending waves in drill rods are piston impact velocity and mass, eccentric impacts induced by chuck wear and malalignment, and rod curvature caused by overthrusting or lack of support for long drill rods.

From data published by Roberts et al. it can be concluded that in a typical airleg-mounted drill in good working order bending stresses of the order of 12,000 psi can be anticipated. These can rise to over 20,000 psi or even greater in a worn machine.

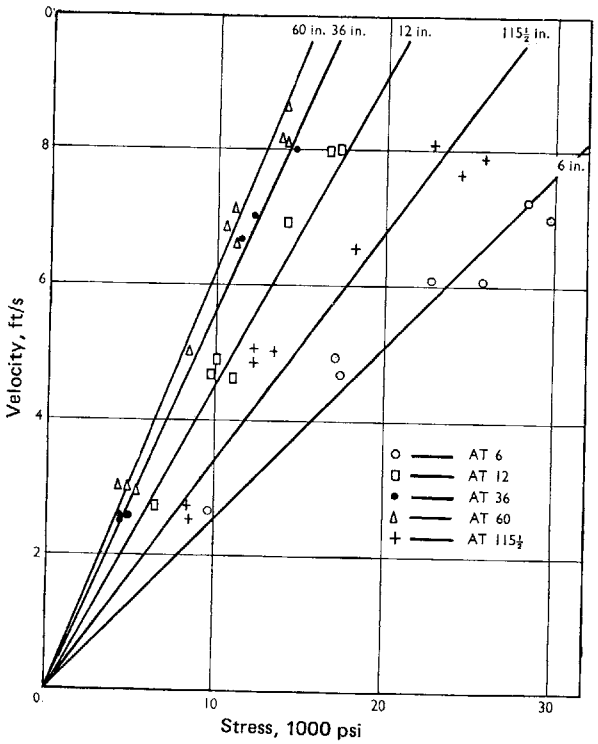


*Figure 13. Bending stresses in a drill rod as a function of impact velocity (impact eccentricity = 1/16 in., rod length 10 ft, rod diameter 0.742 in.). (After Roberts et al. 1962.)*

*Impact velocity.* It has been shown by Takata and Shimizu (1960) and confirmed by Roberts et al. (1962) that the bending wave peak amplitudes increase linearly with piston impact velocity for blows having constant eccentricity relative to the rod axis. Figure 13 shows the bending stresses as a function of impact velocity at five different points along a 10-ft drill rod, obtained from single blow tests after Roberts et al. (1962). For these tests the impact point was located 1/16 in. off the center of the rod axis. The results show that the highest bending stresses are near the shank and bit and the lowest are at the center of the rod. Figure 14 shows a similar result, but the data were acquired during an actual drilling test, on an airleg drill in good condition. This graph also shows the longitudinal stress levels taken during the same drilling tests. Again, the highest bending stresses are close to the shank end and the least at the center of the rod. As mentioned earlier it is not clear exactly what quantity an individual set of strain gauges measures relative to peak amplitudes, and intuitively it is expected that the peak strain would occur at mid-position, at least for the low frequencies.

*Piston mass.* Increasing the piston mass for a given impact velocity, all other factors remaining constant, is equivalent to increasing the impact energy that is absorbed by the bending wave. Figure 15 shows the form of the initial bending wave generated in a drill rod by oblique

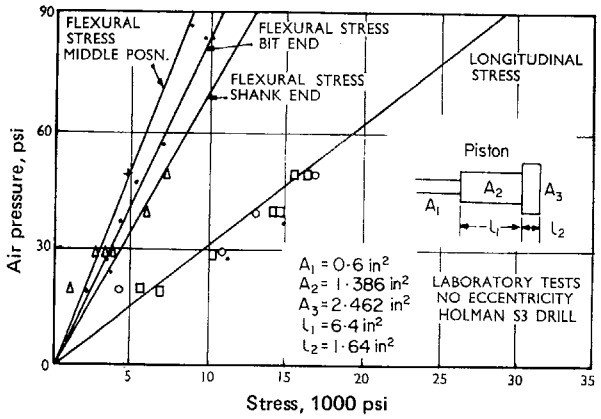


*Figure 14. Bending stresses in drill rod during actual drilling (rod length 10 ft, 7/8 in. hexagon). (After Roberts et al. 1962.)*

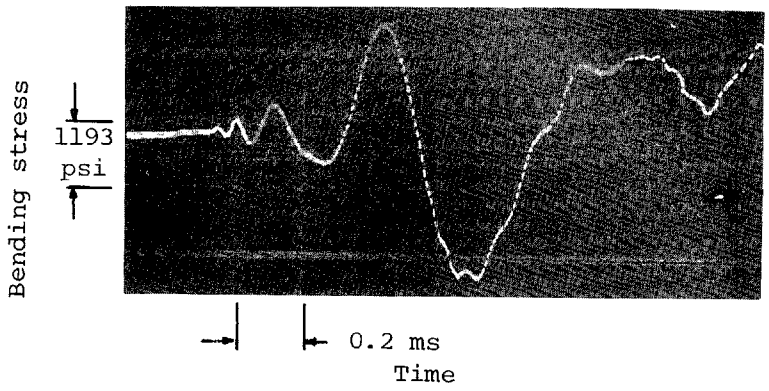


*a. Large hammer, diam = 2.38 in., length = 3 in., mass = 3.76 lb. 7/8 hex rod, 69.5 in. long.*

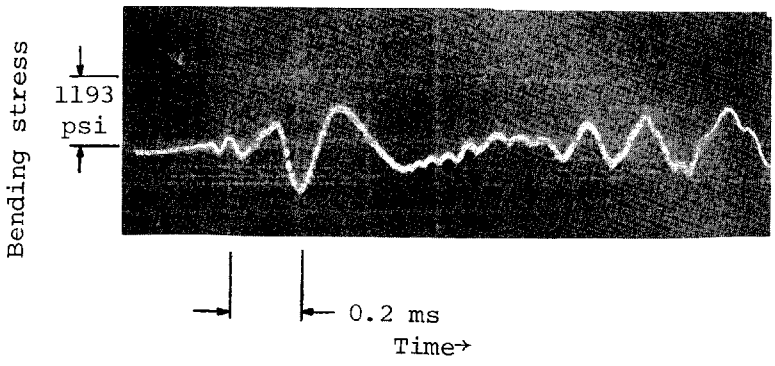


*b. Small hammer, diam = 1 in., length = 2.8 in., mass = 0.62 lb. 7/8 hex rod, 69.5 in. long.*

*Figure 15. Initial shape of bending wave as a function of piston mass (strain gauges mounted 35 in. from the impact end).*

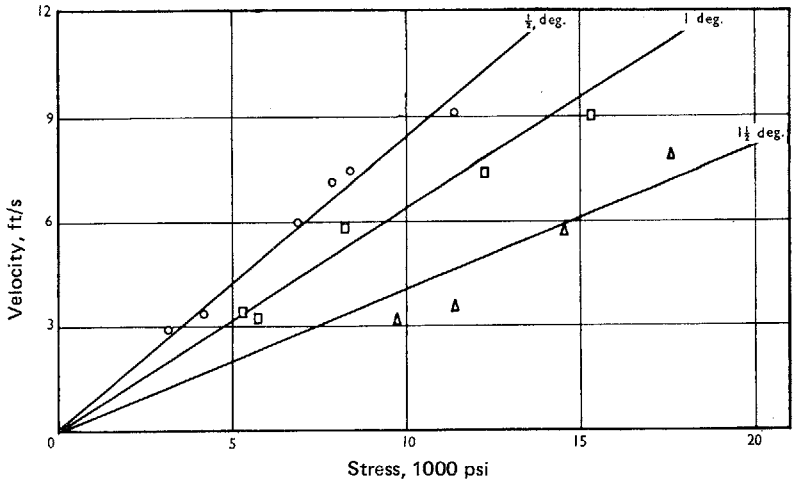


*Figure 16. Bending stresses in drill rods as a function of chuck/rod clearance (rod diameter 0.742 in., piston mass 2.67 lb). (After Roberts et al. 1962.)*

impacts on the end of the rod. For these tests two different hammer masses with approximately constant velocity were used. As the impact energy increases so do the lower frequency components in the bending wave. Roberts et al. showed that the bending stress levels are roughly proportional to the square root of the impact energy, which is in keeping with the theory as will be discussed later.

*Eccentricity of impact.* Lack of rod alignment in the chuck produces an eccentric impact, which in turn generates bending waves. Figure 16, reproduced from Roberts et al. (1962), shows how the bending stresses increase with misalignment of the drill rod in the chuck. Typically a clearance of 0.060 in. in a worn chuck would give a misalignment of 1.2 degrees, with bending stresses well in excess of 20,000 psi.

## 4. NOISE RADIATION FROM DRILL RODS

The original test program was laid out with the intention of determining how the mass, shape and impact velocity of the piston could be optimized to minimize the noise generated by the longitudinal stress waves. However, during the course of the work it became apparent that the bending waves, which develop because of drill imperfections and operating variables, completely dominate noise generation. Thus, the objective of the study was changed to an investigation of the bending waves in drill rods, how they generate noise, and how their influence can be minimized.

Basic theories of the generation of sound by vibrating bodies attempt to make correlations between the sound pressure levels at various distances and the surface velocities or accelerations. The shape of the vibrating surface is important, as is the frequency, which determines the radiation efficiency. A variety of models have been used by researchers investigating the noise radiation from rods and beams, notably dipole arrays based on the concept of an oscillating sphere (Junger 1975) and

simply supported point-driven beams (Blake 1974). However, acoustic models such as these are at best extremely crude representations of a drill rod subjected to bending waves. Some of the problems can be summarized as follows.

a. There are no theories for predicting either the peak stress amplitudes at any particular point in a drill rod or their frequencies, or for calculating the RMS velocities for the rod as a whole, relative to the factors that cause the bending waves to be generated. Thus, even if a correlation could be established between an appropriate RMS surface velocity and radiated noise there is no way to relate this correlation to drill design parameters at present except by using empirical data.

b. Bending waves in drill rods are directional; thus the noise levels will also be directional. This effect is to a large extent canceled out in actual drilling as the rod rotates. However, as the test rods are usually not rotating, the directional nature of the bending waves makes correlation much more difficult.

c. Different points on the drill rod vibrate to different amplitudes at different frequencies, and so the radiated sound field varies continuously in all directions relative to the drill rod.

d. The radiated portion of the sound field is only developed at large distances from the rod; the principal measurement location (1 m) is still within the near field for some of the radiated frequencies where the theory is inexact.

In view of these difficulties and the conflict with the original scope of work, no attempts have been made to provide overall correlations between the sound pressure levels and drilling parameters. The data presented here are only considered to apply for the particular geometry and test conditions used.

The test program was carried out in two locations: a reverberant room and outdoors in free field conditions. Full details are given in Appendix A. The indoor tests were carried out by manually impacting instrumented drill rods, and were made primarily to gain a better understanding of the behavior of the bending waves and to obtain data to correlate with theory. The outdoor tests were made on a special rod-impacting fixture and were aimed at providing quantitative data on the influence of the bending waves on the noise levels. Tests were also made to determine the effects of chuck clearance and rubber collars on the generation and damping of the waves.

Initial and long-term wave form measurements and spectrum analyses were made of the longitudinal and bending waves, surface accelerations, and sound pressure levels on drill rods impacted in three different ways: side (pendulum) impacts, manual end impacts, and impacts using the test fixture.

When the pendulum side impact technique and the test fixture were used, the reproducibility of the results was excellent. For example,

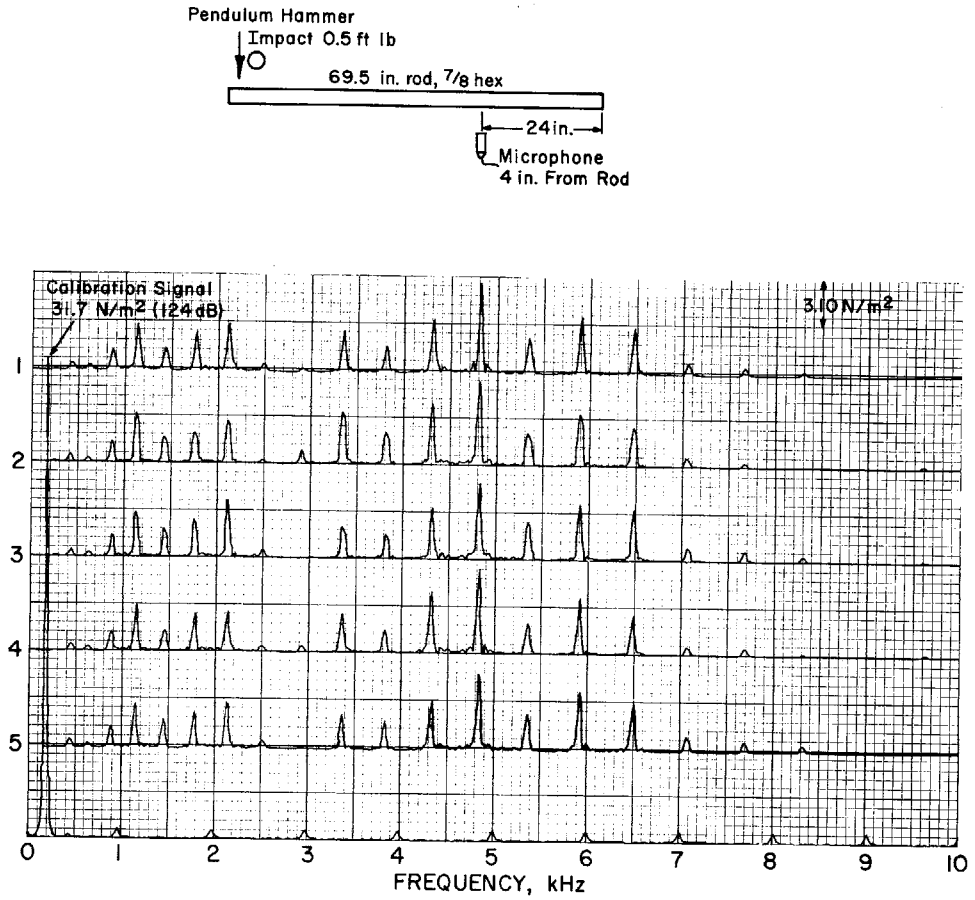


*Figure 17. Spectrum analysis of the drill rod noise from five consecutive side impacts.*

Figure 17 shows the spectrum analysis of the noise generated by five consecutive impacts using the pendulum impact system. Further examples of reproducible records are given in Appendix A.

Figure 18 is a set of spectrum analysis traces for a manual end impact on a freely suspended drill rod, showing the bending wave near the center of the rod, the noise 3 in. from the center, the acceleration, again near the center, and the longitudinal wave near the center and 6 in. from one end.

*Bending wave spectrum.* As discussed in Section 3.3, an equation (eq 25) has been developed which accurately predicts the frequency of the bending waves. In this record every other peak is smaller than the two adjacent peaks. This phenomenon has not been studied.

*Longitudinal wave spectrum.* The longitudinal wave spectrum is shown for two points in the upper two traces of Figure 18, one near the center of the rod and the other near the end. The frequency peaks are shown at the predicted $C_s/2L_r$ (1400 Hz) intervals but the alternate peaks are suppressed for the record taken near the rod center. The reasons for this

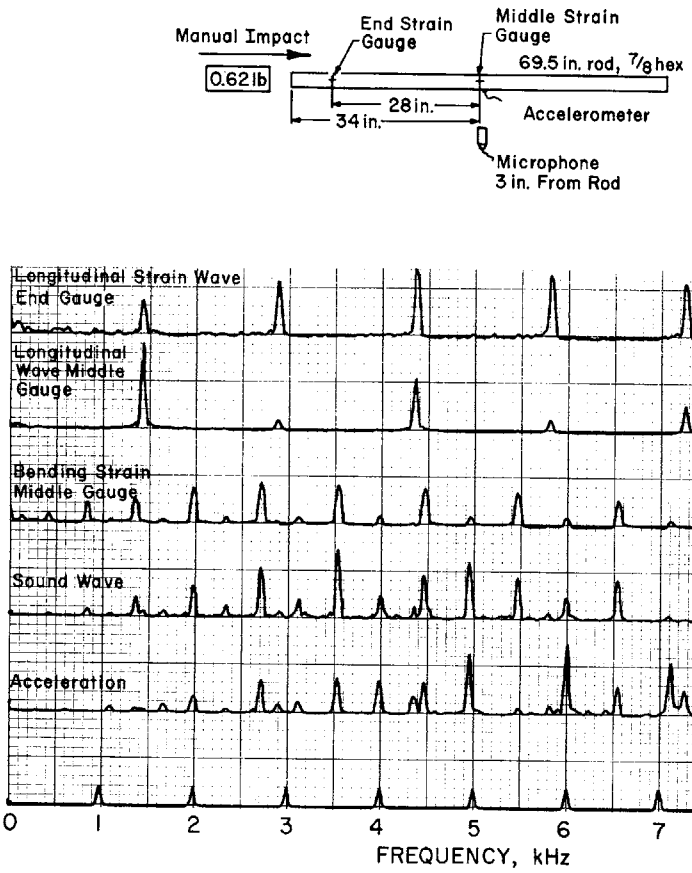


*Figure 18. Longitudinal and bending stress wave, sound, and acceleration frequency spectra from a drill rod.*

are not fully understood but are thought to be associated with the odd and even nature of the wave-overlapping phenomenon at the center of the rod.

*Acceleration spectrum.* As expected the acceleration spectrum coincides mainly with that of the bending wave, but it also shows peaks corresponding to passage of the longitudinal wave.

*Noise spectrum.* For these particular tests the noise spectrum mainly coincides with that of the bending wave, with small peaks indicating the minor contribution of the longitudinal waves.

## 4.1 Relative contribution of bending and longitudinal waves to noise levels

Figure 19 shows the initial bending wave and the corresponding sound pressure wave 1 in. from the rod for test conditions identical to those used to produce the results of Figure 18. The initial sound pressure level close to the rod is an almost exact replica of the bending wave, with no indication of sound pressure from the earlier longitudinal wave. In the tests indoors using manual impacts, the noise levels were always predominantly associated with the bending waves. This was due, in part,

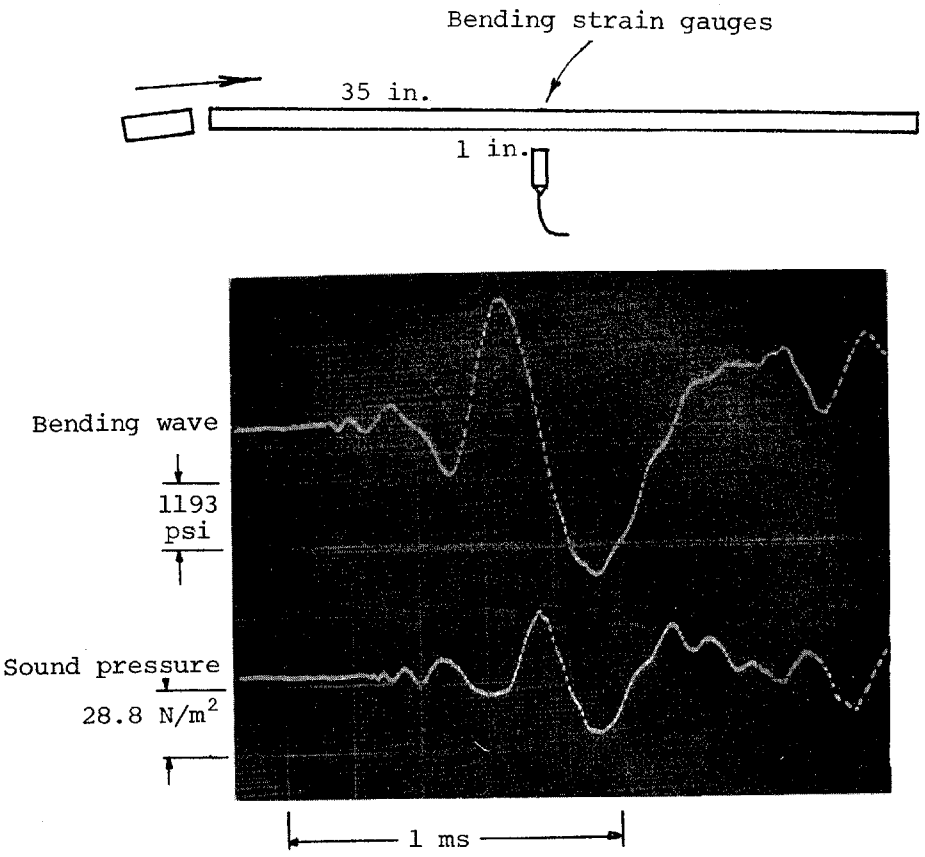


*a. Large hammer (3.76 lb).*

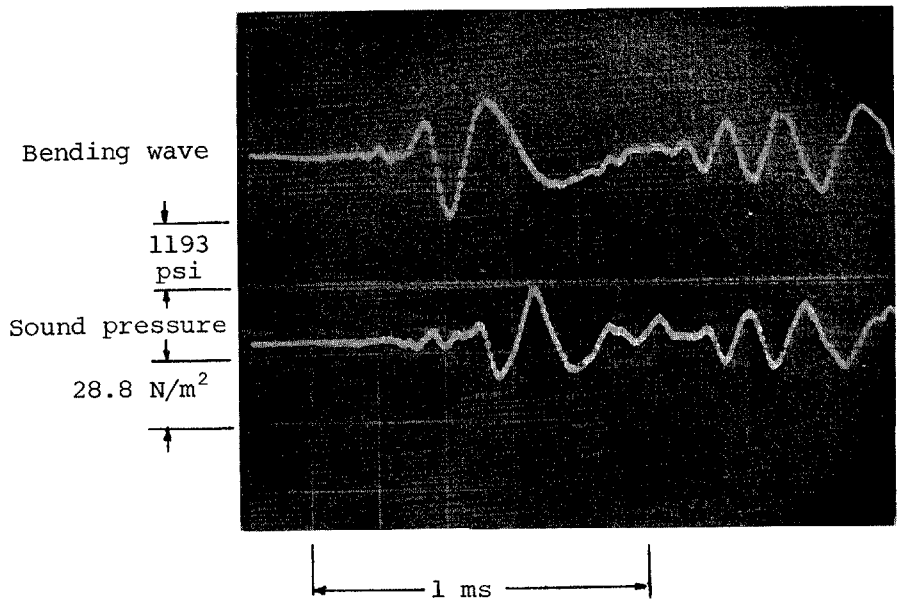


*b. Small hammer (0.62 lb).*

*Figure 19. Simultaneous bending and sound pressure level traces from a 69.5-in.-long, 7/8-in. hexagonal drill rod (manual impact).*

to the difficulty of producing clean axial impacts. However, the impact device used in the outdoor tests and described in Appendix A was especially designed to produce perfectly aligned axial impacts. The piston was dome-shaped so as to contact only the central region of the rod, and the closest possible chuck/rod clearance was used (0.010 in.). Also, great care was taken to align the drill rod in the chuck and to fully support the weight of the rod with the suspension wires.

Figure 20 shows noise spectrum analysis at four distances from a drill rod impacted with a blow energy of 7.6 ft-lb under axially aligned impact conditions. Comparing the noise spectrum with the longitudinal wave spectrum of Figure 18, it will be noted that in Figure 20 the noise peaks are almost all associated with the longitudinal stress wave. For these tests the end face of the drill rod acts as a powerful radiating surface, unlike rock drilling, where the end is enclosed in rock.

During drilling, the close axial alignments achieved in the test fixture are not possible, and most of the noise associated with the drill rod arises from the bending waves. For example, Figure 21 shows the frequency analysis of the noise spectrum of a standard 4-ft drill rod. (The rod length is actually 50 in. and the equivalent diameter is 0.922 in.) The values given in Figure 21, calculated from eq 25 and 10, show an almost perfect correspondence with the measured peaks. Four of the peaks correspond to the longitudinal wave and the remainder to the bending waves.

To clarify the relative contribution of the two kinds of waves to noise generation, we have attempted to calculate the relative RMS radial velocities that the longitudinal and bending waves generate for the drill rod as a whole. Basically, the technique adopted has been to calculate the RMS surface velocities in terms of the relative energy levels in the two kinds of waves by making certain assumptions relative to rise times and to spatial and time variations of the waves. Full details of the assumptions and procedures are given in Appendix C. It is shown that to a first approximation the bending strain energy $E_b$ in the drill rod is given by

$$E_b = \frac{\sigma_{mb}^2 A_r L_r}{16E}. \tag{31}$$

Similarly, assuming that the longitudinal stress wave can be represented by a triangular-shaped pulse of wavelength $q$, as discussed earlier, the energy in the longitudinal wave $E_L$ is given by

$$E_L = \frac{\sigma_{mL}^2}{E} A_r L_r \frac{2}{3} \frac{q}{T} \tag{32}$$

where $\sigma_{mL}$ is the peak stress in the rod and $T$ is the cycle time of the wave ($2L_r/C_s$).

The relationship between the peak radial velocity and the peak bending strains has been presented earlier (Section 3.4, Table 4). The RMS surface velocity in space and time is one-half the peak radial velocity:

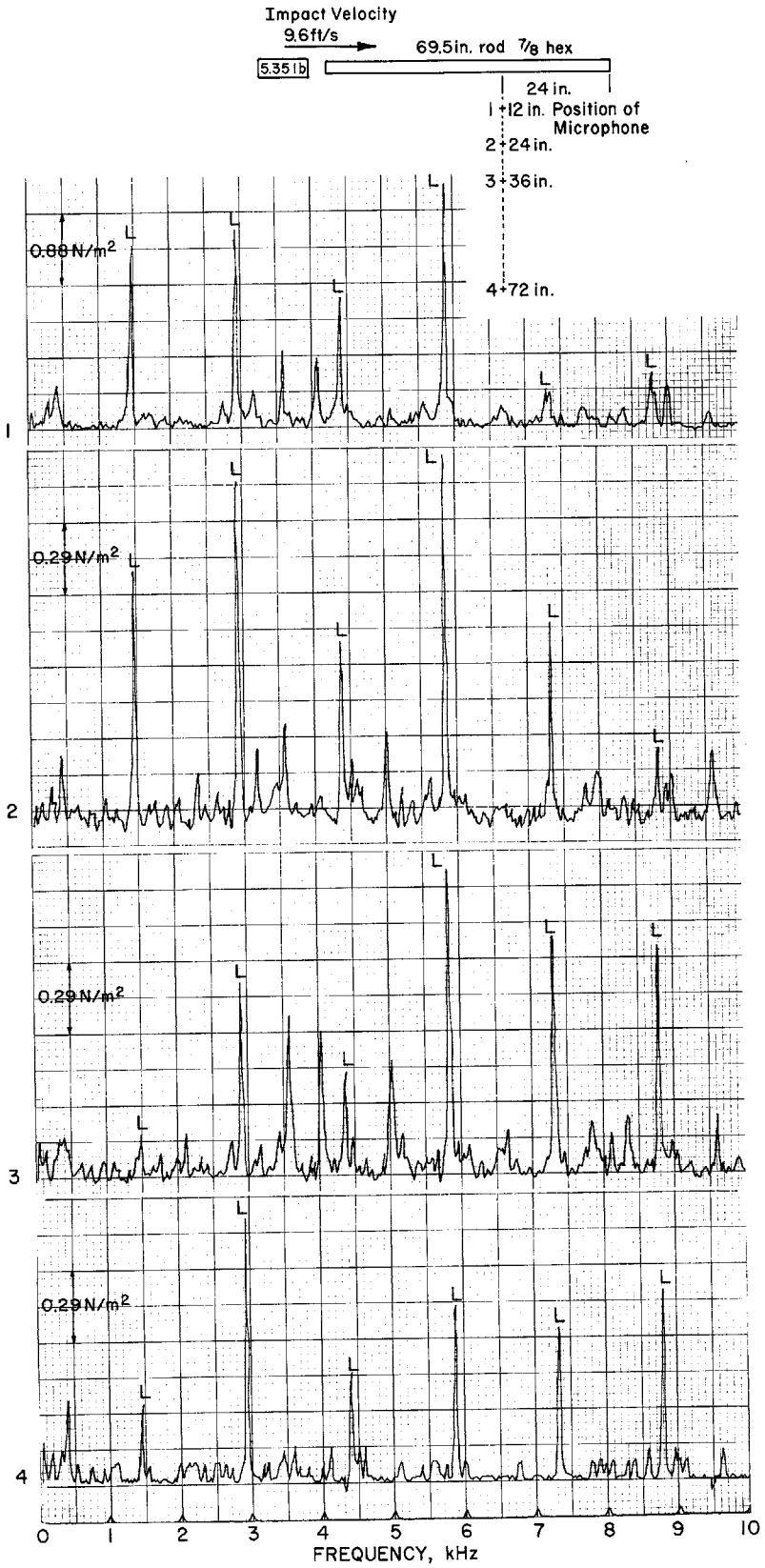


*Figure 20. Sound pressure level spectra for idealized axial impact conditions. Noise corresponding to longitudinal stress wave frequencies is shown by letter L.*

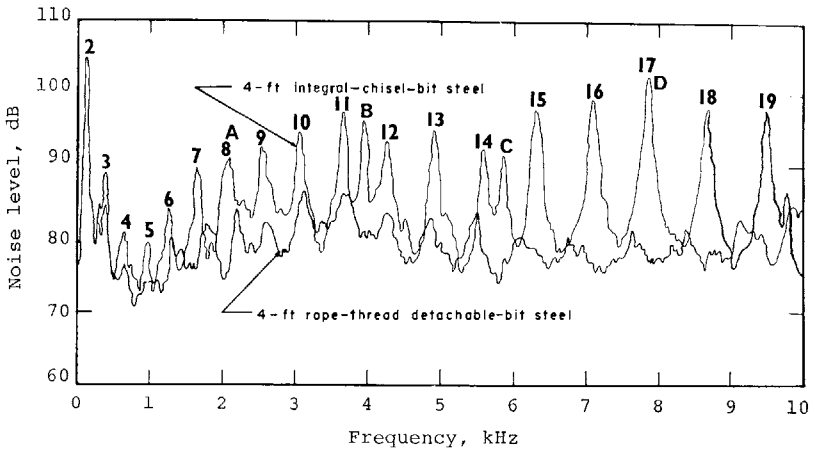


*Figure 21. Calculated and measured drill rod vibration frequencies (rod length 50 in., equivalent diameter 0.922 in.).*

| Frequency (Hz) | | |
|---|---|---|
| Calc (eq 10, 25) | | |
| Longitudinal stress wave | Bending wave | Exp* |
| 2000 | | A |
| 4000 | | B |
| 6000 | | C |
| 8000 | | D |
| | 65.1 | 1† |
| | 181.7 | 2 |
| | 353.5 | 3 |
| | 582.7 | 4 |
| | 867.3 | 5 |
| | 1205.8 | 6 |
| | 1596.7 | 7 |
| | 2038.1 | 8 |
| | 2527.7 | 9 |
| | 3063.1 | 10 |
| | 3641.6 | 11 |
| | 4259.9 | 12 |
| | 4914.9 | 13 |
| | 5602.9 | 14 |
| | 6320.1 | 15 |
| | 7062.1 | 16 |
| | 7824.6 | 17 |
| | 8602.8 | 18 |
| | 9391.7 | 19 |

*Jensen and Visnapuu, 1975.
†Not shown.

$$u_{rb} = u_b \frac{\sqrt{2}}{2} \times \frac{\sqrt{2}}{2} = \frac{u_b}{2} .$$

Thus, assuming sinusoidal mode bending:

$$u_{rb} = \frac{C_s \sigma_{mb}}{4E} . \qquad (33)$$

It is shown in Appendix C that the RMS radial velocity from the longitudinal pulse $u_{rL}$ can be approximated to

$$u_{rL} = \frac{\nu D}{2E} \frac{\sigma_{mL}}{q} (Z) \qquad (34)$$

where Z is a dimensionless factor which accounts for the wave shape and the wavelength relative to the rod length and is given by

$$Z = \left\{ \frac{S_f 2q}{T} + \frac{2q}{T\left[1-(1/S_f)\right]} \right\}^{\frac{1}{2}} .$$

Combining eq 31 and 32, the ratio of the peak bending and longitudinal stress can be obtained in terms of the energies in the two waves:

$$\frac{\sigma_{mb}}{\sigma_{mL}} = \sqrt{\frac{32q}{3T}\frac{E_b}{E_L}} \quad . \tag{35}$$

The RMS radial velocity ratio can be obtained in terms of the stress ratio from eq 33 and 34 as:

$$\frac{u_{rb}}{u_{rL}} = \frac{C_s}{2\nu D}\frac{q}{Z}\frac{\sigma_{mb}}{\sigma_{mL}} \quad . \tag{36}$$

Typical values of the factors in eq 36 for stoper type drills are:

$q = 3.5\times10^{-4}$ s

$T/2 = 3.5\times10^{-4}$ s

$D = 1.0$ in.

$C_s = 2\times10^{5}$ in./s

$\nu = 0.3$

$S_f = 8.$

Substituting these values into eq 35 and 36 gives

$$\frac{u_{rb}}{u_{rL}} = 38.6\,\frac{\sigma_{mb}}{\sigma_{mL}} \tag{37}$$

and

$$\frac{u_{rb}}{u_{rL}} = 89\,\sqrt{E_b/E_L} \quad . \tag{38}$$

Equation 37 means that for the radial velocities from the bending and longitudinal waves to have equal magnitude the peak stress in the longitudinal wave must be 39 times as great as the peak stress in the bending wave.

In terms of the energies in each wave, if the energy in the bending wave is greater than around 0.013% of the energy in the longitudinal wave then the radial velocities associated with the bending wave generate the greatest noise levels. Figure 22 shows the relationships graphically.

The peak stresses in a standard rifle bar drill rod are of the order of one-third the longitudinal stresses (see Fig. 14). In this case, the RMS radial velocity to be associated with the bending waves will therefore be around eight times that due to the longitudinal waves.

## 4.2 Noise generated by bending waves

As discussed earlier, all the measurements of interest, i.e. within 1 m of the drill rod, are within the "near" field where correlation of

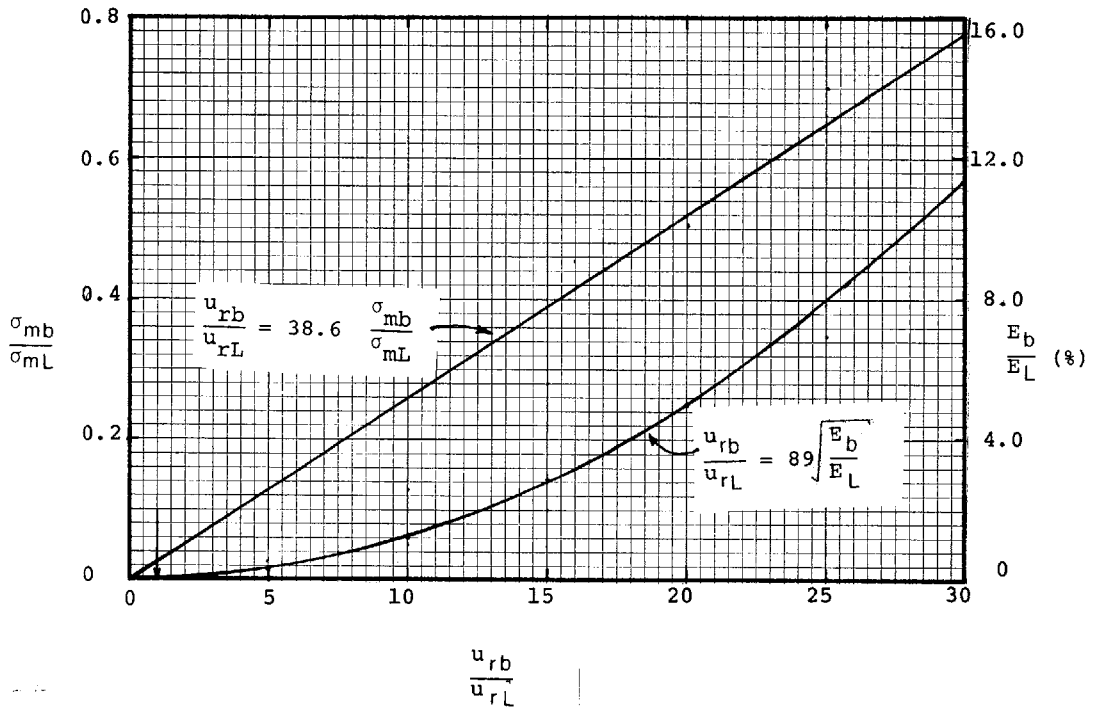


*Figure 22. Relative radial velocities as a function of relative stress levels and energies in longitudinal and bending waves.*

bending amplitude to sound pressure level is very difficult. Strain gauges record the bending waves at only one point, and the sound pressure levels vary in all directions relative to the drill rod, with the different frequencies being reinforced or canceled by sound wave interactions. A series of experiments were made under controlled pendulum impact conditions to demonstrate these effects.

*Bending plane effects.* The plane of the bending waves has a marked influence on the sound pressure level measured around the drill rod. Figure 23a shows the bending waves on planes 60° apart, generated by a side impact. As would be expected, the wave shapes are identical but the amplitudes vary by a factor of three.

Figure 23b shows the bending strains in three planes at 60° to each other and also the sound pressure 6 in. from the rod. In this example, which was of an end impact, the plane of bending was almost parallel to the no. 1 set of strain gauges, which indicate low strains. The other two sets of gauges (2 and 3) show much higher strains.

Figure 23c shows a similar record but for a side impact and with an increased time span (100 ms). The impact point was normal to the no. 1 strain gauge set, which consequently shows the greatest strain amplitudes. In these records the low frequency components are clearly visible and the sound pressure levels fall as the high frequency components are damped.

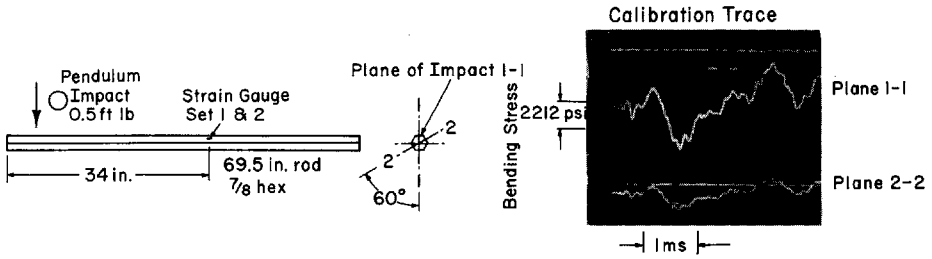


*a. Side impact generated bending waves in planes 60° apart.*

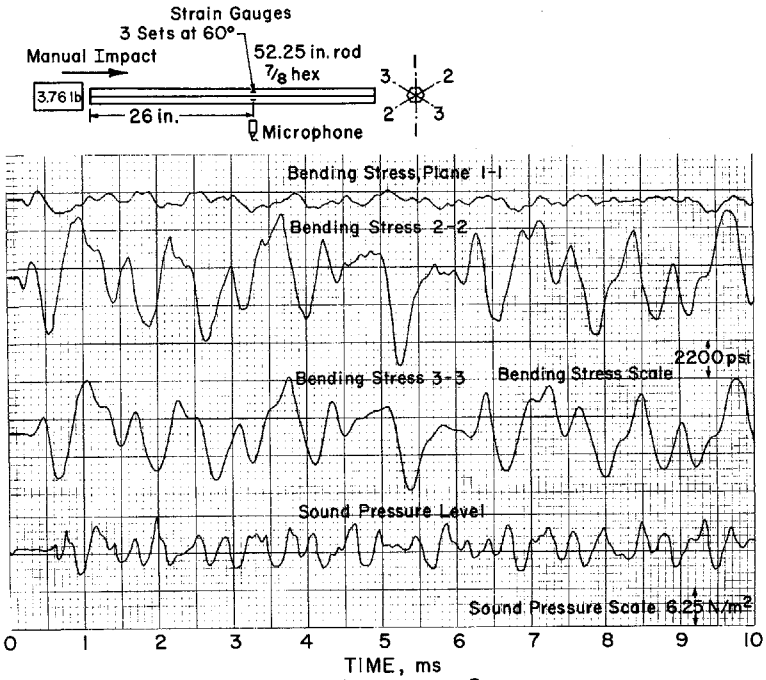


*b. Bending waves in three planes 60° apart, sound pressure at 6 in. from drill rod, 10 ms.*

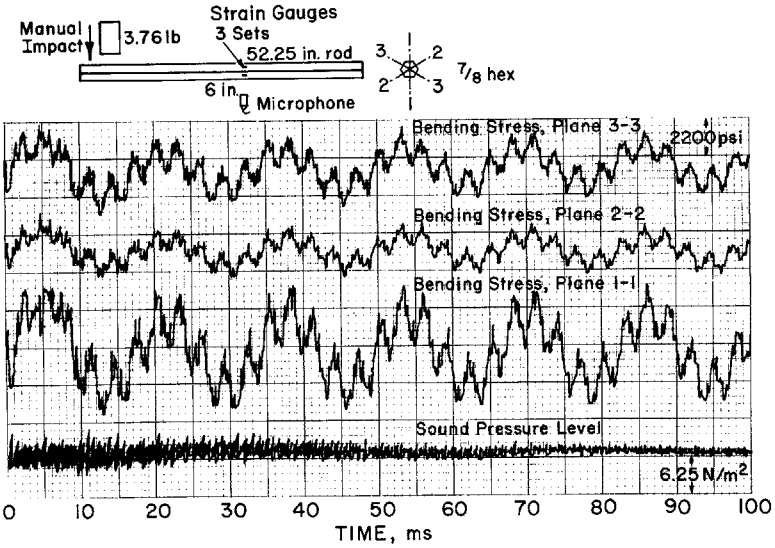


*c. Bending waves in three planes, sound pressure level at 6 in. from drill rod, 100 ms.*

*Figure 23. Drill rod bending waves in different planes.*

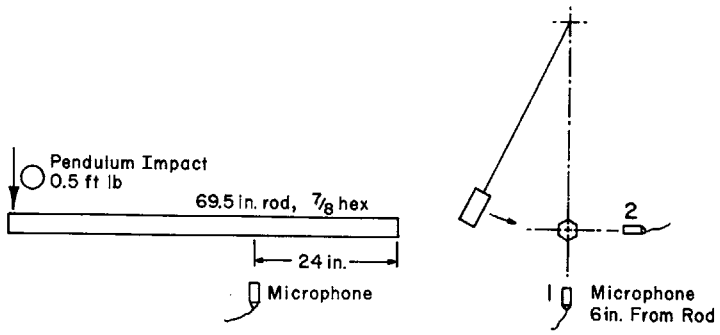


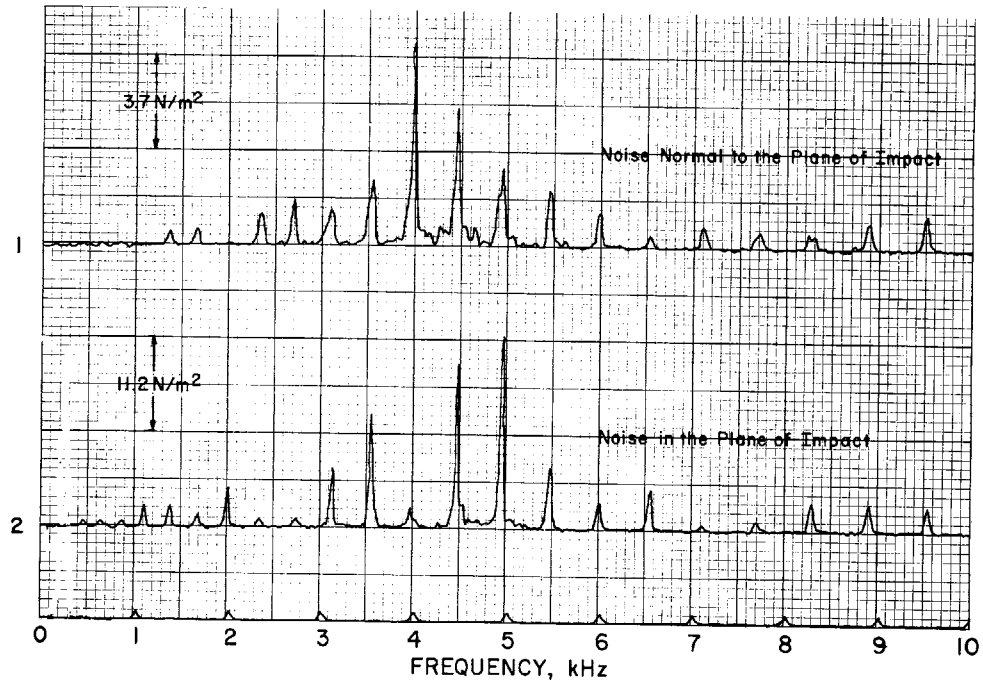


*Figure 24. Noise frequency in two orthogonal planes related to a drill rod.*

Figure 24 shows the noise frequency spectra with the microphone positioned 6 in. from the rod in two orthogonal positions, for side impacts. The frequency peaks for the sound recorded parallel to the bending plane are roughly three times those normal to this direction (the sound level scales are not the same for the two cases.)

*Sound pressure levels in the plane of bending.* The sound pressure levels vary continuously in all directions around the drill rod. Figure 25 shows the spectrum analysis of the sound measured along three different lines normal to the rod axis in the plane of bending, with side impacts. It is very difficult to draw any meaningful conclusion from these results other than the obvious result that very many measurements would have to be taken to obtain a meaningful RMS value. For example, in Figure 25 the frequency peak at 4500 Hz has the highest amplitude of all the peaks at

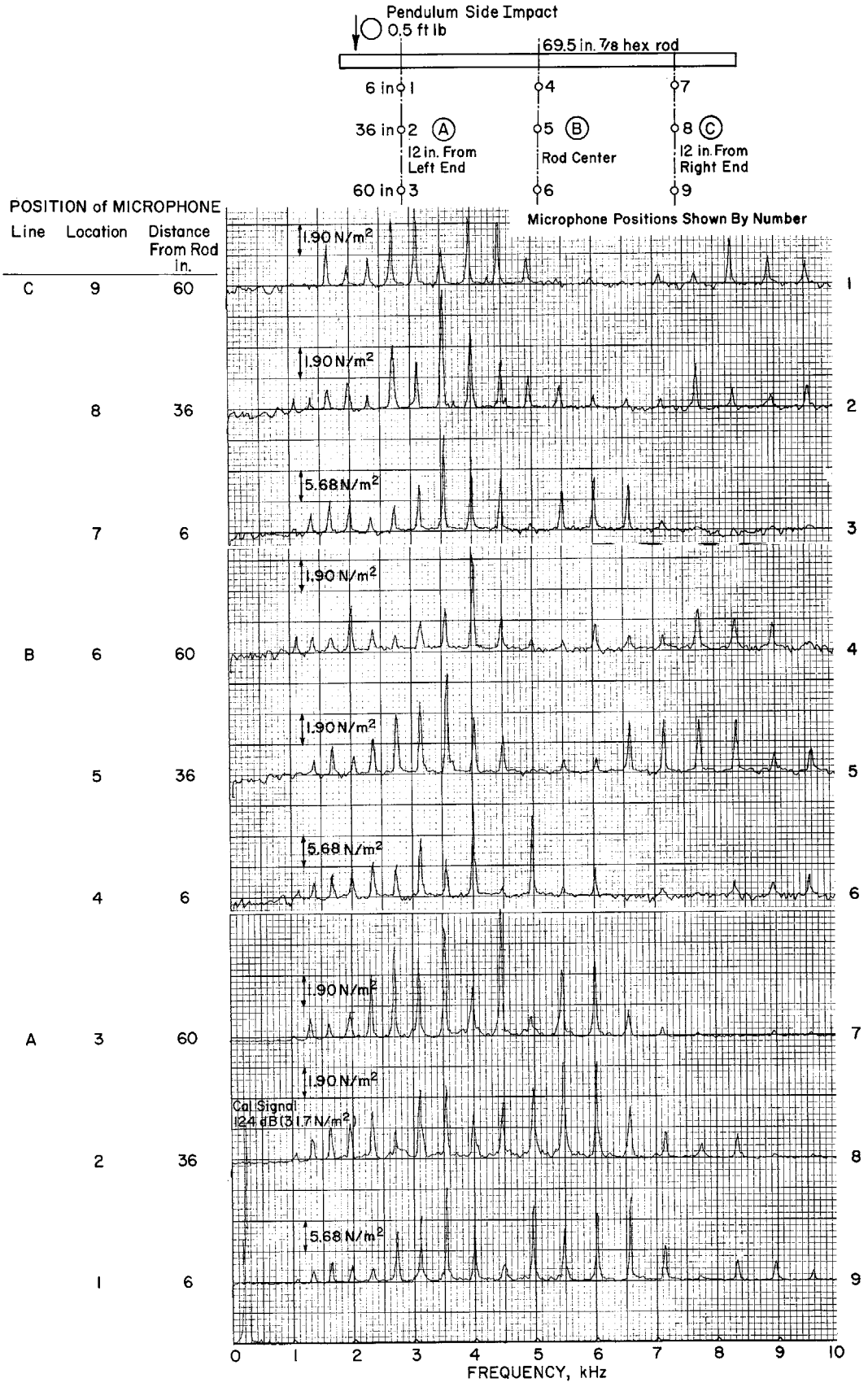


*Figure 25. Noise spectra in the plane of bending at nine different points.*

60 in. from the rod, but one of the lowest at 6 in. The behavior of the adjacent peak at 5000 Hz is directly the opposite, i.e. high at 6 in. but low at 60 in.

## 4.3 Influence of chuck/shank clearance

Roberts et al. showed that misalignment of the drill rod with the axis of the drill was a major cause of bending waves. The extent of rod misalignment is governed primarily by chuck/shank clearance. As discussed in Volume 1 large chuck/shank clearances are required to ensure that drill rods from different manufacturers will fit a given machine. Other factors encouraging loose drill rod/chuck fits are the need to avoid galling and possible seizure due to the influx of cuttings. Typically, chuck/rod clearances are 0.06 in., which represents a misalignment of $1^{o}$ in a typical drill.

Some tests were carried out to try to quantify the bending wave strain level in terms of chuck clearances. Figure 26 shows the results of tests made in the test fixture with two chuck/rod clearances, 0.01 and 0.110 in., corresponding to rod misalignments of $0.13^{o}$ and $1.4^{o}$. The bending stress increases by a factor of around $2\frac{1}{2}$ as the chuck clearance increases, which is in keeping with the results published by Roberts et al. (1962) - see Figure 16. The sound pressure levels over the first 7 ms (Fig. 26b) indicate the increased noise level with the looser chuck (roughly 6 dBA). The sound and bending wave spectra are also given. For the large chuck clearances the contribution of the bending waves to the noise levels increases significantly.

## 4.4 Influence of rubber drill rod collars

The use of coatings to reduce the noise generated by drill rods was discussed in Volume 1. The scope of the study did not permit the testing of coated drill rods, but some tests were made to determine the influence of rubber collars on the drill rod vibrations and noise levels. For these tests a LeRoi AT-60 rubber collar was bonded to $\frac{7}{8}$-in. hexagonal drill rod to give a shank length of $4\frac{1}{4}$ in.

As discussed in Volume 1, Section 2.2, it is generally considered that the use of rubber collars reduces drilling rate. However this is not the case if the optimum thrust is used. At thrusts below optimum more bouncing occurs with rubber-collared rods and so less energy is transferred to the rock. Figure 27a shows the initial longitudinal wave and four reflected waves in a rubber-collared drill and there is no sign of any significant damping, which substantiates this conclusion.

The collar did have a significant effect on the bending wave amplitudes and noise levels generated by side impacts, as will be noted from Figures 27b and c, which show the bending wave and noise levels from rubber-collared and collarless rods. Figure 27d shows the spectrum analysis of the bending waves; again there is considerable reduction in the higher frequency components.

Figure 28 shows how the collar damps the noise level.

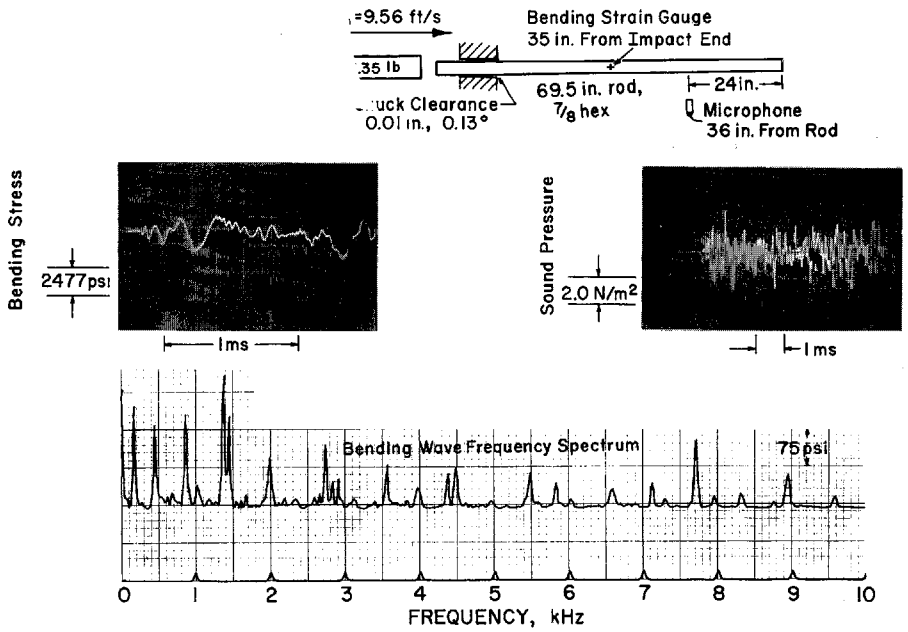


*a. Bending wave and sound pressure, chuck/rod clearance 0.01 in.*

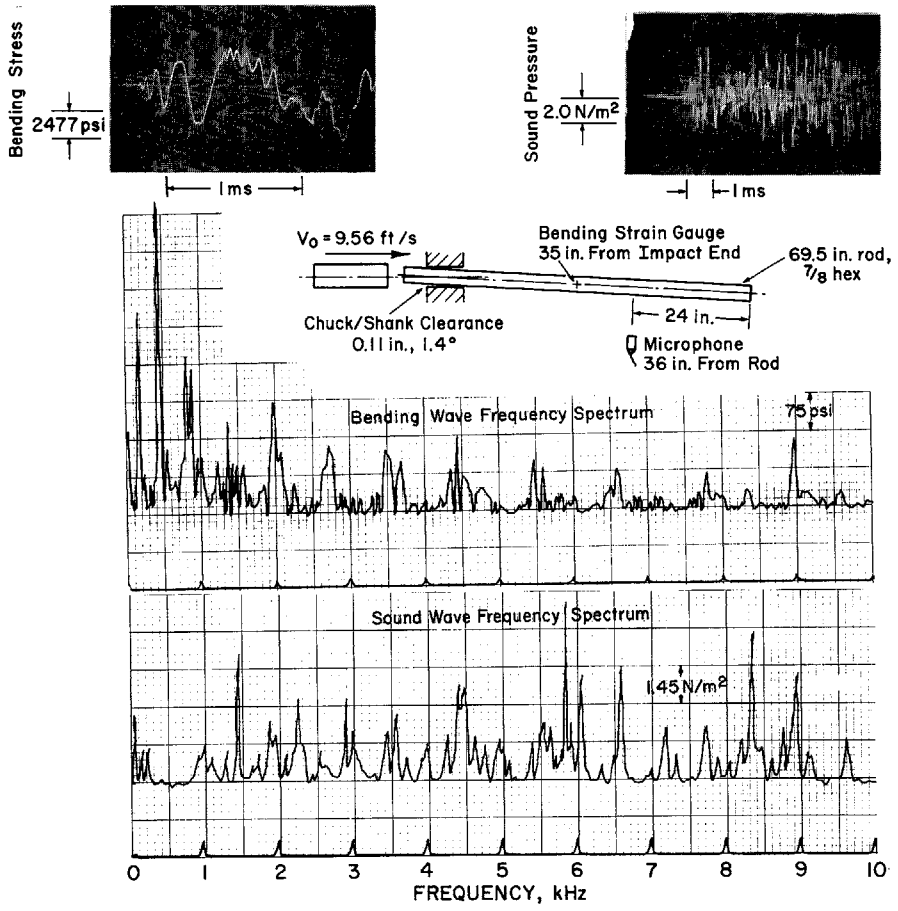


*b. Bending wave and sound pressure, chuck/shank clearance 0.11 in.*

*Figure 26. Influence of chuck/shank clearance on bending and sound frequency.*

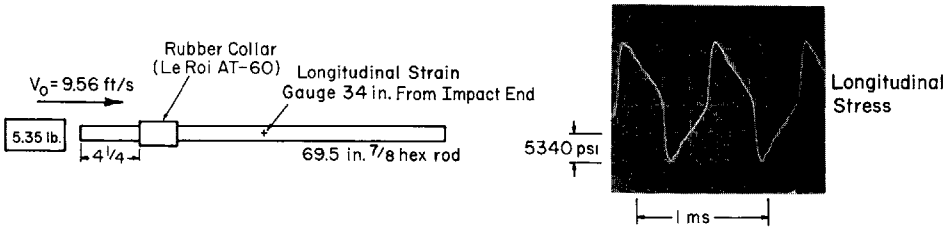


*a. Longitudinal stress wave form in rubber-collared rod.*

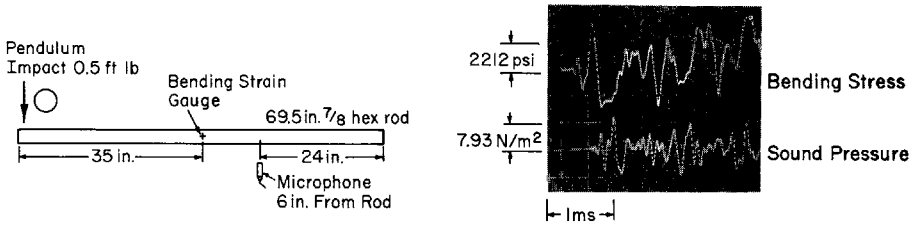


*b. Bending and sound pressure wave form in uncollared rod.*

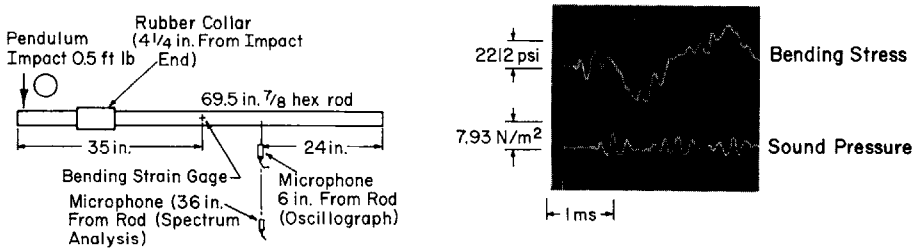


*c. Bending and sound pressure wave form in collared rod.*

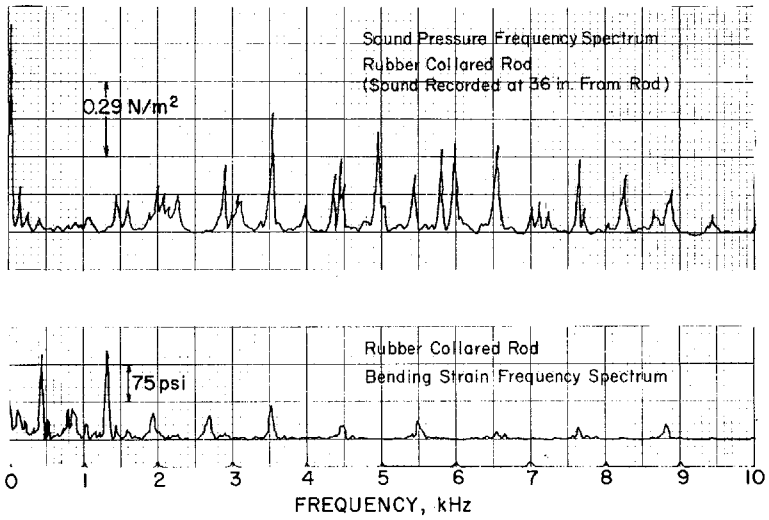


*d. Bending and sound pressure wave frequency spectra, rubber-collared rod.*

*Figure 27. Influence of rubber collars on drill rod stresses and noise levels.*

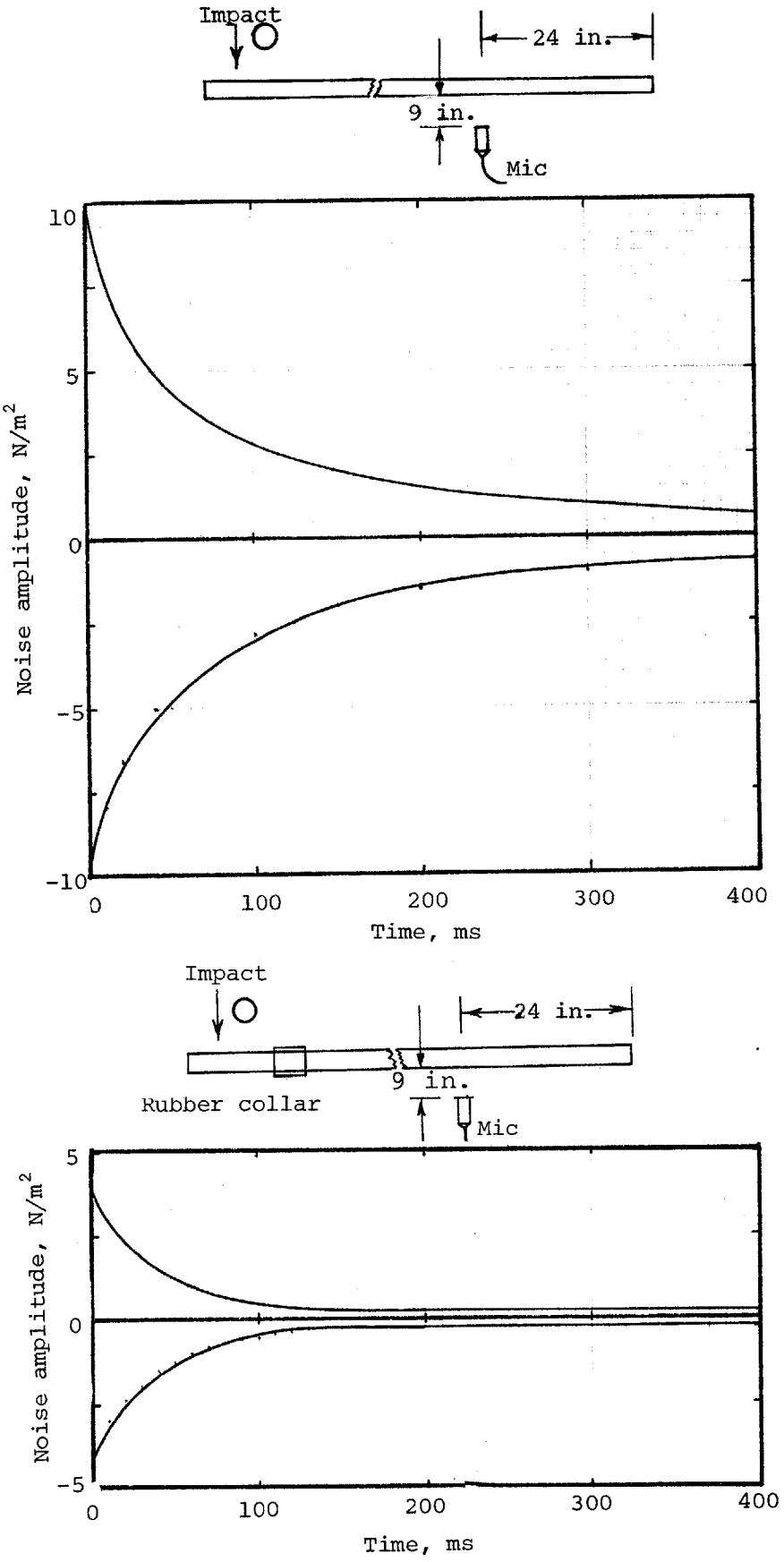


*Figure 28. Noise damping characteristics of collared and collarless rods 69.5 in. long, 7/8 in. hex. Impact energy 0.5 ft-lb.*

## 4.5 Influence of rod diameter

One-inch and seven-eighths-inch hexagonal rods were used during the test program. No discernible differences were noticed relative to the amplitude of the bending waves at corresponding frequencies although insufficient tests were made to really substantiate this conclusion. It seems obvious that the radial velocities must increase as the diameter increases, but in the current tests any effects have been obscured by the different rod lengths used. In a 6-ft rod the slenderness ratio changes very little with a diameter change from 1 to $\frac{7}{8}$-in.

# 5. IMPLICATIONS OF THE STUDY RELATIVE TO DRILL DESIGNS

The study reported here was carried out in conjunction with a parallel effort to evaluate design concepts that will lead to the production of quieter rock drills (reported in Volume 1). Basically, the intention was to better understand how the vibrations in drill rods generate noise so that drill designs can be modified to reduce drill rod generated noise. The original intention at the start of the project was to attempt to correlate the wave form and amplitude of the longitudinal stress wave in the drill rod (which contains the bulk of the energy) with the noise levels around the rod. This has not proved possible, primarily because it was determined early in the study that while drill rod vibrations do in fact consist mainly of longitudinal stress waves, in actual drilling situations the bulk of the noise from the drill rod is generated by the parasitic bending waves.

The main conclusion of the study is that there is no justification for modifying the shape or amplitude of the longitudinal stress wave, for example by changing the piston shape, mass, or impact velocity, in an attempt to reduce the noise levels generated from this source until the amplitude of the bending waves has been reduced. Future efforts at reducing noise levels in drill rods should concentrate on eliminating the bending waves.

Means for reducing the bending waves are as follows.

*a. Tighten chuck/drill rod shank tolerances.* Misalignment of the drill rod with the axis of impact is one of the major sources of bending waves. The current chuck/shank clearances of 0.060 in. and greater can lead to misalignments of up to $1^{o}$ with a $3\frac{1}{4}$-in. chuck. It has been shown that with misalignments of this magnitude the bending waves contribute the major part of the drill rod noise.

The main problem in tightening the chuck/shank tolerances lies in the manufacturing costs and the need for interchangeability of equipment. For example, drill rods are not usually made by drill machine manufacturers, so unilateral decisions on tolerances cannot be made. Tightening the tolerances will undoubtedly lead to higher manufacturing costs, so there is negative incentive in this respect. Other factors encouraging large tolerances are the need to avoid binding the shank in the chuck either by galling, the influx of grit, or plastic deformation of the shank under

repeated impacts. However, despite these problems, attention should be paid to minimizing the tolerance specifications in drills designed for minimum noise. As a first step in this direction it is recommended that common industrial standards be implemented relative to drill rod shanks, setting tolerance limits to +0.000, -0.010 in. The drill machine manufacturers could then build chucks between 0.005 and 0.010 in. larger, thus guaranteeing fits to within 0.020 in.

*b. Increase drill shank length.* Drill shanks vary in length from $2\frac{3}{4}$ to $4\frac{1}{4}$ in. Assuming a typical 0.040-in. chuck/shank clearance the corresponding angular misalignment would range from $0.83^{o}$ to $0.54^{o}$. The length of the shank is not critical and there are no good reasons why shanks up to 5 in. long or longer could not be used. Limitations are ultimately imposed by machine length restrictions and manufacturing difficulties. In the prototype production quiet stoper currently being designed, a shank length of $5\frac{1}{4}$ in. will be used, giving a maximum misalignment of $0.44^{o}$ with the nominal 0.040-in. clearance. In these machines it is expected that the chuck/shank clearances will be closer to 0.020 in., reducing the misalignment to around $0.2^{o}$.

*c. Ensure chuck/bore alignment in the drill.* In typical rifle bar drills the chuck is a loose (0.008- to 0.010-in.) diametrical fit in the chuck housing and there is considerable play in the chuck nut drive assembly. Both these factors contribute to misalignment of the drill rod. In the L-47 quiet drill the chuck was mounted in bearings to estimate all radial and axial movement. In addition to eliminating chuck rattle noise, mounting the chuck in this manner helps to maintain axial alignment of the rod and impact axis.

*d. Damp the bending waves with rubber collars.* Rubber collars, even when short (2 in.), effectively damp bending waves without significantly reducing the amplitude or shape of the initial longitudinal stress waves. However, there are serious practical problems in mounting rubber collars on drill rods that will need to be overcome before the technique can be recommended for widespread use. The shroud tubes developed to reduce noise radiated from the drill rod, described in Volume 1, are mounted on the drill rod with rubber bushings. While we have not made tests, it is likely that these bushings will have added advantages in that they may help to reduce the bending wave amplitudes and damp out the high frequencies. The shroud tubes in the production prototype drills will be mounted to the drill through rubber collars to isolate them from body-generated vibrations and vice-versa.

*e. Eliminate the need for an upset collar on the drill rod.* During drilling, the drill rod of a conventional rifle bar drill rattles between the rock and chuck, generating bending waves. In rifle bar drills it is essential that the rod and bit lift off the rock following energy transfer so that the bit can be rotated; thus impacts in the shank region are unavoidable. However, if the impacts can be cushioned, for example by the use of rubber collars, or if they can be restricted to the shank end, for example by the use of an anvil block, then it is anticipated that the bending waves due to these secondary impacts can be minimized. In the prototype production stoper drill, rods without upset collars will be used.

*f. Optimizing the thrust.* When the drill rod is out of contact with the rock the constraints on rod vibrations are reduced. In Volume 1 it was shown that optimizing the thrust is not only desirable for achieving high drilling rates but it also significantly reduces the noise levels. It is difficult to operate rifle bar drills at optimum thrust levels because rod rotation is generated by the piston on its return stroke. If the machine is overthrusted so that the bit drags over the rock face during rotation, the torque generated by the piston motion is insufficient to rotate the bit, and the machine stalls. Thus, there is a tendency on the part of the operator to underthrust the drill to keep it running smoothly. In drills in which the rotation is provided independently of the piston motion, the thrust is not critical to smooth operation so the thrust levels can be kept closer to the optimum and drill rod bounce minimized. This approach will be taken in the prototype production stoper drill.

## 6. CONCLUSIONS AND RECOMMENDATIONS

The major problem in quietening rock drills is reducing drill-rod-radiated noise. The noise is predominantly due to the bending waves in the drill rods generated by eccentric impacts on the rod ends and by subsequent impacts between the chuck and collar on the bit and rock.

It is concluded that at the current stage in the development of quiet rock drills there is little to be gained by attempting modification of the wave shape or amplitude of the longitudinal stress waves and that emphasis should be placed on reducing the bending waves.

Specific recommendations are:

a. Increase the length of the drill rod shank.

b. Tighten shank/chuck clearances to around 0.02 in.

c. Mount the chuck rigidly to maintain its axial alignment with the drill bore.

d. Use short rubber damping collars or bushings in contact with the drill rod wherever practical.

e. Eliminate collar/chuck impacts or reduce their intensity by using rubber collars.

f. Optimize machine thrust by reducing rod bounce between the rock and chuck to a practical level; this is best achieved by arranging for independent rotation of the drill rod.

All of these measures to reduce noise radiation from the drill rod will be incorporated into the design of the production prototype currently being developed.

In relation to the studies some specific findings are as follows:

An equation has been derived which enables the bending wave frequencies to be precisely predicted, based on knowledge of the drill rod length and diameter. This should prove very useful in future studies where it is of interest to isolate the drill rod noise frequencies from the overall noise spectrum.

It has been proved that bending waves in drill rods, as measured by strain gauges mounted on opposite sides of the rod and coupled so as to isolate the strain difference across the rod, can be directly related to the radial surface velocities generated by the waves. Conversion factors are given for RMS and peak strain values.

The region of interest, from the point of view of predicting noise levels at the operator's ear, is within the near field of the noise source. Experimental correlations of bending wave frequencies and amplitudes with sound pressure levels proved impractical to make in this region because of the constantly changing nature of the sound field with distance and position relative to the rod.

## 7. REFERENCES


Arndt, F.K. (1960) *The Percussive Process in Piston and Drill Steel in Percussive Drilling.* Gluckauf, Sehr Gang 96, Nov.

Beiers, J.L. (1966) *A Study of Noise Sources in Pneumatic Rock Drills.* J. Sound Vib. 3, 166-194.

Blake, W.K. (1974) *The Radiation from Free-Free Beams in Air and in Water.* J. Sound Vib. 33(4), 427-450.

Cremer, L.; Heckl, M.; Ungar, E.E. (1973) *Structure-Borne Sound, Transaction and Review.* Springer-Verlag, New York.

Dutta, P.K. (1968) *The Determination of Stress Waveforms Produced by Percussive Drill Pistons of Various Geometric Designs.* Int. J. Rock Mech. Min. Sci. 5, 501-518.

Harris, C.M. and Crede, C.E., Ed. (1976) *Shock and Vibration Handbook.* McGraw-Hill, New York, 2nd edition.

Hawkes, I. and Chakravarty, P.K. (1961) *Strain Wave Behavior in Percussive Drill Steels During Drilling Operations.* Mine Quarry Eng. 27(7), 318-326; 27(8), 367-373.

Holdo, J. (1958) *Energy Consumed by Rock Drill Noise.* Mining Mag. (Also Atlas Copco Publication 5013.)

Hustrulid, W.A. and Fairhurst, C. (1971/72) *A Theoretical and Experimental Study of the Percussive Drilling of Rock.* Int. J. Rock Mech. Min. Sci. 8, 311-333; also 9, 417-449.

Junger, M.C. (1975) *Radiation and Scattering by Submerged Elastic Structures.* J. Acoust. Soc. Am. 57(6), Part 1.

Morse, P.M. and Ingard, K.U. (1968) *Theoretical Acoustics*. McGraw-Hill, New York.

Pretlove, A.J. (1969) *Road Noise: Noise Reduction on Road-Breaking Drills*. Phil. Trans., Series A, 263, 425-439.

Roberts, A., Hawkes, I. and Furby, J. (1962) *Transmission of Energy in Percussive Drilling: The Influence of the Flexural Strain Waves in the Drill Steel*. Mine Quarry Eng, Oct.

Shepherd, B.F. (1954) *The Connecting Link in Percussion Drilling*. Min. Cong. J. 40(11), 28-31.

Summers, C.R. and Murphy, J.N. (1974) *Noise Abatement of Pneumatic Rock Drill*. USBM RI 7998.

Takata, M. and Shimizu, O. (1960) *Dynamic Stresses in the Drilling Rod*. Memoirs Faculty Eng., Kywshu Univ. 19(3).

Timoshenko, S. and Goodier, J.N. (1951) *Theory of Elasticity*. McGraw-Hill, New York.

Visnapuu, A. and Jensen, J.W. (1975) *Noise Reduction of a Pneumatic Rock Drill*. USBM RI 8082.

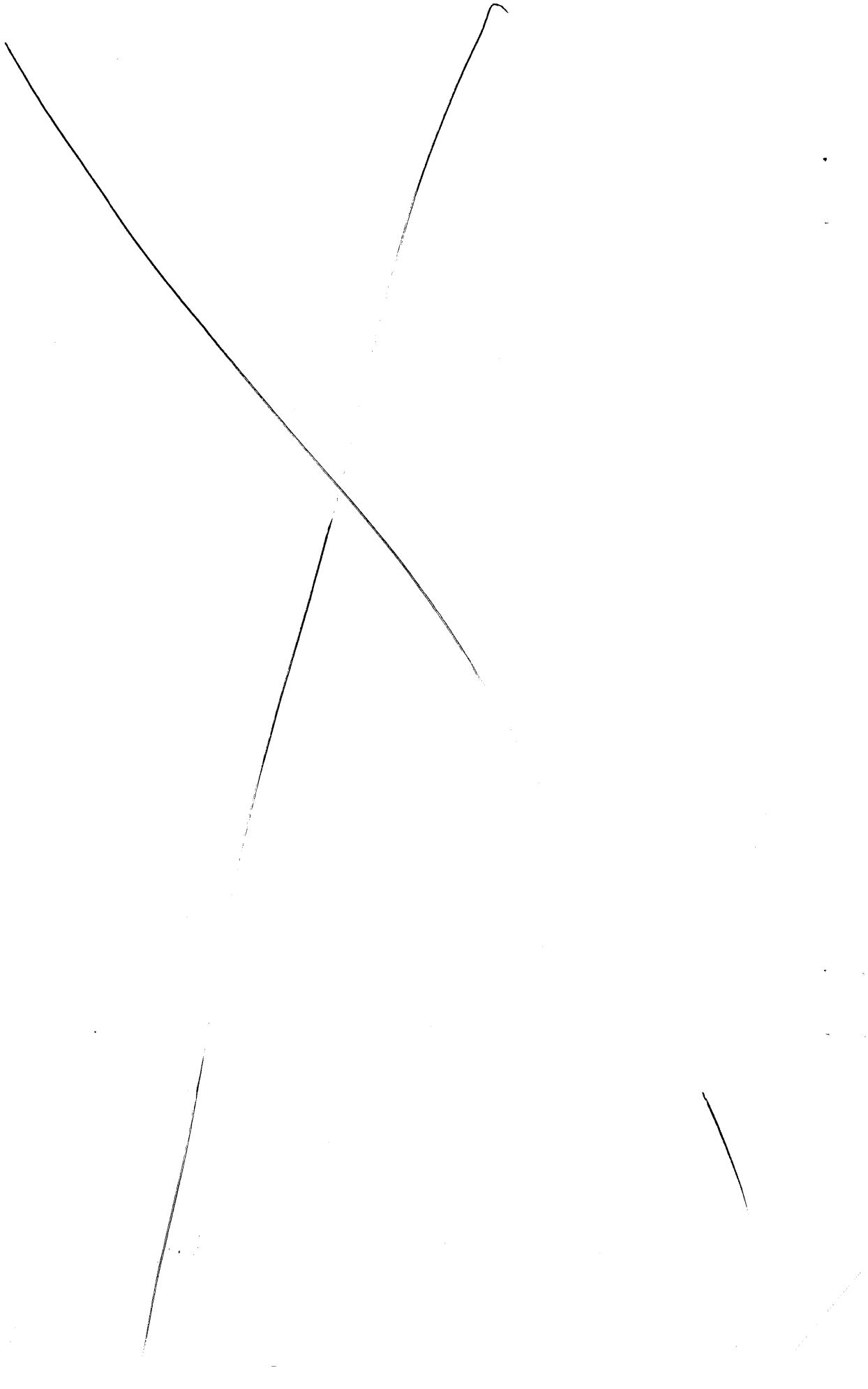

## APPENDIX A. EXPERIMENTAL EQUIPMENT AND TECHNIQUES

This appendix describes the basic equipment and techniques used to generate stress waves in drill rods and to measure the following quantities: longitudinal stress waves, bending waves, drill rod surface accelerations and sound pressure levels.

### A.1 Basic equipment

During the tests three methods of impacting a drill rod were used: manual impacts on the end of the rod, pendulum impacts on the side of the rod, and axial impacts on the end of the rod using an impactor mechanism. Details of the drill rods and impact hammers are given in Tables A1 and A2. The manual and pendulum impacts were made on drill rods suspended from a beam in a reverberant room, 11 × 10 × 8 ft. The impactor tests were made in a special test fixture outdoors in free field conditions.

Table A1. Details of drill rods.

| *No.* | *Length (in.)* | *Section* | *Diameter (in.)* | *Area ($in.^2$)* | *Weight (lb)* | *Remarks* |
|---|---|---|---|---|---|---|
| 1 | 21.90 | Hex | 7/8 | 0.62 | 3.84 | Strain gauge |
| 2 | 69.50 | Hex | 7/8 | 0.62 | 12.19 | Strain gauge |
| 3 | 52.13 | Hex | 7/8 | 0.62 | 9.15 | Strain gauge |
| 4 | 53.75 | Hex | 1 | 0.76 | 11.56 | Strain gauge |
| 5 | 69.50 | Hex | 7/8 | 0.62 | 12.19 | Strain gauge and rubber collar |
| 6 | 71.70 | Round | 1 1/8 | 1.01 | 20.49 | Strain gauge |
| 7 | 71.70 | Round | 1 | 0.79 | 15.94 | No gauge |
| 8 | 71.70 | Round | 7/8 | 0.60 | 12.25 | No gauge |
| 9 | 71.70 | Round | 5/8 | 0.31 | 6.25 | No gauge |

Table A2. Details of impact hammers.

| *No.* | *Diameter (in.)* | *Length (in.)* | *Area ($in.^2$)* | *Weight (lb)* | *Remarks* |
|---|---|---|---|---|---|
| 1 | 1.00 | 2.80 | 0.79 | 0.62 | Manual impact |
| 2 | 2.38 | 3.00 | 4.45 | 3.76 | Manual impact |
| 3 | 1.75 | 3.00 | 2.40 | 2.06 | Pendulum impact |
| 4 | 2.00 | 6.00 | 3.14 | 5.35 | Compressed air actuated axial impact |

Preceding page blank

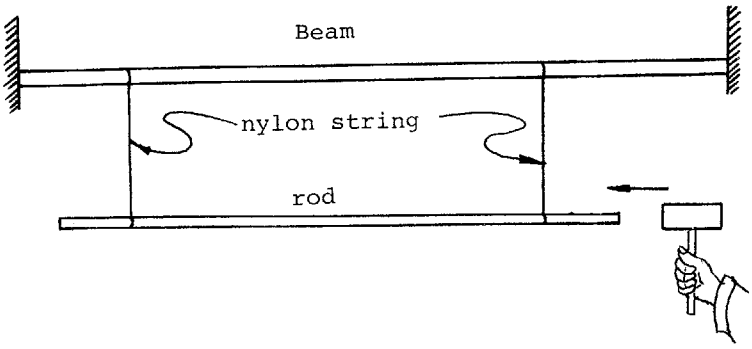


*a. Manual impact setup.*

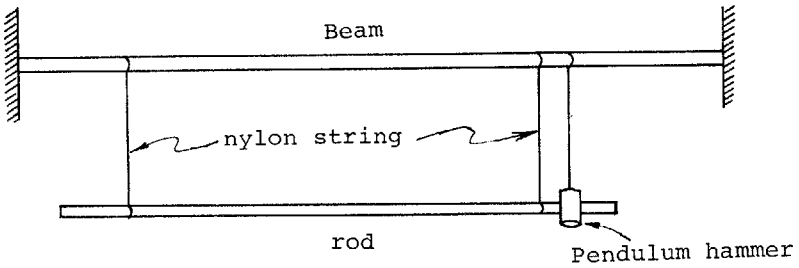


*b. Pendulum impact setup (mass of pendulum 2.06 lb, swing 12 in., impact energy 0.5 ft-lb).*

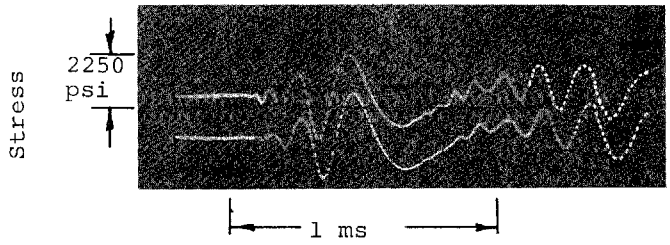


*c. Bending waves generated by pendulum impact (no. 2 drill rod; strain measured at center of rod).*

*Figure A1. Indoor test setup.*

*Manual impacts.* A large number of tests were made by manually impacting the ends of the various drill rods using hammers 1 and 2 (Fig. A1a). No attempt was made to calibrate the blows or measure the impact energy for these tests.

*Pendulum impacts.* For these tests, which were intended to generate mainly bending waves, impact hammer 3 was suspended on a string and allowed to swing through a distance of 12 in. to give an impact of 0.5 ft-lb on the side of the rod (Fig. A1b). The bending waves produced by this technique were reproducible, as will be noted from the records given in Figure A1c.

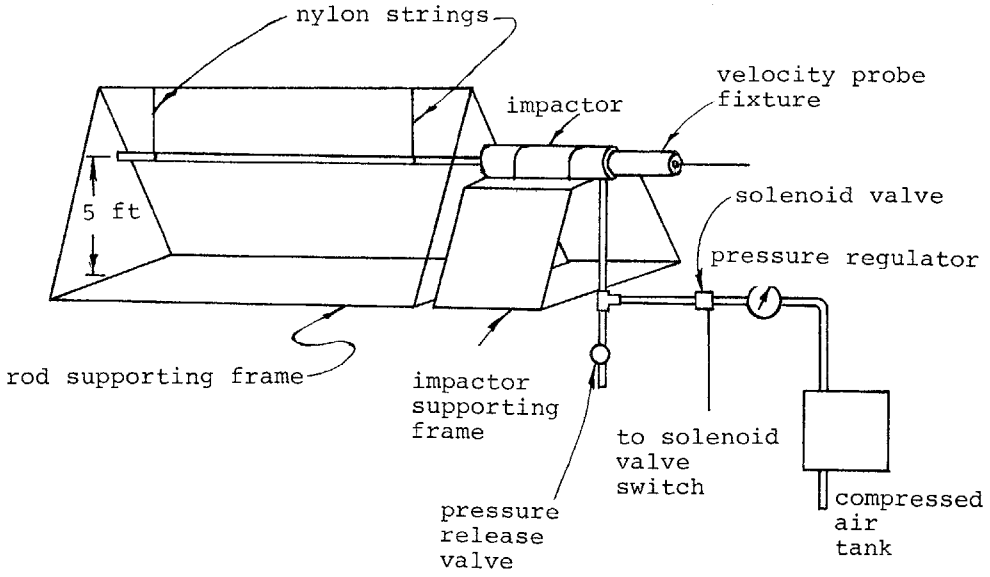


*a. Schematic of the outdoor test fixture.*

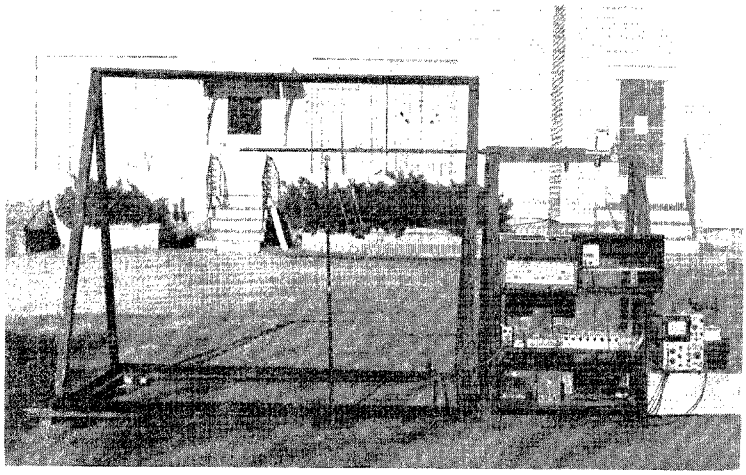

*b. Actual test rig.*

*Figure A2. Outdoor drill rod test rig.*

*Axial impacts.* Figure A2a is a schematic of the test fixture designed to produce axial impacts. Figure A2b shows the actual fixture with some of the measurement and analyzing equipment. Details of the impactor are given in Figure A3a, and Figure A3b shows an instrumented drill rod mounted in the impactor chuck.

Basically the unit consists of a cylinder containing a solid piston (hammer), with a chuck mounted at the front of the cylinder to accept a drill rod. Compressed air was fed to the back of the hammer through a regulator and a solenoid valve to accelerate it down the cylinder bore and into contact with the drill rod shank. The piston velocity at impact was measured with a Sanborn LV Syn (coil/magnet) velocity transducer,

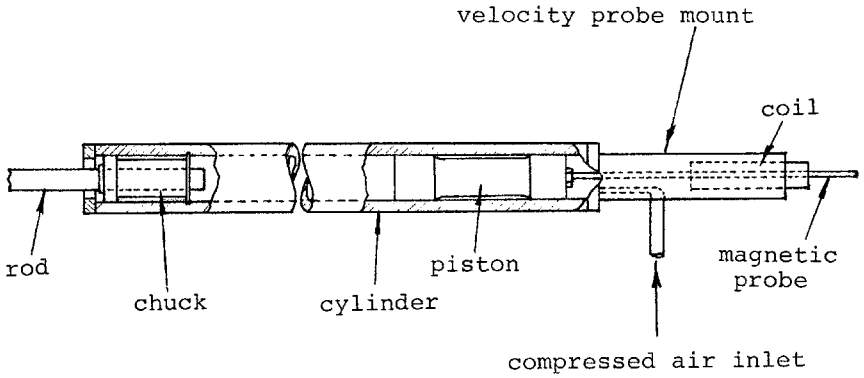


*a. Pneumatically operated axial drill rod in impactor.*

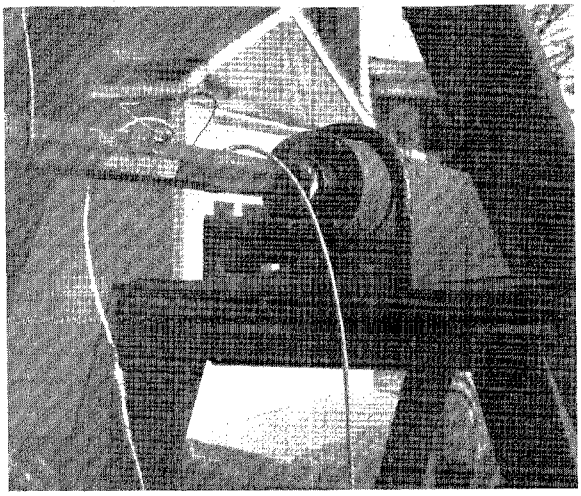

*b. Instrumented drill rod in the chuck.*

*Figure A3. Axial impactor.*

consisting of a coil mounted on the cylinder and a magnet attached to the hammer as shown in Figure A3a.

Figure A4a shows the circuit diagram for the velocity transducer, Figure A4b the calibrated output of the transducer, and Figures A4c and A4d typical test results. The form of the records shown in Figures A4c and A4d is typical for this type of transducer, with the output changing sign as the magnet passes through the coil. The peak output is a measure of the impact velocity. The sensitivity of the transducer with the circuitry, as illustrated in Figure A4a, was 115 mV/in.-s. The impact velocity was calculated from the transducer output as in the following example.

Peak voltage output at impact = 1.2 V

Voltage output of probe = $\frac{1100}{100} \times 1.2 = 13.2$ V

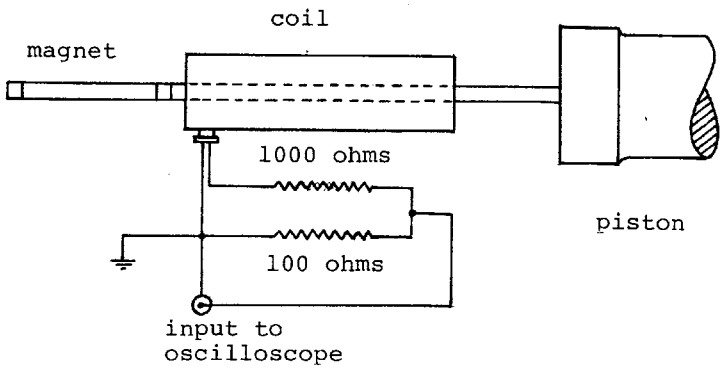


*a. Circuitry for Sanborn LV Syn velocity transducer.*

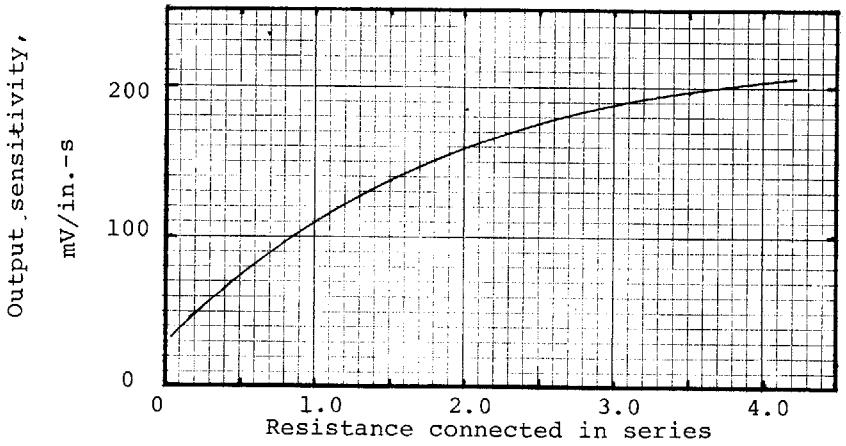


*b. Manufacturer's calibration graph.*

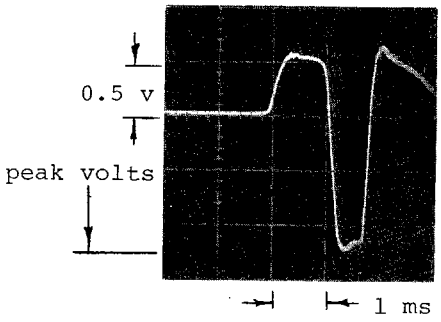


*c. Voltage output calibration signal.*

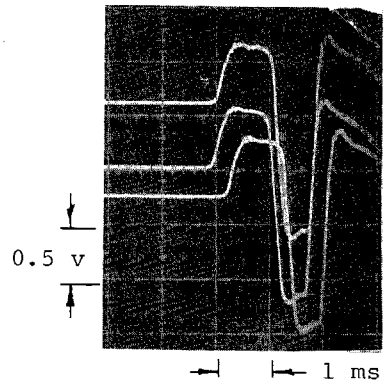


*d. Three consecutive output traces.*

*Figure A4. Piston impact velocity measurements.*

$$\text{Impact velocity} = \frac{13.2 \times 1000}{115 \times 12} = 9.56 \text{ ft/s}$$

$$\text{Impact stress level } \sigma_0 = 1760 V_0 \frac{A_p}{A_p + A_r}$$

Substituting $A_p = 3.142$ in.$^2$, $A_r = 0.62$ in.$^2$,

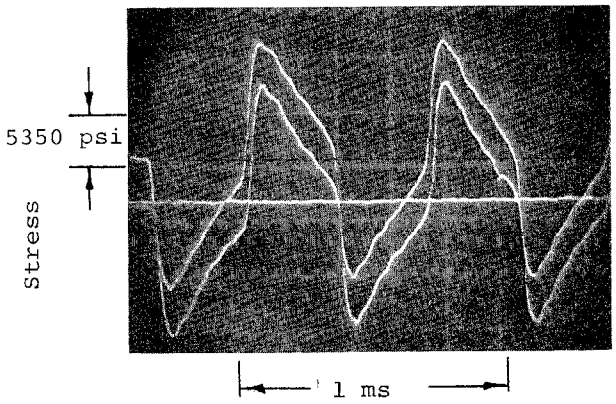


*a. Longitudinal stress waves, two consecutive impacts.*

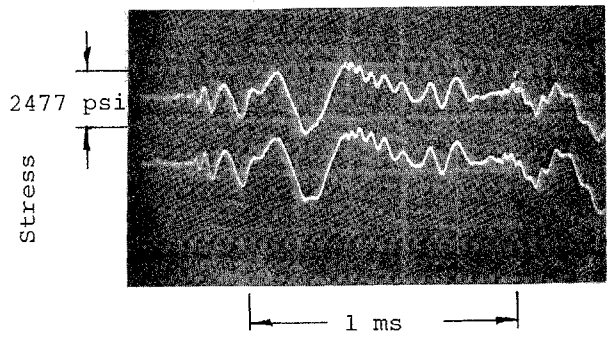


*b. Bending stress waves, two consecutive impacts.*

*Figure A5. Stress waves in drill rods generated by axial impactor.*

and $V_0$ = 9.56 ft/s, the longitudinal impact stress is calculated to be 14,060 psi.

Repeated impacts are closely reproducible, as will be noted from Figure A4d, which shows the impact velocity for three consecutive blows at the same pressure.

Figures A5a and A5b show the longitudinal and bending waves for the impacts measured in two of the tests of Figures A4c and A4d. Techniques for obtaining these records will be discussed later. As expected, they show excellent reproducibility, with a measured peak stress level for the longitudinal wave of 13,350 psi. This is slightly less than the value calculated from the impact velocity but is to be expected as some of the impact energy goes to generating the bending waves, as discussed in the main text.

Most of the tests on the outdoor fixture were made with hammer 4 impacting at a velocity of 9.56 ft/s, giving an impact energy of 7.6 ft-lb.

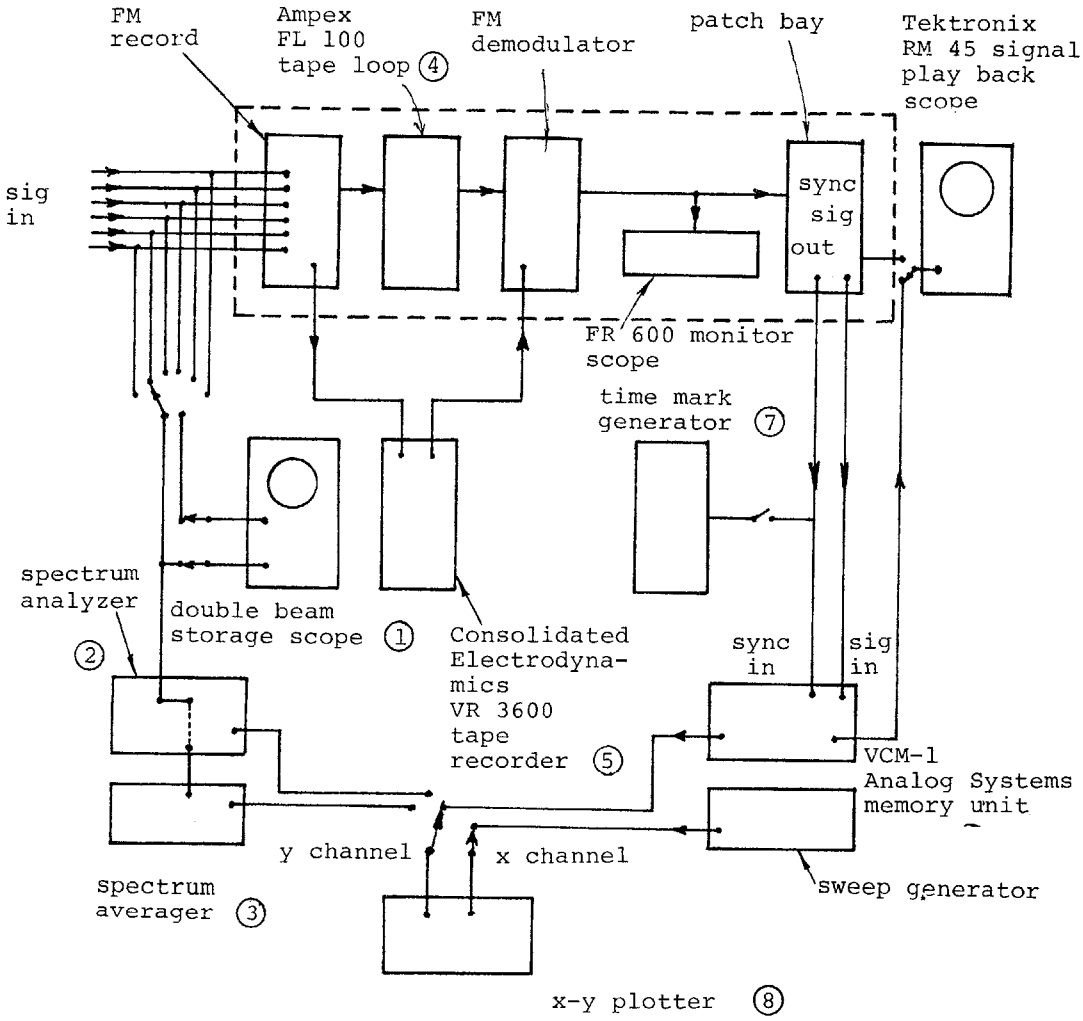


*Figure A6. Recording and analyzing equipment - layout schematic.*

## A.2 Measurement and analyzing equipment

*System description.* The equipment used for recording and analyzing the strain, acceleration and sound pressure level signals was designed to accept six simultaneous signals; it is shown schematically in Figure A6. Specifications are as follows:

1. Double beam storage oscilloscope, Tektronix Model 564

   y amplifier: Type 3A6, band width dc to 10 MHz
   x amplifier: Time base Type 3Bc, 0.5 μs/div

2. Spectrum analyzer, Federal Scientific Model UA-14A

   Input signal amplitude level 10 V RMS to 0.1 V RMS
   Input impedance 100,000 ohms
   Analysis range 0-50,000 Hz

Length of signal stored in memory varies from 0.008 s for 0-50,000 Hz coverage to 40 s for 0-10 Hz coverage.
Linearity of output: ±0.25% of the full analysis range

3. Spectrum averager, Federal Scientific Model 1014

   Input signal +5 mV to +5 V
   Input impedance 10,000 ohms
   Automatic averaging 1, 4, 16, 32, 64, 128, 256, 512 or 1024 spectra

4. Tape loop, Ampex Model FL 100

   Frequency response dc to 10 kHz
   Tape speed (maximum) 60 in./s
   Number of tracks - 14

   FM record electronics, Ampex Model FM 100

   Channel 1, 3, 5 dc to 100 kHz
   Channel 2, 4, 6 dc to 5 kHz

5. Tape recorder, Consolidated Electrodynamics VR 3600

   Frequency response 400 Hz to 102 MHz
   Tape speed 3.75, 7.5, 15, 30, 60, 120 in./s
   Number of tracks - 7

6. Memory unit, Analog Systems Model VCM-1

   High speed digital mode dc to 10 kHz
   Low speed digital mode dc to 10 Hz
   Maximum memory storage 4096 words × 12 bits/word

7. Timing mark generator, Hewlett Packard Model 650A Test Oscillator and Hewlett Packard Model 523CR Digital Counter, output 1 kHz 2v pp

8. X-Y Plotter, Federal Scientific Model 131B

   X axis gain 1 mV/in. to 10 V/in. in 5 steps
   Y axis gain 1 mV/in. to 10 V/in. in 5 steps
   Graph size 7 × 11 in.

The recorded signals were transient (short duration), steady-state (long duration), or frequency signals.

The transient signals were mostly recorded on the storage oscilloscope and the trace photographed to provide a permanent record.

The steady-state signals (up to 100 ms) were recorded on the Ampex tape loop used in conjunction with the VCM-1 Analog Systems memory unit. The records from the tape loop were plotted on the x-y plotter at two writing speeds representing 1 ms and 10 ms/in.

For frequency analysis the signals were taken directly from the signal conditioners to the spectrum analyzer. When statistical averaging was required the signals from the analyzer were fed into the spectrum averager and then recorded on the x-y plotter. The analysis normally covered a frequency range from 0 to 10 kHz over a time period of 40 ms.

3. Drill rod stress wave measurements

The longitudinal and bending strains in the drill rods were measured using metal foil electrical resistance strain gauges bonded axially to the rod surface.

Two strain gauges were bonded onto diametrically opposite sides of the rod at each measurement point. For longitudinal wave measurements the gauges were coupled in series into a quarter bridge network and for the bending wave measurements the gauges were coupled into a half bridge network (Fig. A7). These are standard strain gauge measurement techniques to cancel out the bending strains for the longitudinal wave measurements and the longitudinal strains for the bending wave measurements.

Details of the gauges used are as follows:

| | |
|---|---|
| Type: | Micromeasurement CEA-06-125-UW-120 with fully encapsulated grid. |
| Width: | 0.125 in. |
| Length: | 0.125 in. |
| Resistance: | 120 ohms ±0.3% |
| Gauge factor: | 2.075 ±0.5% |
| Self-temperature compensation: | ±1% variation of gauge factor between -100°F and +400°F |
| Cement: | Micromeasurement M Bond AE-10 System |

Circuit triggering was achieved either by using the output of an accelerometer mounted near the impact point or alternatively using the output of a strain gauge also mounted adjacent to the impact point.

Details of the test set-up for direct strain measurements on a scope and for frequency analysis of the signals are given in Figure A7.

*Strain gauge calibration.* The strain amplitudes recorded on the oscilloscope were calibrated by inserting a shunt resistance into the individual bridges in the conventional manner. Referring to the strain gauge bridges in Figure A7,

$$\text{Equivalent longitudinal strain} = \frac{R_4}{R_5 \times GF}$$

$$\text{Bending strain} = \frac{R_4}{2R_5 \times GF}$$

where $GF$ is the manufacturer's gauge factor.

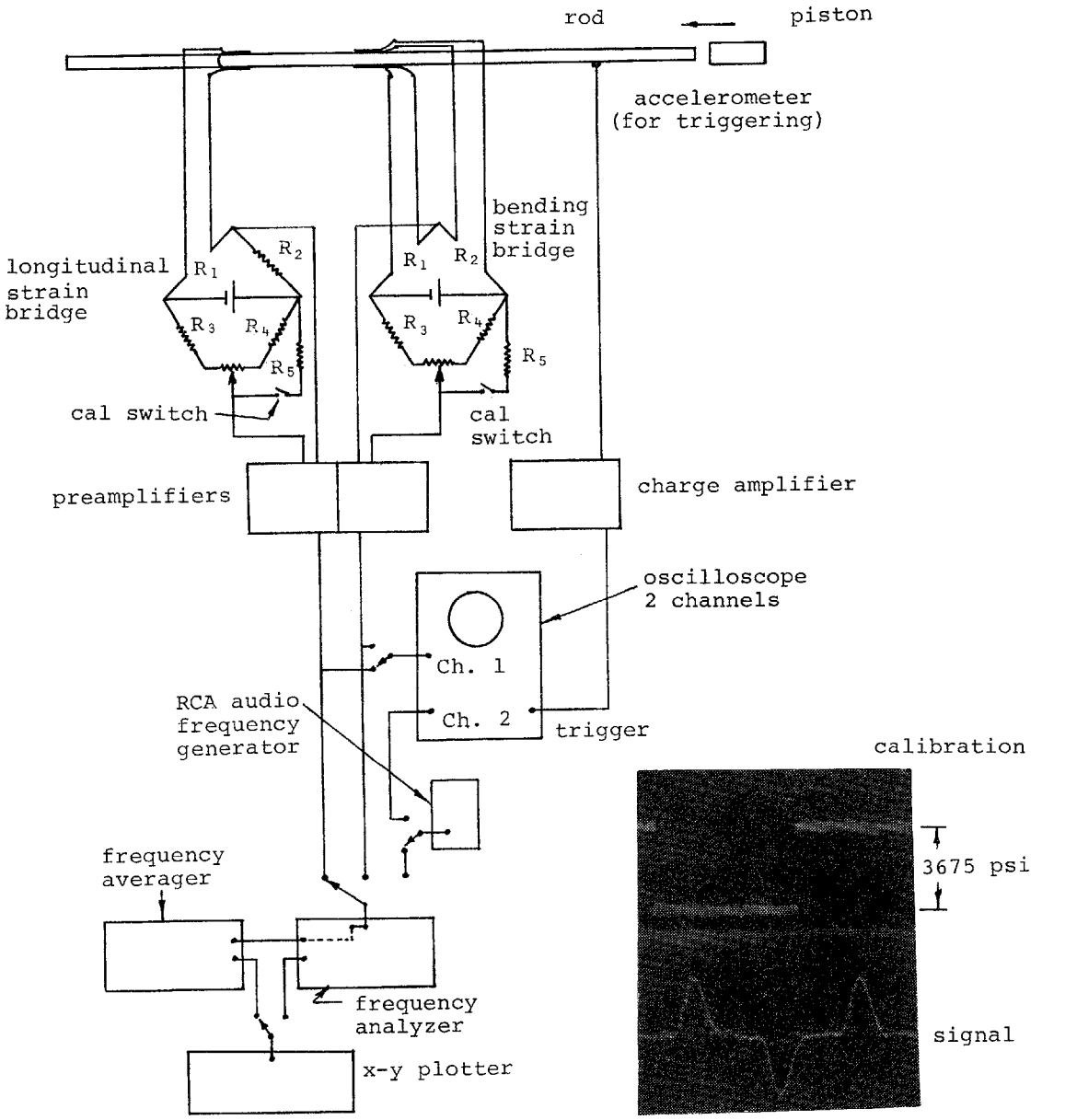


*a. Schematic.*

*b. Calibration of longitudinal strain wave signals.*

*Figure A7. Strain measurement instrumentation.*

The oscillograph insert in Figure A7 shows a typical calibration trace and a record of longitudinal strain. In this example the scope Y axis setting was 0.5 V/div, $R_4$ = 250 ohms, $R_5$ = 1000 kohms, and the scope calibration deflection was 2.75 divisions.

$$\text{Equivalent strain} = \frac{250}{10^6 \times 2.075} = 120.5 \text{ microstrains}$$

$$\text{Equivalent stress} = \text{strain} \times \text{modulus}$$

$$= 120.5 \times 10^{-6} \times 30.5 \times 10^6 = 3675 \text{ psi.}$$

Many of the tests involved making a spectrum analysis of strain gauge signals. This presented a calibration problem as equivalent strain signal is not at a unique frequency. The system finally adopted was to generate a calibration strain signal on the oscilloscope screen, as described earlier, and then use a signal generator with a variable voltage output to generate a 1000-Hz signal with an equivalent amplitude. This signal, when fed to the frequency analyzer and plotted on the x-y plotter, gives a strain amplitude peak at 1000 Hz equivalent to the calibration signal.

## A.4 Acceleration measurements

Radial accelerations of the rod surface were measured using a miniature quartz accelerometer screwed into small surface blocks bonded to the drill rod surface.

Details of the accelerometer and associated charge amplifier are as follows:

*Accelerometer*

| | |
|---|---|
| Type | Columbia Research Laboratories Model 606-3 |
| Voltage sensitivity | 3.04 mV/g with 100-pf load |
| Charge sensitivity | 1.43 pk pcmb/g |
| Range | 1 cps to 8 kHz |
| Acceleration range | 0.1 to 5000 g |

*Charge amplifier*

| | |
|---|---|
| Type | Columbia Research Laboratories Model 4012 |
| Source impedance | should be > 50 Mohms |
| Maximum input | 10,000 pcmb |
| Range (peak to peak) | 1.0 to 10,000 g, depending on transducer sensitivity |
| Gain maximum | 250 mV/pcmb |
| Accuracy | ±2% |
| Frequency response | 1 Hz to 10 kHz |
| Output maximum linear voltage | 5.0 V (peak to peak) |

The manufacturer's calibration factors were assumed for the accelerometer. The charge amplifier settings were adjusted to give a 5-V peak-to-peak output with 1000 g's input to the accelerometer.

The scale on the x-y plotter was adjusted using a 2-V peak-to-peak signal at 1 kHz in place of the output of the charge amplifier.

Tests were made to ensure that the cross sensitivity of the accelerometer was small so that the radial drill rod motion would not be swamped by the much higher axial motions associated with the longitudinal stress waves. The accelerometer was mounted at the end of a cantilever bar and vibrated with its sensitive axis in the direction of motion and also at right angle to it, and the outputs compared. Cross sensitivity was about 5% or less and this may explain why the longitudinal stress wave frequencies are noticeable in the acceleration frequency spectrum, but not in the noise spectrum. See, for example, Figure 18.

## A.5 Sound pressure level measurements

Sound pressure levels were measured with a Bruel and Kjaer ¼-in. condenser microphone and associated equipment with the following specifications:

*Microphone Type 4135*

| | |
|---|---|
| Nominal diameter | ¼ in. |
| Frequency response | free field, 0 incidence |
| Open circuit frequency response | 3.9 Hz to 100 kHz |
| Open circuit sensitivity | 3.47 mV/(N/m$^2$) or -49.2 dB re 1V/(N/m$^2$) |
| Cartridge diameter | 6.35 mm |
| Resonant frequency | 100 kHz |
| Influence of relative humidity | < 0.1 dB |

*Preamplifier Type 2619T*

| | |
|---|---|
| DC power supply | 120 V/2 mA |
| Input impedance | > 10 Gohms/0.8 pF |
| Frequency response | 2 Hz to 200 kHz |
| Output impedance | < 25 ohms |
| Maximum output current | 1.5 mA peak |
| Temperature range | -20$^o$ to +60$^o$C |
| Attenuation | 0.1 dB |

*Power supply*

| | |
|---|---|
| Input/output voltage ratio | 1:1 |
| Polarization voltage | 200 V |
| Noise | 20 Hz to 200 kHz, 30 μV |
| Hum | 50 Hz to 180 Hz, 8 μV |

*Noise level calibration.* The noise records were directly calibrated by using a General Radio Type 1562A Sound Level Calibrator, later itself calibrated against a B&K Type 4220 Pistophone. The specifications of these two types of calibrator are as below:

| General Radio Type 1562A Sound Level Calibrator | B&K Type 4220 Pistophone |
|---|---|
| Acoustic output:<br>Frequencies 125, 250, 500, 1000 and 2000 Hz ±3%<br>SPL: 114 dB ±0.3 dB at 500 Hz | Acoustic output:<br>Pure tone: 250 Hz ±1%<br>SPL: 124 dB ±0.2 dB |

The output of the two calibrators agreed within 2% (0.18 dB).

*Indoor sound field evaluation.* Most of the measurements were made within an 11- × 10- × 8-ft room. The reverberation effect of the room was evaluated by calculating the room constant $R_0$ for a frequency of 4000 Hz. The room surface areas and their absorption coefficients are given below.

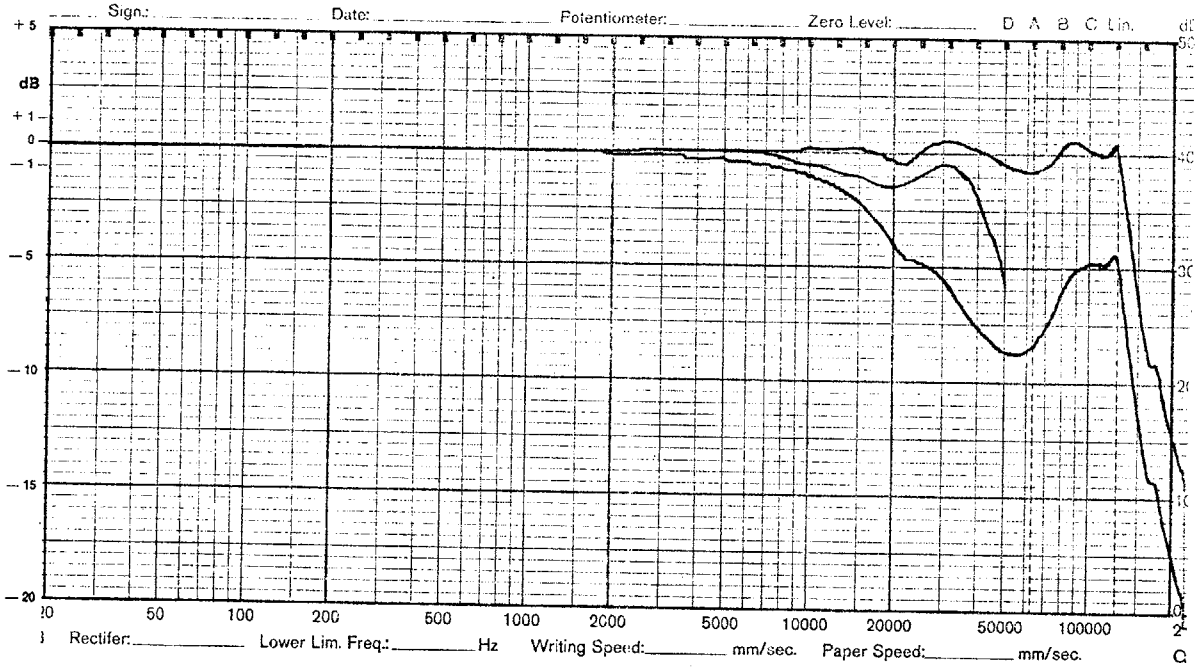


*Figure A8. Frequency response calibration curve of type 4135 ¼-in. B&K microphone used in tests. Frequency response characteristics: The upper curve is the open circuit free-field characteristic, valid for the Microphone Cartridge without protecting grid. Sound waves perpendicular to diaphragm. The lower curve is the open circuit pressure response recorded with electrostatic actuator. The middle curve is the open circuit random incidence response. Conditions of tests: Frequency 250 Hz, polarization voltage 200 V, barometric pressure 1021 mbar, relative humidity 56%, temperature 23°C.*

| Surface | Area ($ft^2$) | Absorption noise coefficient at 4000 Hz |
|---|---|---|
| Carpeted floor | 122.70 | 0.3* |
| Ceiling | 472.55 | 0.11† |
| Window glass | 15.80 | 0.04† |
| Hard surface | 52.09 | 0.04† |

*Taylor, R. (1970) *Noise*. Penguin Books Ltd., p. 262.

†Diehl, G.M. (1973) *Machinery Acoustics*. John Wiley and Sons, p. 59.

The area average absorption coefficient $\alpha$ is calculated from the table above to be 0.14. The room constant $R_0$ is given by

$$R_0 = \frac{S_t\bar{\alpha}}{1-\bar{\alpha}} = \frac{663.14\times0.14}{1-0.14} = 107.95$$

where $S_t$ = total area of the room (663.14 $ft^2$).

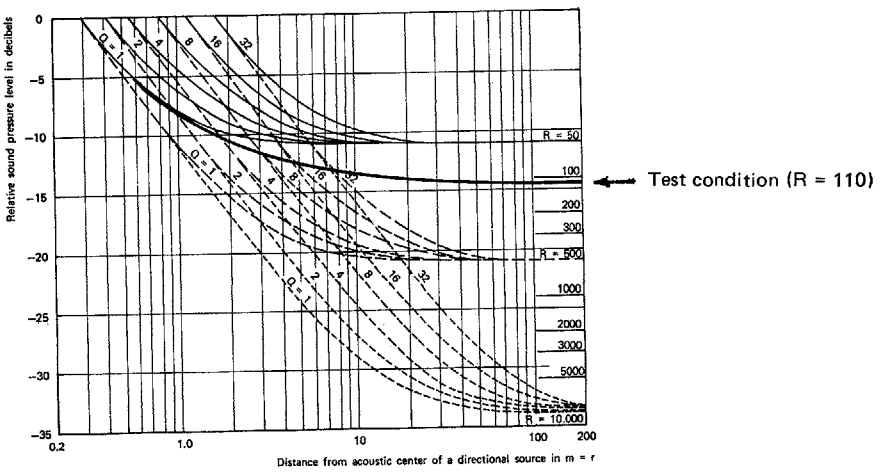


*Figure A9. Chart for determination of the sound pressure level in a large room as a function of the distance from the sound source. The room constant, $R_Q$, and the directivity factor, $Q$, are plotted as parameters. (After Broch 1971.)*

Figure A9 (from Broch*) indicates that for a room constant $R_Q$ = 110 and $Q$ = 1 the "reverberant" field starts and extends beyond 0.6 m from the rod for 4000 Hz. ($Q$ is the directing factor; $Q$ = 1 corresponds to the free suspension of a nondirectional sound source.)

The measurements made within the distance of 0.6 m (≃ 24 in.) should essentially be free from reverberation effects.

*Broch, J.T. (1971) *Application of the Bruel & Kjaer Measuring Systems to Acoustic Noise Measurements.* B & K, p. 189.

## APPENDIX B. DERIVATION OF RADIAL SURFACE VELOCITIES IN BENDING WAVES

The relationship between the drill rod surface velocity and surface strain is derived rigorously to verify the simple development that these two quantities are directly proportional to each other. The derivation applies to standing waves, as opposed to transient waves which exist prior to the formation of standing waves. Any transverse rod motions may be represented as a series, each term of which applies to a single standing wave mode. Mathematically,

$$y = \sum_{\ell=0}^{\infty} y_\ell \exp i(k_\ell x - \omega_\ell t + \phi_\ell) \tag{B1}$$

where $k_\ell$, $\omega_\ell$ and $\phi_\ell$ are constants characterizing the $\ell th$ mode of vibration (i.e. the $\ell th$ standing wave), and $y_\ell$ is a function to be determined.

To verify that eq B1 is an allowable representation for the standing waves, substitute into the bending wave equation

$$\frac{\partial^4 y}{\partial x^4} = \frac{-\rho A_r}{EI} \frac{\partial^2 y}{\partial t^2} . \tag{B2}$$

For each term in the series the derivatives required in eq B2 can be evaluated. (Note that $y_\ell$ is allowed to be a variable function.) The required derivatives are:

$$\frac{\partial^4 y}{\partial x^4} = \sum_{\ell=0}^{\infty} \exp i(k_\ell x - \omega_\ell t + \phi_\ell) \left[ y_\ell (ik)^4 + 4 \frac{\partial y_\ell}{\partial x} (ik)^3 + 6 \frac{\partial^2 y_\ell}{\partial x^2} (ik)^2 + 4 \frac{\partial^3 y_\ell}{\partial x^3} (ik) + \frac{\partial^4 y_\ell}{\partial x^4} \right] \tag{B3}$$

$$\frac{\partial^2 y}{\partial t^2} = \sum_{\ell=0}^{\infty} \exp i(k_\ell x - \omega_\ell t + \phi_\ell) \left[ y_\ell (-i\omega)^2 + 2 \frac{\partial y_\ell}{\partial t} (-i\omega) + \frac{\partial^2 y_\ell}{\partial t^2} \right]. \tag{B4}$$

Dropping the summation signs and proceeding on a term-by-term basis, each function, $y_\ell$, must obey an equation of the form:

$$\frac{\partial^4 y_\ell}{\partial x^4} + 4 \frac{\partial^3 y_\ell}{\partial x^3} (ik) + 6 \frac{\partial^2 y_\ell}{\partial x^2} (ik)^2 + 4 \frac{\partial y_\ell}{\partial x} (ik)^3 + y_\ell \left[ (ik)^4 + \frac{\rho A_r}{EI} (-i\omega)^2 \right] = \frac{2\rho A_r}{EI} \frac{\partial y_\ell}{\partial t} (i\omega) - \frac{\rho A_r}{EI} \frac{\partial^2 y_\ell}{\partial t^2} . \tag{B5}$$

The term in brackets is identically zero, as this condition describes the relationship between the temporal and spatial variation of the standing bending waves. The rest of the terms are either spatial derivatives (left-hand side of the equals sign) or temporal derivatives (right-hand side of the equals sign). The spatial variation of the wave is assumed to be sinusoidal and this standing wave mode shape is already incorporated into the exponential factor $e^{i(kx-\omega t+\phi)}$. Thus the spatial derivatives can all be set to zero by assumption, and eq B5 reduces to:

$$\frac{d^2 y_\ell}{dt^2} = 2i\omega \frac{dy_\ell}{dt} . \tag{B6}$$

There are two general solutions to eq B6:

$$\begin{aligned} y_\ell &= \text{Constant} \\ y_\ell &= A\ e^{2i\omega t}. \end{aligned} \tag{B7}$$

The first solution verifies the assertion made earlier that the $y_\ell$'s are constant, while the second states that left-running waves are also allowable solutions to the bending wave equation. Thus, if the second solution was selected, the sign in front of the $\omega t$ term in the exponential factor would be positive rather than negative, and this change of sign merely reflects a change in direction for the propagation of the waves. Direction of wave propagation does not affect the conclusion that the wave amplitude is constant in time.

The drill rod surface velocity is the time derivative of the surface motion and may be calculated directly from eq B1:

$$u_b = \frac{dy}{dt} = \sum_{\ell=0}^{\infty} y_\ell(-i\omega_\ell)\ \exp\ i(k_\ell x-\omega_\ell t+\phi_\ell). \tag{B8}$$

This series may be related to the surface strain through the beam equation for thin rods:

$$\frac{M}{EI} = \frac{d^2 y}{dx^2} . \tag{B9}$$

The bending moment is related to rod stress by the well known formula

$$\sigma_b = \frac{Mc}{I} \tag{B10}$$

where $c$ is the distance from the radial axis. Finally, the stress is related to strain by Hooke's law:

$$\sigma_b = E\,\varepsilon_b. \tag{B11}$$

Combining eq B9-B11 and using $c = D/2$ for a circular rod gives

$$\varepsilon_b = \frac{D}{2}\frac{d^2y}{dx^2} . \tag{B12}$$

Performing the indicated differentiations:

$$\varepsilon = \frac{D}{2}\sum_{\ell=0}^{\infty} y_\ell(-k_\ell^2) \exp i(k_\ell x - \omega_\ell t + \phi_\ell) . \tag{B13}$$

This result can be further simplified and put into a form comparable to eq B8 by substituting the bending wave frequency equation (the bracketed term in eq B8), i.e.

$$k_\ell^2 = \sqrt{\frac{\rho A}{EI}}\,\omega_\ell = \frac{4}{C_s D}\omega_\ell . \tag{B14}$$

Finally, on substituting eq B14 into eq B13 and comparing to eq B8 we deduce that

$$u_b = \frac{\varepsilon_b C_s}{2} i. \tag{B15}$$

The factor $i$ represents a phase shift between the surface strain and surface velocity, and the factor $C_s/2$ is the constant of proportionality. This result applies in both the time and frequency domains, which means that the power spectrum of the surface velocity will be identical to that of the surface strain as well as that the wave forms will be the same, i.e. $|i| = 1$. The limitations to the generality of eq B15 are:

1. The bending waves must be standing (i.e. steady-state).

2. The rod must be linearly elastic.

3. The slender beam approximation must be valid.

Another important question to be addressed is: What does a strain gauge mounted on the rod measure in terms of the peak surface velocity? This is a matter of speculation because the exact placement of the strain gauge relative to the mode shape of the standing waves will have an important effect. In the absence of specific information concerning the strain gauge placement, if it is assumed that the strain gauge measures the spatial RMS strain, then the peak surface velocity will be greater than that calculated from eq B15 by the factor $\sqrt{2}$, i.e.

$$u_b = \frac{\varepsilon_b C_s}{2}\sqrt{2} . \tag{B16}$$

The assumption that a randomly placed strain gauge will read the RMS average strain is made for the following reason. The average energy in a sinusoidal signal over one period of vibration corresponds to the RMS average level of the signal. If the energy of each mode is independent of that of all other modes and if the vibration nodes are equally spaced, then the total energy indicated by the strain gauge will be half of the

true energy and the correction factor will be exactly $\sqrt{2}$. However, if the real time signals are added and (if they were) uncorrelated, the average correction factor would be $\pi/2$ rather than $\sqrt{2}$. Neither condition is strictly fulfilled, but the first is assumed to be more valid.

## APPENDIX C. DRILL ROD SURFACE VELOCITY AND ENERGY FOR BENDING AND LONGITUDINAL WAVES

The mathematical formulas relating surface radial velocity and wave energy to "measurable" quantities such as stress, strain, rod length, rod area, and material properties are summarized in this appendix. Because they are not available in the literature in the form required for the present study, most of these formulas are derived from the elementary principles of mechanics. The derivations for bending wave energy are given in Section C.1, and for the longitudinal wave energy in Section C.3. Section C.2 gives the relationship between surface radial velocity and stress for the longitudinal wave based on the triangular wave approximation. The surface radial velocity for bending waves has already been given in Appendix B and is not repeated here.

### C.1 Bending wave energy formulas

As the bending waves do not travel at constant speed, it is necessary to integrate the stress and kinetic energy expressions throughout the drill rod to do calculations. The integrations are performed in terms of stress levels for the case of standing waves and it is not expected that the formulas will strictly apply during the transient period, although they should be approximately valid.

The bending wave energy formulas are derived on the basis of a single frequency of oscillation corresponding to a single mode of vibration. The total energy in oscillations of all frequencies is obtained by adding the energy for each mode of vibration, so the most commonly used averaging is RMS, which is an "energy average." In relation to sound radiation it should be remembered that not all modes of vibration radiate equally efficiently, so the RMS radial velocity is not necessarily the one which best represents the radiated sound level. This additional complexity is ignored on the grounds that the present study does not attempt to correlate sound and vibration levels; also, the radiation efficiency is unity over the range of frequencies where the bending wave energy is significant so the correction for this effect is small in any event.

*Kinetic energy.* The kinetic energy of the rod motion associated with the transverse bending vibration is calculated by adding the energy from the motions at every point along the rod. The effects which must be accounted for include:

1. The plane of the bending waves.
2. The time variation of the bending waves.
3. The spatial (along the rod) variation of the bending waves.
4. The different vibration frequencies (resonances) of the bending waves.

Consider a section of rod:

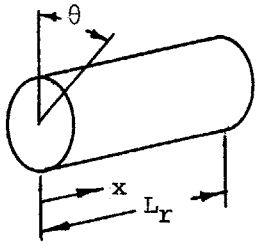


The radial velocity $u$ at any point on the rod surface subject to a standing wave* is given by

$$u = u_0 \cos\theta \cos\omega t \sin n\pi \frac{x}{L_r} \tag{C1}$$

where $\theta$ = angle to the point from the plane of bending
$t$ = time variable. The $\cos\omega t$ factor is used rather than a more general expression because time phase information is not important.
$x$ = spatial coordinate along a rod length $L$.

The average kinetic energy of the whole rod over one cycle of vibration is represented by the integral

$$KE = \frac{1}{M}\int_0^M \frac{1}{2} u^2 dm = \frac{\omega}{2\pi}\frac{1}{L_r}\int_0^{2\pi/\omega}\int_0^{L_r} \frac{m}{2} u_0^2 \cos^2\theta \cos^2\omega t \sin^2 n\pi \frac{x}{L_r} dx dt \tag{C2}$$

For $\theta = 0$ corresponding to the plane of bending, eq C2 integrates to $KE = (mu_0^2)/8$ where $m$ is the mass of the rod.

It has been shown in Appendix B that the relationship between the peak radial velocity $u_0$ and the peak bending strain $\varepsilon_0$ is given by

$$u_0 = \frac{\varepsilon_0 C_s}{2} = \frac{\sigma_{mb} C_s}{2E} \tag{C3}$$

where $\sigma_{mb}$ is the peak bending stress.

Thus the kinetic energy in the bending wave can be expressed in terms of peak bending stress by

$$KE = \frac{1}{8} A_r L_r \rho \left(\frac{\sigma_{mb} C_s}{2E}\right)^2 = \frac{1}{32}\frac{A_r \sigma_{mb}^2 L_r}{E}. \tag{C4}$$

*Strain energy.* The strain energy associated with the bending waves is found by integrating the strain energy expression throughout the cross section of the rod.

---

**Note that the end conditions are assumed to be hinged-hinged for these computations. The same results are also obtained for other end conditions, e.g. free-free or clamped-free.*

$$SE = \int \frac{\sigma^2}{2E} \, d_{vol}$$

$$d_{vol} = 2x dy L_r$$

$$x = \sqrt{r^2 - y^2}$$

$$\sigma = \sigma_{mb} \frac{y}{r} \left( \cos\theta \, \cos\omega t \, \sin n\pi \frac{x}{2} \right)$$

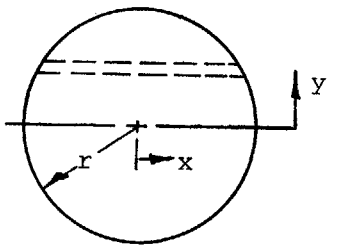


where the bracketed term reminds that to obtain a space and time average strain energy, a factor of ¼ must be included, because $\sigma$ is oscillating harmonically along the rod length and also in time, whereas the integral is performed for $\sigma$ constant. The factor ¼ corrects for the difference between RMS and peak quantities.

$$SE = 2 \frac{\sigma_{mb}^2 L_r}{2E} \int_0^r \left( \frac{y}{r} \right)^2 2\sqrt{r^2 - y^2} \, dy$$

$$= 2 \frac{\sigma_{mb}^2 L_r}{2E} \frac{2}{r^2} \left[ \frac{-y(r^2 - y^2)^{3/2}}{4} + \frac{r^2 y \sqrt{r^2 - y^2}}{8} + \frac{r^4}{8} \sin^{-1} \frac{y}{r} \right]_0^r$$

$$= 2 \frac{\sigma_{mb}^2 L_r}{2E} \frac{2}{r^2} \left( \frac{\pi}{2} \frac{r^4}{8} \right)$$

$$= \frac{\sigma_{mb}^2}{2E} \pi r^2 L_r \frac{1}{4}. \qquad \text{(C5)}$$

Multiplying by ¼ to include the effects of the space and time average, the strain energy of the rod is

$$SE = \frac{\sigma_{mb}^2}{2E} A_r L_r \frac{1}{16}. \qquad \text{(C6)}$$

Comparison of eq C6 with C4 reveals that the total energy in a bending wave is made up of half kinetic and half strain energy, just as is the case in a longitudinal stress wave. Thus the total energy is given by peak stress $\sigma_{mb}$ as

$$E_b = \frac{1}{16} \frac{\sigma_{mb}^2}{E} L_r A_r. \qquad \text{(C7)}$$

## C.2 Surface RMS radial velocity for longitudinal stress waves

There is a fundamental difference between calculations for bending (transverse) and stress (longitudinal) waves. Bending waves exhibit dispersion and thus quickly occupy the whole rod. Longitudinal stress waves, on the other hand, travel at constant velocity, and hence stay together in a "cohesive" packet. Thus the stress wave is concentrated in a definite portion of the drill rod at any instant of time. To calculate the RMS radial surface velocity from the longitudinal stress wave

it is necessary to integrate over the stress wave length and then divide by the ratio of rod length to stress wave length rather than to attempt to integrate over the rod length in both space and time.

A simple model has been developed to relate surface radial velocity to the stress and energy levels. The model approximates the stress wave to a triangular-shaped wave and the justification for the model is given in Section 3.2.

The stress wave form is modeled by three parameters: the peak stress $\sigma_{mL}$, the stress wave length $q$, and the rise time $\tau$. In addition, the stress wave period is defined by $T = 2L_r/C_s$. These quantities are illustrated in Figure C1.

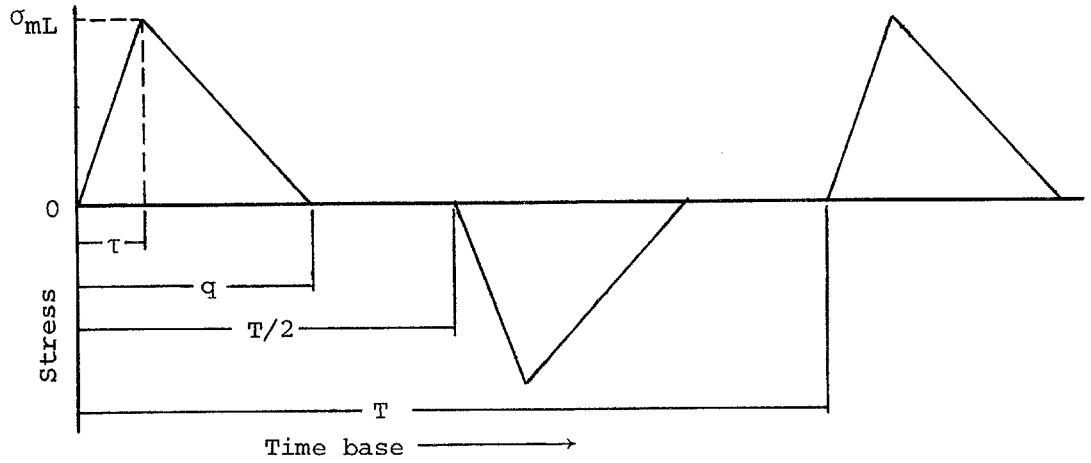


*Figure C1. Longitudinal stress wave model.*

It has been shown in Section 3.2 that the radial surface velocity $u_L$ is given by

$$u_L = \frac{\nu D}{2E} \frac{d\sigma}{dt} . \qquad \text{(C8)}$$

The derivative in the rise time region is

$$\frac{d\sigma}{dt} = \frac{\sigma_{mL}}{\tau}$$

while during the rest of the wave

$$\frac{d\sigma}{dt} = - \frac{\sigma_{mL}}{q-\tau} .$$

Finally, $d\sigma/dt = 0$ when there is no wave, i.e. for $q < t < T/2$.

The radial velocities in the initial wave are calculated from eq C8 as

$$\frac{\nu D}{2E} \frac{\sigma_{mL}}{\tau}$$

and

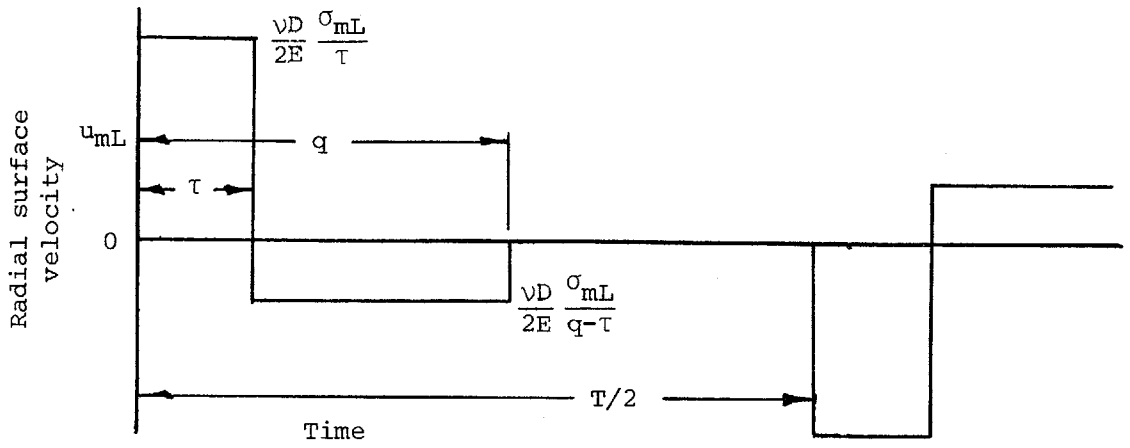


*Figure C2. Radial velocity from longitudinal stress wave model.*

$$\frac{\nu D}{2E}\frac{\sigma_{mL}}{q-\tau}.$$

The radial velocity distribution is shown in Figure C2.

The RMS radial velocity averaged over the entire rod is given by

$$u_{rL} = \frac{\nu D}{2E}\left[\left(\frac{\sigma_{mL}}{\tau}\right)^2 \frac{2\tau}{T} + \left(\frac{\sigma_{mL}}{q-\tau}\right)^2 (q-\tau)\frac{2}{T}\right]^{\frac{1}{2}}. \qquad \text{(C9)}$$

For convenience, the factor $S_f$ can be used to define the form of the wave form, where

$$S_f = \frac{q}{\tau}.$$

Substituting for τ in eq C9, the RMS radial velocity is given by

$$u_{rL} = \frac{\nu D}{2E}\frac{\sigma_{mL}}{q}\left[S_f \frac{2q}{T} + \frac{(2q/T)}{1-(1/S_f)}\right]^{\frac{1}{2}}. \qquad \text{(C10)}$$

*Kinetic and strain energy.* The energy in a longitudinal stress wave is given by the well known formula

$$KE = SE = \int_0^q \frac{\sigma_{mL}^2}{2E} A_r C_s dt.$$

Evaluating this integral for the triangular wave form leads directly to the result:

$$\text{total energy} = \frac{2\sigma_{mL}^2}{2E}\frac{A_r}{3} q C_s$$

$$= \frac{\sigma_{mL}^2}{E} A_r L_r \frac{2}{3}\frac{q}{T}. \qquad \text{(C11)}$$